U.S.NRC

United States Nuclear Regulatory Commission

Protecting People and the Environment

NUREG/CR-6982
ANL-05/44

Assessment of Noise Level for Eddy Current Inspection of Steam Generator Tubes

Office of Nuclear Regulatory Research

AVAILABILITY OF REFERENCE MATERIALS IN NRC PUBLICATIONS

NRC Reference Material

As of November 1999, you may electronically access NUREG-series publications and other NRC records at NRC's Public Electronic Reading Room at http://www.nrc.gov/reading-rm.html. Publicly released records include, to name a few, NUREG-series publications; *Federal Register* notices; applicant, licensee, and vendor documents and correspondence; NRC correspondence and internal memoranda; bulletins and information notices; inspection and investigative reports; licensee event reports; and Commission papers and their attachments.

NRC publications in the NUREG series, NRC regulations, and *Title 10, Energy*, in the Code of *Federal Regulations* may also be purchased from one of these two sources.

1. The Superintendent of Documents
   U.S. Government Printing Office
   Mail Stop SSOP
   Washington, DC 20402–0001
   Internet: bookstore.gpo.gov
   Telephone: 202-512-1800
   Fax: 202-512-2250
2. The National Technical Information Service
   Springfield, VA 22161–0002
   www.ntis.gov
   1–800–553–6847 or, locally, 703–605–6000

A single copy of each NRC draft report for comment is available free, to the extent of supply, upon written request as follows:

Address: U.S. Nuclear Regulatory Commission
Office of Administration
Mail, Distribution and Messenger Team
Washington, DC 20555-0001
E-mail: DISTRIBUTION@nrc.gov
Facsimile: 301–415–2289

Some publications in the NUREG series that are posted at NRC's Web site address http://www.nrc.gov/reading-rm/doc-collections/nuregs are updated periodically and may differ from the last printed version. Although references to material found on a Web site bear the date the material was accessed, the material available on the date cited may subsequently be removed from the site.

Non-NRC Reference Material

Documents available from public and special technical libraries include all open literature items, such as books, journal articles, and transactions, *Federal Register* notices, Federal and State legislation, and congressional reports. Such documents as theses, dissertations, foreign reports and translations, and non-NRC conference proceedings may be purchased from their sponsoring organization.

Copies of industry codes and standards used in a substantive manner in the NRC regulatory process are maintained at—

The NRC Technical Library
Two White Flint North
11545 Rockville Pike
Rockville, MD 20852–2738

These standards are available in the library for reference use by the public. Codes and standards are usually copyrighted and may be purchased from the originating organization or, if they are American National Standards, from—

American National Standards Institute
11 West 42nd Street
New York, NY 10036–8002
www.ansi.org
212–642–4900

Legally binding regulatory requirements are stated only in laws; NRC regulations; licenses, including technical specifications; or orders, not in NUREG-series publications. The views expressed in contractor-prepared publications in this series are not necessarily those of the NRC.

The NUREG series comprises (1) technical and administrative reports and books prepared by the staff (NUREG–XXXX) or agency contractors (NUREG/CR–XXXX), (2) proceedings of conferences (NUREG/CP–XXXX), (3) reports resulting from international agreements (NUREG/IA–XXXX), (4) brochures (NUREG/BR–XXXX), and (5) compilations of legal decisions and orders of the Commission and Atomic and Safety Licensing Boards and of Directors' decisions under Section 2.206 of NRC's regulations (NUREG–0750).

DISCLAIMER: This report was prepared as an account of work sponsored by an agency of the U.S. Government. Neither the U.S. Government nor any agency thereof, nor any employee, makes any warranty, expressed or implied, or assumes any legal liability or responsibility for any third party's use, or the results of such use, of any information, apparatus, product, or process disclosed in this publication, or represents that its use by such third party would not infringe privately owned rights.

U.S.NRC
United States Nuclear Regulatory Commission
Protecting People and the Environment

NUREG/CR-6982
ANL-05/44

Assessment of Noise Level for Eddy Current Inspection of Steam Generator Tubes

Manuscript Completed: January 2008
Date Published: March 2009

Prepared by
S. Bakhtiari, D.S. Kupperman, and W.J. Shack

Argonne National Laboratory
9700 South Cass Avenue
Argonne, IL 60439

M. Stambaugh, NRC Project Manager

NRC Job Code Y6588

Office of Nuclear Regulatory Research

Abstract

This report provides an overview of research activities associated with eddy current (EC) inspection of steam generator tubes that was carried out at Argonne National Laboratory (ANL) as part of the Steam Generator Tube Integrity Program sponsored by the U.S. Nuclear Regulatory Commission. Results of recent studies on assessing the influence of noise on detection of EC flaw signals are presented. In particular, methodologies for measuring the level of noise in bobbin-coil inspection data are examined. Although the primary focus is on spatially one-dimensional calculations for bobbin probe noise, limited investigations on the measurement of noise in rotating probe data are also discussed. In the first part of the report, the basic concepts and common sources of signal distortion in EC data from in-service inspection are initially reviewed. Next, various algorithms for the simulation, superposition, and measurement of noise that were developed at ANL are described. Results of studies on the effect of measurement variables (e.g., measurement window size and region of interest) on various measures of noise level are also presented. Based on these investigations, viable indicators of the noise level are identified and the associated measurement procedures are outlined. A distinction is made between the global noise levels that are important for data quality assessment and the more localized noise levels that directly affect detection capability. The second part of the report deals with measurement of the level of noise present in the tube bundle mock-up at ANL. Selected tubes were identified as having flaw signals that were borderline for detectability, i.e., they were missed by at least one of the round–robin teams or by a number of individual analysts from different teams. By analysis of these signals and the associated noise levels, inferences were made regarding the limit of detection. The implications of the results concerning the detection probability are discussed. Finally, application of the proposed methodologies for the measurement of noise level is addressed.

Foreword

This report discusses a study conducted by Argonne National Laboratory (ANL) under contract with the U.S. Nuclear Regulatory Commission (NRC), Office of Nuclear Regulatory Research (RES). RES initiated this study as part of the agency's Steam Generator Tube Integrity Program. The study aims to support the NRC's evaluation of licensee inspection programs that utilize eddy current examination technology. This report identifies the key properties of eddy current noise and evaluates their affect on the detection and sizing of flaws. The results of this work will ultimately aid in implementing improved methodologies for evaluating the effect of noise on the detection and sizing of flaws. NRC staff will use these findings to perform independent assessments of inspection technology reliability and to inform decisions related to licensing actions.

In eddy current technology there are many possible sources of noise as well as various ways to measure noise. Each method of measuring noise can provide information useful in assessing the ability to both detect and size flaws. This study examined noise sources and noise measurement methods as well as measurement repeatability.

The first part of the report discusses measurement and simulation of unwanted eddy current signals (i.e., noise). This includes the basic concepts of noise and common sources of eddy current signal distortion in steam generator tubes. Additionally, the report discusses the algorithms that were used to analyze eddy current signals. The algorithms can be used to measure noise and to inject noise into the eddy current data. The sensitivity of the noise measurement to various parameters is also discussed. The second part of the report discusses the measurement of noise level from a tube bundle mock-up at ANL. The ability to detect signals is evaluated as a function of noise level using various measures of noise. Finally, there is a discussion of a method to adjust the probability of detection for different levels of noise.

The study determined that it is best to quantify the noise for a flaw signal by using inspection data which is directly adjacent to the flaw. Furthermore, the study noted that noise can constructively or destructively affect an eddy current signal. It was also determined that the vertical amplitude of a noise signal affects flaw detection but the total noise is more important in sizing flaws. As a result, it may be appropriate to have separate criteria for assessing the effects that noise can have on detecting and sizing flaws. Finally, the study identified that if certain noise measurement parameters are maintained within a particular range, a more repeatable measurement of noise is possible. These conclusions along with the other analyses in the report provide a useful assessment of the effects that noise can have on detecting and sizing flaws in steam generator tubes using eddy current technology.

Contents

Abstract iii

Foreword v

Contents vii

Figures viii

Tables xiii

Executive Summary xv

Acknowledgments xvii

Acronyms and Abbreviations xix

1 Introduction 1

2 Simulation and Measurement of Eddy Current Noise 3

2.1 Sources of Signal Distortion in Steam Generator Tube Inspections 3

2.2 Noise Simulation and Measurement 5

2.2.1 Simulation and Superposition of Noise 6

2.2.2 Data Analysis and Measurement Routines 11

2.2.3 Effect of Measurement Parameters on Estimation of Noise Level 11

2.2.4 Measurement Repeatability 23

2.2.5 Assessment of Noise Level in Rotating Probe Data 46

3 Influence of Eddy Current Noise on Detection of Mock-up Flaws 57

3.1 Assessment of Noise Level 57

3.1.1 Data Selection Criteria 57

3.1.2 Calibration Procedure for Bobbin Coil Data 57

3.1.3 Procedure for Measurement of Noise Level 58

3.2 Evaluation of Parameters for Establishing Detection Limit 59

3.2.1 Composition of Database for Noise Level Assessments 59

3.2.2 Analysis of Measurement Results for Establishing Detection Probability 71

3.3 Adjustment of POD Based on Noise Level 77

4 Concluding Remarks 83

5 References 85

Figures

2.1 Representative display of superimposed TSP signal (captured from a separate calibration standard tube) on rotating probe data from a laboratory-cracked specimen with primarily OD-initiated SCC.. 8

2.2 Representative display of superimposed random noise on rotating probe data from a laboratory-cracked specimen with primarily OD-initiated SCC.. 9

2.3 Representative display of superimposed periodic noise on rotating probe data from a laboratory-cracked specimen with primarily OD-initiated SCC. 10

2.4 Evaluation of bobbin coil mix results for an ASME calibration standard tube. 13

2.5 Evaluation of bobbin coil mix results for TSP-level test section #4 with ODSCC indication.. 14

2.6 Evaluation of bobbin coil mix results for TSP-level test section #6 with ODSCC indication. 14

2.7 Evaluation of noise influence on bobbin coil signal for TSP-level test section #4 with an ODSCC indication. 15

2.8 Evaluation of noise influence on bobbin coil signal for TSP-level test section #6 with an ODSCC indication.. 15

2.9 Depiction of the measurement region and the associated variables for the measurement of noise outside a TSP intersection. 18

2.10 Evaluation of the influence of noise on bobbin coil data from mock-up test section #1 with an ODSCC indication at a TSP intersection. 18

2.11 Second evaluation of the influence of noise on bobbin coil data from mock-up test section #1 with ODSCC indication at a TSP intersection. 19

2.12 Third evaluation of the influence of noise on bobbin coil data from mock-up test section #1 with an ODSCC indication at a TSP intersection. 19

2.13 Fourth evaluation of the influence of noise on bobbin coil data from mock-up test section #1 with an ODSCC indication at a TSP intersection. 20

2.14 Evaluation of the influence of noise on bobbin coil data from mock-up test section #4 with an ODSCC indication at a TSP intersection. 20

2.15 Second evaluation of the influence of noise on bobbin coil data from mock-up test section #4 with an ODSCC indication at a TSP intersection.. 21

2.16 Evaluation of the influence of noise on bobbin coil data from mock-up test section #14 with an ODSCC indication at a TSP intersection. 21

2.17 Second evaluation of the influence of noise on bobbin coil data from mock-up test section #14 with an ODSCC indication at a TSP intersection. 22

2.18 Evaluation of the influence of random and periodic noise on bobbin coil data from mock-up test section #1 with an ODSCC indication at a TSP intersection. 28

2.19 First parametric evaluation of the influence of noise on bobbin coil data from mock-up test section of Fig. 2.18. 29

2.20 Second parametric evaluation of the influence of noise on bobbin coil data from mock-up test section of Fig. 2.18. 30

2.21 Third parametric evaluation of the influence of noise on bobbin coil data from mock-up test section of Fig. 2.18. 31

2.22 Fourth parametric evaluation of the influence of noise on bobbin coil data from mock-up test section of Fig. 2.18. 32

2.23 Evaluation of the influence of random and periodic noise on bobbin coil data from mock-up test section #4 with an ODSCC indication at a TSP intersection.. 33

2.24 Parametric evaluation of the influence of noise on bobbin coil data from mock-up test section of Fig. 2.23. 34

2.25 Second parametric evaluation of the influence of noise on bobbin coil data from mock-up test section of Fig. 2.23. 35

2.26 Third parametric evaluation of the influence of noise on bobbin coil data from mock-up test section of Fig. 2.23. 36

2.27 Fourth parametric evaluation of the influence of noise on bobbin coil data from mock-up test section of Fig. 2.23 37

2.28 Fifth parametric evaluation of the influence of noise on bobbin coil data from mock-up test section of Fig. 2.18 38

2.29 Sixth parametric evaluation of the influence of noise on bobbin coil data from mock-up test section of Fig. 2.18 39

2.30 Seventh parametric evaluation of the influence of noise on bobbin coil data from mock-up test section of Fig. 2.18 40

2.31 Eighth parametric evaluation of the influence of noise on bobbin coil data from mock-up test section of Fig. 2.18 41

2.32 Parametric evaluation of the influence of noise on bobbin coil data from mock-up test section of Fig. 2.23. 42

2.33 Second parametric evaluation of the influence of noise on bobbin coil data from mock-up test section of Fig. 2.23 43

2.34 Third parametric evaluation of the influence of noise on bobbin coil data from mock-up test section of Fig. 2.23 44

2.35 Fourth parametric evaluation of the influence of noise on bobbin coil data from mock-up test section of Fig. 2.23 45

2.36 Evaluation of the influence of noise on rotating probe data from mock-up test section with an ODSCC indication at a TSP intersection. 49

2.37 Measurement of maximum amplitude (V_{max}) and RMS (V_{rms}) noise based on the vertical component of data along the tube axis for the specimen shown in Fig. 2.36(a). 50

2.38 Parametric evaluation of noise influence on rotating probe data from mock-up test section of Fig. 2.36(b) 51

2.39 Second parametric evaluation of noise influence on rotating probe data from mock-up test section of Fig. 2.36(b). 52

2.40 Measurement of noise at the same location as the flaw. 53

2.41 Measurement of noise in rotating probe data from mock-up test section with dent at TSP intersection. 54

2.42 Measurement of noise in rotating probe data from flaw-free mock-up TS test section. 55

2.43 Measurement of noise in rotating probe data from mock-up TS test section with large difference in level of noise above and below the roll transition region.. 56

3.1 Eddy current data collected with bobbin coil from test section #1 with flaw at TSP intersection. 61

3.2 Eddy current data collected with bobbin coil from test section #2 with flaw at TSP intersection. 62

3.3 Eddy current data collected with bobbin coil from test section #3 with flaw at free-span region. 63

3.4 Eddy current data collected with bobbin coil from test section #4 with flaw at TSP intersection. 63

3.5 Eddy current data collected with bobbin coil from test section #5 with flaw at TSP intersection. 64

3.6 Eddy current data collected with bobbin coil from test section #6 with flaw at TSP intersection. 64

3.7 Eddy current data collected with bobbin coil from test section #7 with flaw at free-span region. 65

3.8 Eddy current data collected with bobbin coil from test section #8 with flaw at TSP intersection. 65

3.9 Eddy current data collected with bobbin coil from test section #9 with flaw at TSP intersection. 66

3.10 Eddy current data collected with bobbin coil from test section #10 with flaw at TSP intersection.. 66

3.11 Eddy current data collected with bobbin coil from test section #11 with flaw at TSP intersection. 67

3.12 Eddy current data collected with bobbin coil from test section #12 with flaw at TSP intersection. 67

3.13 Eddy current data collected with bobbin coil from test section #13 with flaw at TSP intersection. 68

3.14 Eddy current data collected with bobbin coil from test section #14 with flaw at TSP intersection. 68

3.15 Eddy current data collected with bobbin coil from test section #15 with flaw at TSP intersection. 69

3.16 Eddy current data collected with bobbin coil from test section #16 with flaw at TSP intersection. 69

3.17 Eddy current data collected with bobbin coil from test section #17 with flaw at TSP intersection. 70

3.18 Eddy current data collected with bobbin coil from test section #18 with flaw at free-span region. 70

3.19 Solid dots show probability of detection measured for round–robin (number of hits/11 trials). Solid curve shows log–logistic fit for POD based on round–robin data. Chain-dot curves show estimated bounds (95th percentile) on the expected values of POD obtained in 11 trials if the true binomial POD is given by the log–logistic fit. 77

3.20 Probability of detection as a function of $(S/N)^{V}$. 77

3.21 Probability of detection as a function of S/N. Although flaws are predominantly ODSCC, the data includes some IDSCC. 78

3.22 Probability of detection as a function of voltage. POD RR denotes the probability of detection . 79

3.23 Probability of detection as a function of signal voltage for average noise levels of 0.6 V and 0.9 V. 80

3.24 Range of probabilities of detection expected for a given voltage for log–normal noise with a mean value of 0.6 V. 80

3.25 Range of probabilities of detection expected for a given voltage for log–normal noise with a mean value of 0.9 V. 81

3.26 Range of probabilities of detection expected for a given voltage for log–normal noise with a mean value of 0.9 V based on the POPCD curve. 81

Tables

2.1 Calculated values of signal and noise without and with various levels of simulated noise for the test sections shown in Figs. 2.10 to 2.17. 22

3.1 Measured minimum and average values of probe response from calibration standard tube. 73

3.2 Measured average and maximum value of noise level in free-span regions of the test sections shown in Figs. 3.1-3.6 and 3.8-3.18 from mix channel data. 73

3.3 Measured average and maximum value of noise level in free-span regions of the test sections shown in Figs. 3.1-3.6 and 3.8-3.18 from mix channel data with simulated noise. 74

3.4 Measured maximum value of noise level and *S/N* over the region of interest, which includes the TSP for the test sections shown in Figs. 3.1-3.6 and 3.8-3.18 from mix channel data. 75

3.5 Measured maximum value of noise level and *S/N* over the region of interest, which includes the TSP for the test sections shown in Figs. 3.1-3.6 and 3.8-3.18 from mix channel data with simulated noise. 76

Executive Summary

Proper assessment of the influence of noise on nondestructive evaluation (NDE) results from the in-service inspection (ISI) of steam generator (SG) tubes is important for reliable evaluation of flaw indications. Site-specific industry guidelines define how to measure the level of noise and, in turn, to determine its effect on the detection probability for specific flaw locations in a steam generator. The suggested methodologies in these guidelines are general and applicable only to the free-span region of SG tubing. The nuclear industry is currently striving to develop a more systematic approach to define and measure the noise level in SG tubes.

This report provides an overview of research activities associated with eddy current (EC) inspection of SG tubes that was carried out at Argonne National Laboratory (ANL) as part of the Steam Generator Tube Integrity Program sponsored by the U.S. Nuclear Regulatory Commission (NRC). Recent studies have assessed the influence of noise on the detection of EC flaw signals. Efforts to date have focused primarily on evaluation of methodologies for measuring the level of noise in bobbin coil data and its effect on the detection of flaws that are present in the tube bundle mock-up at ANL. These investigations could ultimately aid in implementing more uniform procedures for evaluating the effect of noise on the detection and sizing of EC flaw indications.

The first part of this report deals with the simulation and measurement of unwanted EC signals. The basic concepts and common sources of signal distortion associated with EC inspection of SG tubes are discussed first. Algorithms for simulation, superposition, and measurement of signal and noise are subsequently described. Next, the effect of measurement variables (i.e., window size, segment length, and region of interest) on several measures of noise level is discussed. A distinction is made between global noise levels for the purpose of data quality assessment and localized noise levels that more directly influence detection capability.

The second part of this report deals with the measurement of noise level in the tube bundle mock-up at ANL. Eddy-current inspection data from a subset of test sections containing indications that were borderline for detectability, i.e., they were missed by at least one of the round–robin teams or by a number of individual analysts from different teams, were evaluated. Calculations were then performed to determine the level of noise present in the bobbin-coil inspection data. The viability of different parameters for estimating the influence of noise is discussed, and a detection limit based on the observable trends in detectability for different signals and the associated noise levels is examined. Implications of the results concerning the detection probability are discussed. A generic example of the adjustment of detection probability based on the measured level of noise is presented. This example suggests that in addition to the effect on probability of detection (POD) curves of an increase in the average noise level there can be significant variability in the detectability of a given flaw signal from location–to–location within a given steam generator due to variability expected in noise. Finally, concluding remarks are presented on the results of the analyses and on the application of the proposed methodologies for the measurement of noise.

Acknowledgments

This work is sponsored by the Office of Nuclear Regulatory Research, U.S. Nuclear Regulatory Commission (NRC), under Job Code Y6588. The NRC Project Manager is M. Stambaugh. T. Mintz and J. Muscara provided useful guidance in the performance of this work. K. Karwoski and E. Reichelt provided comments on earlier versions of this report

Acronyms and Abbreviations

ANL	Argonne National Laboratory
ASME	American Society of Mechanical Engineers
EC	eddy current
FBH	flat-bottom hole
GUI	graphical user interface
ISI	in-service inspection
NDE	nondestructive evaluation
NRC	U.S. Nuclear Regulatory Commission
OD	outer diameter
ODSCC	outer-diameter stress corrosion crack/cracking
PC	(Windows) personal computer
POD	probability of detection
POPCD	probability of prior-cycle detection
RMS	root mean square
ROI	region of interest
RR	round robin
SCC	stress corrosion crack/cracking
SG	steam generator
S/N	signal-to-noise ratio
TS	tube sheet
TSP	tube support plate
TTS	top of the tube sheet
TW	throughwall

1 Introduction

This report provides an overview of research activities carried out at Argonne National Laboratory (ANL) as part of the Steam Generator Tube Integrity Program sponsored by the U.S. Nuclear Regulatory Commission. Eddy current (EC) testing is currently the primary nondestructive evaluation (NDE) method employed for in-service inspection (ISI) of steam generator (SG) tubes. In general, depending on the technique being employed, the measured EC probe response provides information about an indication's location, origin (e.g., whether initiated from inner or outer surface of the tube), spatial extent, and relative orientation (axial, circumferential, or volumetric), as well as the electrical properties (conductivity and permeability) of the tube. Because of the sensitivity of the EC probe to a wide range of tubing discontinuities, however, proper assessment of the influence of noise on the EC probe signal is essential for reliable evaluation of flaw indications. Studies have thus concentrated on methodologies for measuring the level of noise and its effect on detection of flaws present in the tube bundle mock-up at ANL. These investigations could ultimately aid in implementing improved methodologies for evaluating the effect of noise on detection and sizing of flaws in SG tubes.

The first part of this report deals with simulation and measurement of unwanted EC signals. This part includes the following:

- a brief discussion of basic concepts and common sources of signal distortion in EC data from SG tube inspections,
- a description of the algorithms used for simulation, superposition, and measurement of signals and noise, and
- results from investigations on the effect of measurement parameters (i.e., window size and the region of interest) on various measures of noise level.

The second part of this report deals with the measurement of noise level in the tube bundle mock-up at ANL. Data from a subset of test sections containing mostly borderline indications were used for this purpose. The ability to detect signals was evaluated as a function of noise level using different parameters to estimate the influence of noise. Finally, the viability of each parameter for establishing a detection limit and, in turn, for adjusting the detection probability is discussed.

2 Simulation and Measurement of Eddy Current Noise

Categorization of various types and sources of unwanted signals associated with EC inspection of SG tubing is briefly discussed in Sec. 2.1. Section 2.2 describes several algorithms that were implemented at ANL to allow off-line manipulation of EC data for the studies associated with the influence of noise on detection and sizing. Development and application of software-based tools for simulation, superposition, and measurement of probe response are also discussed in that section. Parametric evaluations on the effect of measurement window size and the test region of interest (ROI) on estimates of noise level are provided in Sec. 2.3. Measurements and evaluations are based primarily on bobbin coil data acquired from selected test sections of the tube bundle mock-up at ANL, although some results on rotating probe data are also presented.

2.1 Sources of Signal Distortion in Steam Generator Tube Inspections

For general EC inspection applications, "signal" essentially refers to the probe response to any consequential indication associated with various forms of tube wall degradation. This response includes all volumetric and crack-like signals. Any undesirable probe response from any extraneous source that complicates the detection and interpretation of flaw signals would be considered as noise. For SG tubing, this definition covers a wide range of electronic and physical sources that may be located either internal or external to the tube. In certain EC inspection applications, probe response that is generally regarded as noise can be considered as the signal of interest. Examples include low-frequency mapping of outer-diameter (OD) deposits, locating of landmarks, and measuring of material property variations. Unwanted signals can be classified broadly as either random or deterministic. Deterministic noise exhibits a predictable spatial (i.e., as a function of position) and frequency distribution. Random noise, on the other hand, is non-stationary and thus exhibits incoherent spatial and frequency distribution. Examples of both of these sources of signal distortion are presented below. Because of the diversity and variability of the sources of noise, it is difficult to classify certain types of noise as purely random or deterministic.

Common sources of deterministic signal distortion are support structures, uniform deposits due to corrosion products, changes in manufactured tube dimensions and geometry, and probe wobble and lift-off. Probe response associated with material property variations, non-uniform surface conditions, and electronic noise from the test equipment can be categorized as sources of random noise. The degree to which all of these sources perturb the EC signal, in turn, depends on many other factors and does not exclude the amplitude of the signal itself.

Support structures have diverse designs and are made of materials that produce dissimilar characteristic responses. For instance, the EC probe response from drilled support structures is typically easier to analyze than that from broached and lattice supports. This is due to the difference in uniformity in the geometry of the support structure itself. The material properties of such structures can also have a significant effect on the probe response at these intersections.

Corrosion products, which can deposit either on the inside or outside surface of the tube, can vary widely in composition and electrical properties (conductivity and permeability). Thin layers of mostly ferromagnetic deposits do not produce, in general, a large response at primary test frequencies because they do not conduct electrical currents and have a relatively low effective permeability. Conducting constituents or films can induce a large probe response, which may be difficult to separate from true flaw signals. A random distribution of particles could further complicate analysis of the data at such locations. Conducting

and ferromagnetic deposits inside a flaw opening can result in a reduction of the probe response due to the flaw because current passes with less resistance through the flaw region. This condition could potentially mask low amplitude signals.

Changes in tube dimension and geometry typically cause the most pronounced distortion of EC signals. Such changes include the transition of an expanded tube to its nominal dimension, which typically occurs near the top of the tube sheet (TTS); reduction of the tube diameter due to denting; and ovalization of the tube at small radius U-bends. These sites have also historically been more prone to various forms of degradation, which is due, in part, to the higher levels of residual stresses. The response in all of these cases is essentially due to changes in probe lift-off (for rotating probes) or fill factor (for bobbin probes) and probe alignment. An increase in probe lift-off (or reduction in fill factor) produces an exponential drop in the amplitude response from flaws and is directly connected with the degree of coupling between the probe and the tube. Signal distortion due to localized deformations, in many cases, is more difficult to deal with than that associated with gradual transitions of tube diameter. The level of noise produced at the expansion transition region is dependent on the expansion method employed. Kinetic expansion of tubes is known to produce smoother transitions and, in turn, lower levels of EC noise than methods that apply a mechanical process.

Probe wobble exhibits itself as a low-frequency semi-periodic response that is due to a change in the alignment of the probe with respect to the tube axis. This effect is typically caused by a problem with the probe positioning mechanism. Uneven wearing of the centering device, probe guide, or coil housing can produce this effect. While some level of wobble is always present in the EC baseline signal, excessive wobbling of the probe can significantly distort signal amplitude and phase. Small changes in lift-off for surface probes (e.g., rotating pancake-type probes) and asymmetric alignment for bobbin probes affect the induction of currents within the tube wall, which consequently gives rise to changes in the probe impedance.

Random noise can be generated by spatial variability of the electrical conductivity and magnetic permeability of the tubing. Depending on the type of variability, both the resistive and reactive components of the probe impedance could be affected. Heat treatment and cold work are possible sources of this type of noise. Special probe designs can be used to reduce the signal fluctuations due to permeability variations in the material. Magnetically biased probes that typically incorporate permanent magnets to saturate the magnetic material have a reduced response to permeability variations. Such approaches could result, however, in some reduction in probe sensitivity.

Electronic or system noise can originate either from the EC test equipment or by interference from external sources. Electronic noise can exhibit itself either as a gradual signal drift caused by temperature fluctuation in the circuit components and probe or as random fluctuations about the baseline. Electromagnetic or electrical interference can be caused by power lines, cable connections, and nearby electrical equipment. Probe wear in extreme cases can also lead to spike-like noise that is randomly distributed.

Various NDE techniques have been developed over the years for dealing with noise in EC inspection. Noise suppression techniques may be implemented through either hardware or software. Either way, the goal is to increase the signal-to-noise ratio (*S/N*) and thus improve the technique's capability to detect consequential signals in the presence of noise. The conventional approach for discriminating EC flaw signals from noise is based on examining the impedance plane response as a function of frequency. Multifrequency mixing techniques are routinely employed for suppressing unwanted signals.[1,2] Calibration standards with simulated design discontinuities that resemble those present in the SG are typically used for this purpose. The level of noise can also be significantly reduced by applying appropriate frequency and spatial domain filtering schemes.[1,2] For ISI applications, digital filters are often applied only to data used for screening purposes. This approach is taken primarily to minimize any variability in the analysis results that could be introduced by

the filtering process. Knowledge about the plant's history, location along the tube, characteristic response, and distribution of indications always plays an important role in discriminating flaw signals from artifacts (i.e., any inconsequential probe response). This information may be used on a site-specific basis to implement more effective noise suppression schemes that can help improve the capability of a technique to detect difficult flaws.

Suppression of noise is also achieved by using specialized probe designs. Surface-riding probes (e.g., multi-coil rotating probes with absolute pancake and directional or orthogonally wound coils) either with absolute or differential coil configurations can reduce the effect of many localized sources of noise in comparison to bobbin probes. Partial or full saturation of the tube using magnetically biased probes can drastically suppress the noise caused by permeability variations in the material. Specially designed centering and balancing mechanisms (e.g., flexible and gimbaled probe heads) can help reduce the effect of noise caused by tube deformation and geometry change.

As discussed above, many sources of signal distortion are always present during EC inspection of SG tubes. Aside from its diversity, noise is inherently difficult to characterize because of the ambiguity involved in separating it from the signal. Another complicating factor is the statistical nature of many types of noise. Noise can interfere both constructively (in phase) and destructively (out of phase) with flaw signals. The effect of noise on detection of EC signals, therefore, depends on many factors, such as the origin, amplitude, and spatial and frequency distributions of the signal itself.

Plant operating history (e.g., number of years in service, operating conditions, water chemistry, and maintenance activities) and design-related features (e.g., type of tube support structures, repair or design related tube expansion methods, and tube manufacturing processes) are the primary factors that determine the level of noise present during in-service inspection (ISI) of SG tubing. Obvious potential consequences of this dependence on operating history and design include variability in the level of noise at different elevations in the same SG, variability among generators in the same unit, and variability among plants with similar SG designs. Because of differences in the intrinsic electrical properties (i.e., electrical conductivity and magnetic permeability) of common non-ferromagnetic alloy tubes such as Alloy 600, 690, and 800, the tubing material itself often plays a secondary role with regard to the level of EC noise. Tube manufacturing processes such as heat treatment and cold work, on the other hand, could affect the electrical properties of the tube, and in turn, result in atypical levels of noise.

The remainder of this report deals with the investigations carried out at ANL on evaluation of methods for simulation and measurement of noise. The analyses presented here are based on EC data from a subset of flaws and artifacts in the tube bundle mock-up. The studies have focused on bobbin coil data with limited consideration of the measurement of noise in rotating probe data. In conformance with conventional terminology, signal and noise will be used interchangeably through the rest of this report for certain types of deterministic noise.

2.2 Noise Simulation and Measurement

This section discusses the data analysis tools that were developed to investigate various parameters associated with the measurement of noise and the effect of noise on the flaw signal. The simulation tool for combining simulated and recorded noise with EC data from different locations along a SG tube is described first. Analyses here are based only on data collected on test sections of the tube bundle mock-up at ANL. Algorithms for generating two prevalent types of noise are presented afterward. The last section deals with studies on the effect of measurement parameters and different estimates of noise level. The implications of the results are also discussed in that section.

2.2.1 Simulation and Superposition of Noise

To study the effect of various sources of signal distortion on EC inspection data, software-based tools were developed to combine simulated or recorded noise with data collected by standard bobbin and rotating probes. The algorithms for simulation and measurement of EC probe response and a graphical user interface (GUI) were developed under the MATLAB[3] environment. Embedded routines permit simulation of several random and deterministic types of noise. Data from arbitrarily selected sections of tubes can be combined to create a composite probe response that simulates various forms of signal distortion. To help carry out the examination of various parameters associated with measurement of noise, which is discussed in the following sections, additional functions were integrated into the code.

All data manipulations for either bobbin or rotating probes are controlled through a single user interface. Data may be displayed in image, isometric, strip-chart, and lissajous formats. Various standard data analysis functions can be evoked for closer examination of selected data segments at the recorded test frequencies. Multiple processes may sequentially be applied to the original data (i.e., calibrated raw data), and the processed result (i.e., manipulated data) may then be saved for further analysis.

Figures 2.1-2.3 show representative graphics that demonstrate electronic addition of various types of noise to signals. The EC data are from a mid-range pancake coil [2.92-mm (0.115-in) diameter] of a standard three-coil rotating probe that is used for ISI of tubes having 22.2-mm (0.875-in) diameter. Figure 2.1 shows the original and composite data for a laboratory-cracked specimen with and without a simulated tube support plate (TSP); the defect is primarily due to stress corrosion cracking (SCC) initiated at the OD. The data segment encompassing the 270° removable collar was captured (i.e., imported) from data acquired on a separate calibration standard tube and superimposed over the cracked segment of the tube.

Figure 2.2 shows the original and composite data after addition of random noise. The noise in this case has a 2-D Gaussian (normal) bivariate distribution (complex distribution) that was generated from a 2-D uniform distribution using the Box-Muller transformation.[4] The transformation algorithm can be stated as follows. Starting with deviates (i.e., random variables) x_1 and x_2 that are independently and uniformly distributed between 0 and 1 [i.e., $x_1, x_2 \rightarrow U(0,1)$], define a new pair of transformed variables

$$z_1 = \sqrt{-2\,ln(x_1)} \cdot cos(2\pi x_2) \tag{2.1}$$

$$z_2 = \sqrt{-2\,ln(x_1)} \cdot sin(2\pi x_2) \tag{2.2}$$

with $z_1, z_2 \rightarrow N(0,1)$. Alternatively, one may use the polar form of the Box-Muller method to avoid trigonometric calculations:

$$v_i = 2x_i - 1\ ,\ i = 1,2 \tag{2.3}$$

$$w = \sum_{i=1}^{2} v_i^2 \tag{2.4}$$

$$y = \sqrt{\frac{-2\,ln(w)}{w}} \tag{2.5}$$

$$z_i = v_i \cdot y \tag{2.6}$$

where a conditional statement should be placed to check whether w in Eq. 2.4 lies within the unit circle. The process will be repeated if w is greater than 1. The new quantities, z_i, representing simulated random noise for the in-phase and quadrature components of the EC data, can be scaled on the basis of the mean and variance of the noise in the original data, which is typically calculated from a data segment in the vicinity of an indication.

Figure 2.3 shows the original and composite data with simulated periodic noise. The sinusoidal noise in this case was generated from an expression of the form

$$N_i = A \cdot e^{j\phi} \cdot \left[cos(\theta_i) + j \cdot sin(\theta_i + d\theta) \right] \tag{2.7}$$

in which $j = \sqrt{-1}$, and A, ϕ, and $d\theta$ can be manipulated to adjust the amplitude, rotation, and eccentricity of the impedance plane trajectory, respectively. For $d\theta = 0$, the locus of the term in the bracket would trace the perimeter of a unit circle. Equation 2.7 can be used to simulate various sources of periodic noise, such as deformed geometries (e.g., ovalized or pilgered tube) and probe wobble.

Field-induced periodic noise often contains more than a single-frequency component, resulting in a more complex probe response. This response may be approximated by a more general form of Eq. 2.7,

$$N_i = \sum_{k=1}^{M} A_k \cdot e^{j\phi_k} \cdot \left[cos(\theta_{i,k}) + j \cdot sin(\theta_{i,k} + \Delta\theta_k) \right] \tag{2.8}$$

where $k = 1,2,\ldots,M$ denotes the index of summation over the arbitrary number of frequency components that are present in the composite series.

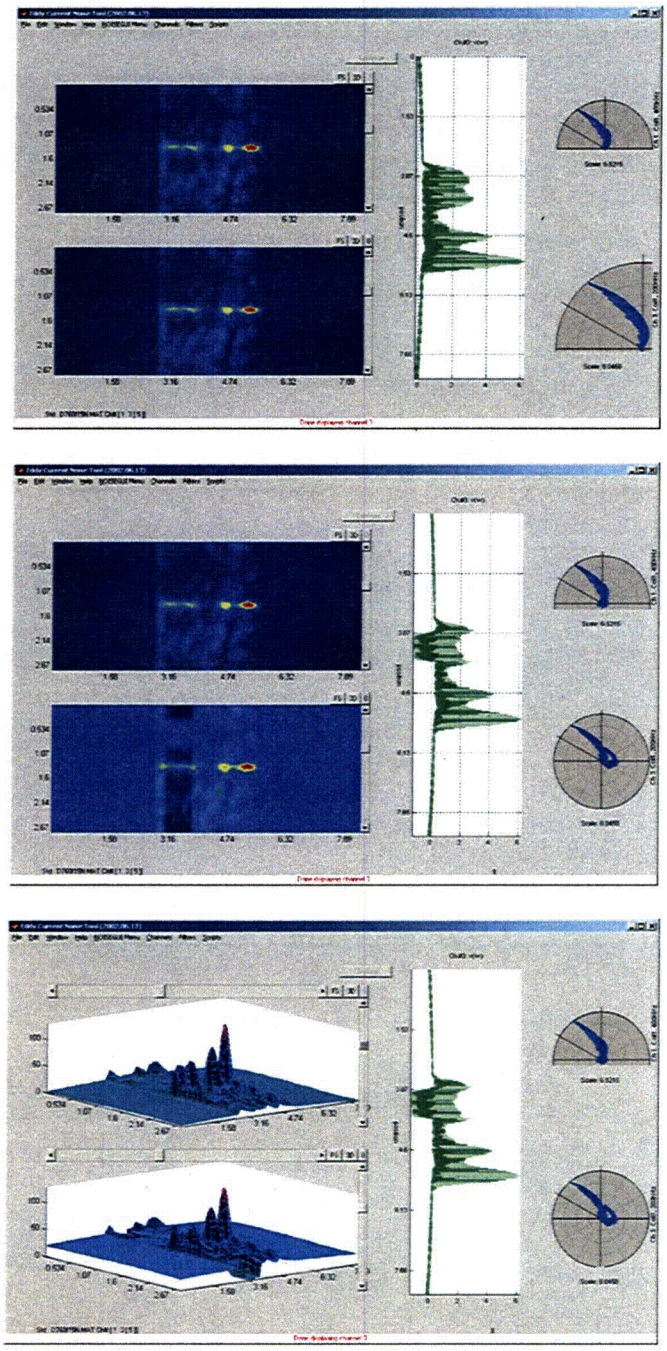

Figure 2.1 *Representative display of superimposed TSP signal (captured from a separate calibration standard tube) on rotating probe data from a laboratory-cracked specimen with primarily OD-initiated SCC. The (top window) original and (middle and bottom windows) composite data are shown in image and isometric format, respectively. Each window displays the vertical (top) and horizontal (bottom) component of data.*

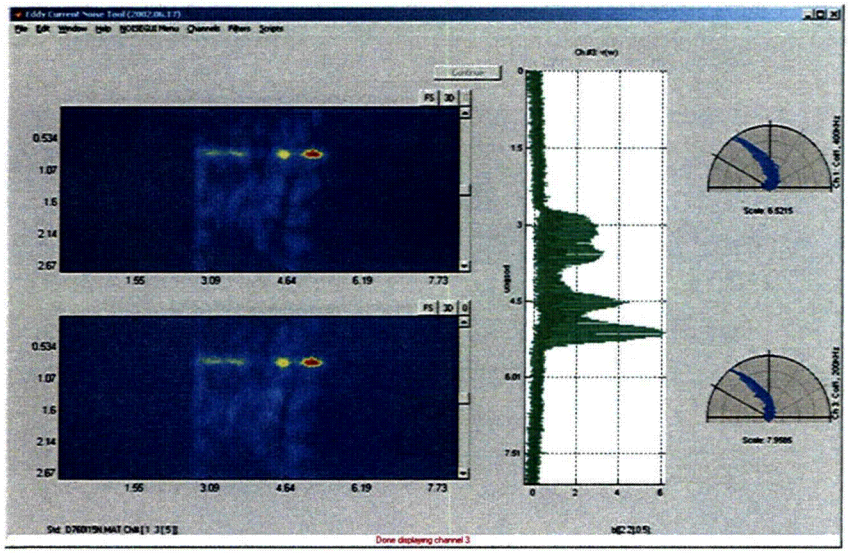

(a)

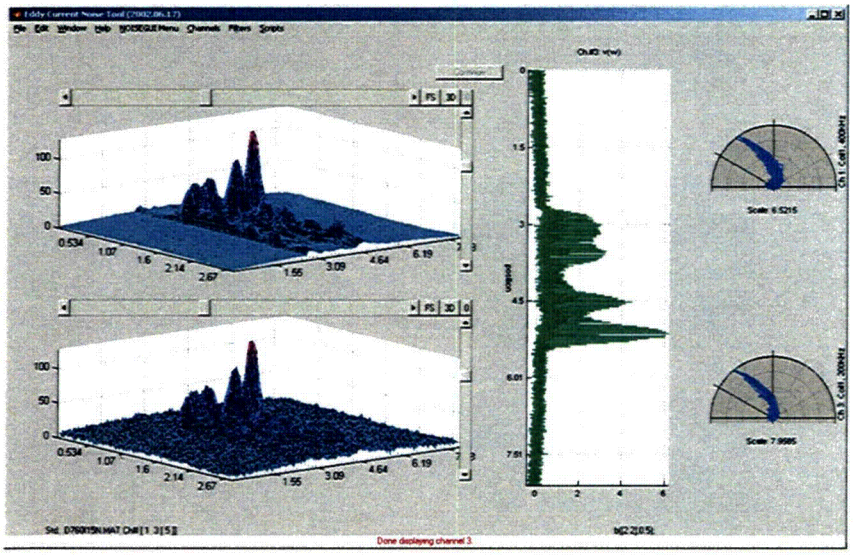

(b)

Figure 2.2 *Representative display of superimposed random noise on rotating probe data from a laboratory-cracked specimen with primarily OD-initiated SCC. Graphics show (a) image and (b) isometric plot of the (top) original and (bottom) composite data with simulated random noise.*

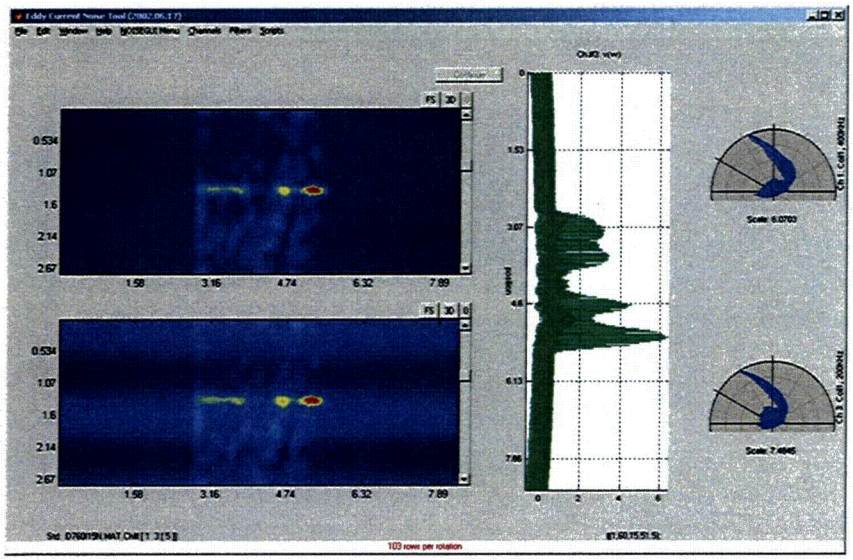

(a)

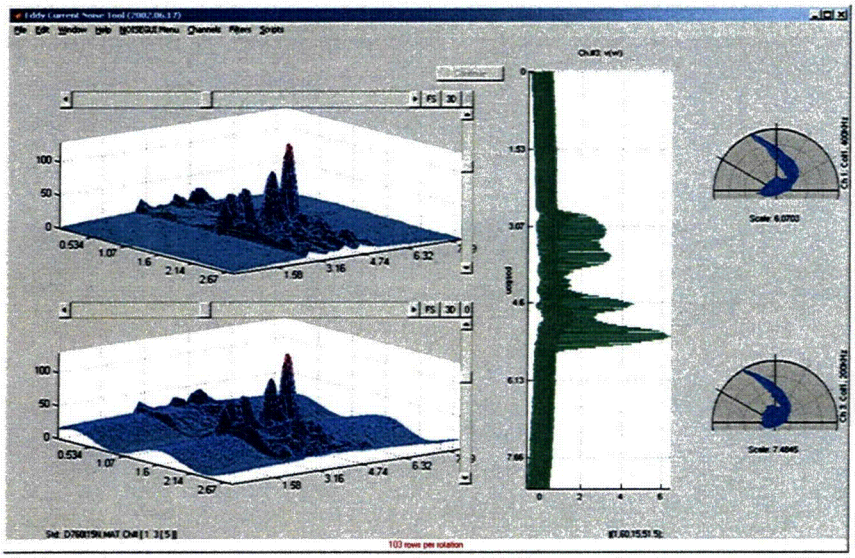

(b)

Figure 2.3 *Representative display of superimposed periodic noise on rotating probe data from a laboratory-cracked specimen with primarily OD-initiated SCC. Graphics show (a) image and (b) isometric plot of the (top) original and (bottom) composite data with simulated periodic noise.*

2.2.2 Data Analysis and Measurement Routines

Several algorithms have been developed for off-line manipulation of data acquired with commercial EC inspection systems. These algorithms include those that duplicate the methods used by commercial data analysis software for measuring the amplitude and phase of the EC signal and incorporate standard methods for data processing that are employed for suppression of unwanted signals. Various levels of noise were added to the data to assess the ability to detect signals as a function of noise level using standard statistical indicators. The intent of these studies was to establish procedures for assessing the effect of noise on the detection probability.

Bobbin coil data from a selected subset of mock-up test sections were selected for parametric studies on the influence of noise. The degradation type in this set of data was outer-diameter stress corrosion cracking (ODSCC) at the TSP intersection. According to conventional data analysis guidelines, bobbin coil calls are based on the processed channel information, which is a two-frequency differential mix. For SG tubing having 22.2-mm (0.875-in) diameter and 1.27-mm (0.05-in) wall thickness, 400 kHz primary and 100 kHz auxiliary frequency channels are used.

A series of tests was carried out to compare data processed off-line with the original recordings and to demonstrate equivalency of our algorithms with the mix channel results obtained using commercial software. Figure 2.4(a) shows the strip chart and lissajous plot of the primary and mix channel data for an American Society of Mechanical Engineers (ASME) calibration standard tube. The vertical and horizontal components of the EC data in the strip chart are shown as solid and dotted lines, respectively. The lissajous plots display only the section of the tube covered by the simulated TSP ring. A comparison of the process channel data shown in Fig. 2.4(a) with the data in Fig. 2.4(b) from the commercial software shows there is good agreement between the two results. Test cases are also shown in Figs. 2.5 and 2.6 for mix channel results using representative data from laboratory-degraded tubes with ODSCC at the TSP intersection. For all cases examined so far, the two-frequency mix results produced off-line are in good agreement with those generated by the commercial software.

The software tool described earlier was used to add noise to the EC inspection data from the mock-up. Figures 2.7 and 2.8 are representative graphics from the simulation of random noise added to the bobbin coil recordings shown in Figs. 2.5 and 2.6. The added noise was calculated for each signal component (i.e., horizontal and vertical) as twice the standard deviation of baseline data near the TSP intersection. Qualitative examination of the data in Fig. 2.7 indicated that the added noise produced a significant distortion of the impedance plane trajectory for this particular test section. In contrast, a smaller influence of noise on the ability to detect the signal is seen in the case of a flaw signal in the middle of the TSP shown in Fig. 2.8. Comparison of the data in Figs. 2.7 and 2.8 indicated that the degree of influence is directly dependent on the *S/N*, with the larger signal being less affected by a comparable level of noise. The software-based tool used for simulating the effect of noise also provides some standard statistical indicators for quantifying the level of signal and noise.

2.2.3 Effect of Measurement Parameters on Estimation of Noise Level

Quantifying the influence of noise on EC inspection results is difficult due to the ambiguity involved in separating the flaw signal from the noise and the variability associated with the origin of the noise itself. These factors complicate the process of establishing a general criterion for determining the minimum detectable signal in the presence of noise. For practical inspection applications, a useful indicator for measuring the effect of EC noise should not be too sensitive to typical measurement inaccuracies but, at the

same time, should be responsive to changes in the level of noise. Such an indicator should ideally provide an absolute measure of the noise level and its influence on detection and sizing to limit the need for comparative measurements.

Using bobbin coil data from the mock-up, parametric evaluations of various indicators of noise level have been carried out to help determine the most appropriate methods for assessing the influence of noise on detection of flaws. The suggested approach in the industry guidelines for measuring the level of noise in the area of interest employs root-mean-square (RMS) quantities. The RMS components of noise in the baseline data can be determined from [5]

$$N_{RMS}^{h,v} = \sqrt{\frac{1}{n}\sum_{i=1}^{n}\left(N_i^{h,v} - \bar{N}^{h,v}\right)^2} \tag{2.9}$$

where

$$\bar{N}^{h,v} = \frac{1}{n}\sum_{i=1}^{n} N_i^{h,v} \tag{2.10}$$

and the superscripts h and v denote the horizontal or vertical component of the noise, respectively. Equation 2.9 defines the variance of a sample about its mean and thus provides the best estimate of truly random fluctuations.[6] The total RMS noise in the area of interest may then be calculated from

$$N_{RMS}^{T} = \sqrt{\left(N_{RMS}^{h}\right)^2 + \left(N_{RMS}^{v}\right)^2} \tag{2.11}$$

The second indicator of the noise level that was examined is the *S/N* ratio, which can be expressed as

$$\left(S/N\right)^{h,v} = \frac{|S^{h,v}|}{|N^{h,v}|} = \frac{\left(S_{max}^{h,v} - S_{min}^{h,v}\right)}{\left(N_{max}^{h,v} - N_{min}^{h,v}\right)} \tag{2.12}$$

where the numerator and the denominator on the right hand side of Eq. 2.12 represent the magnitude of the horizontal or vertical components of the signal and noise, respectively. The terms inside the parentheses denote the maximum and minimum value of the signal and noise. For detection purposes, *S/N* ratios based on the vertical components of signal and noise are of primary interest. A limitation of Eq. 2.12 is that variability in the noise amplitude, particularly for small baseline values, could significantly affect the *S/N* value. To minimize this problem, *S/N* was also determined from a modified version of Eq. 2.12, which can be written as

$$\left(S/N\right)^{h,v} = \frac{|S^{h,v}|}{|N^{h,v}| + N_c} \tag{2.13}$$

where N_c is a small positive constant representing the minimum level of baseline noise. A clean section (e.g., a free-span region of tube with no flaw indications) of the tube or the calibration standard may be used to estimate N_c. For the studies presented here, a value of N_c = 0.1 V was used for the calculation of the *S/N*

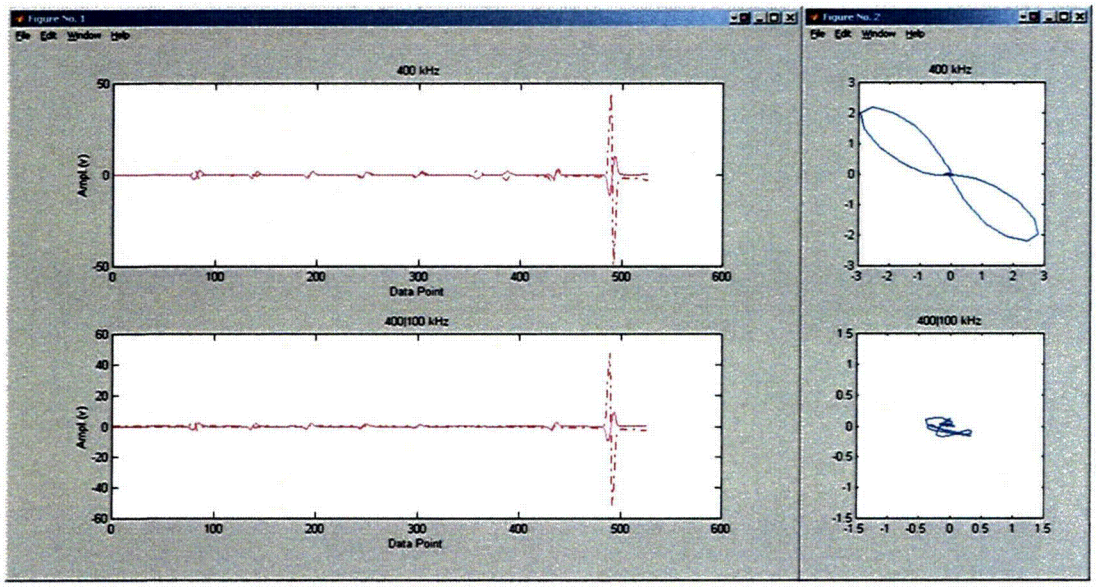

(a)

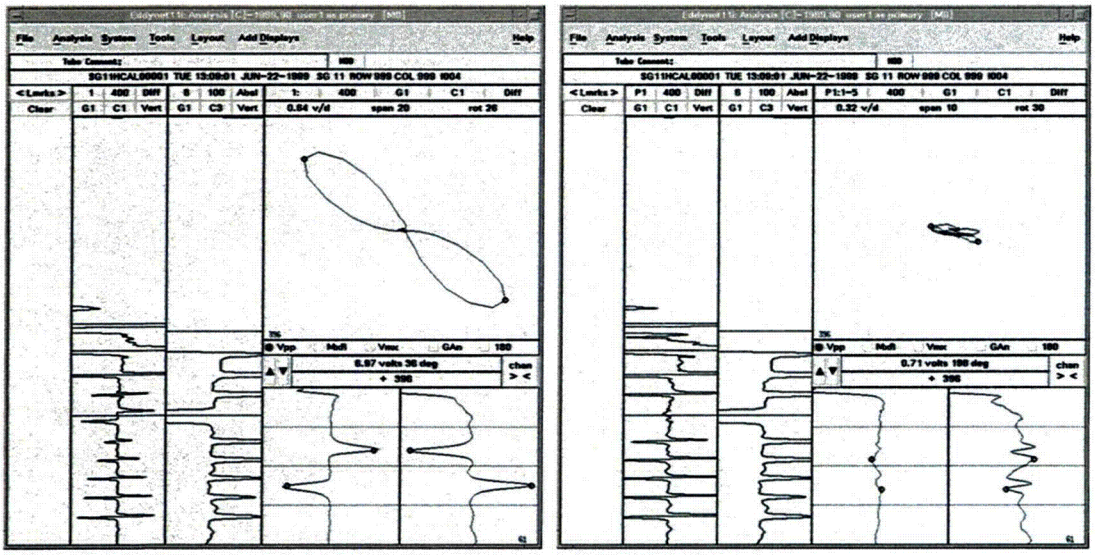

(b)

Figure 2.4 *Evaluation of bobbin coil mix results for an ASME calibration standard tube. Graphics in Fig. 2.4(a) show (top left) primary and (bottom left) mix channel traces and lissajous plot of results for TSP zone before (top right) and after (bottom right) mix process. For comparison, Fig. 2.4(b) shows (left) primary and (right) mix channel data for TSP region of the same tube using commercial software.*

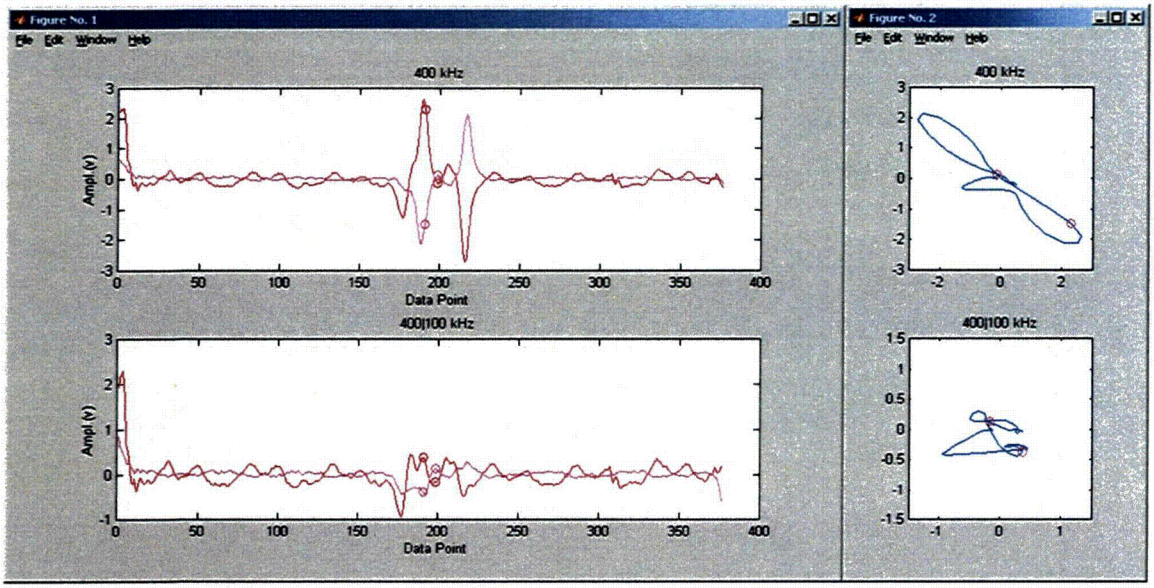

Figure 2.5 *Evaluation of bobbin coil mix results for TSP-level test section #4 with ODSCC indication. Graphics show original (top left) and processed (bottom left) traces and lissajous plot of results for TSP zone before (top right) and after (bottom right) mix.*

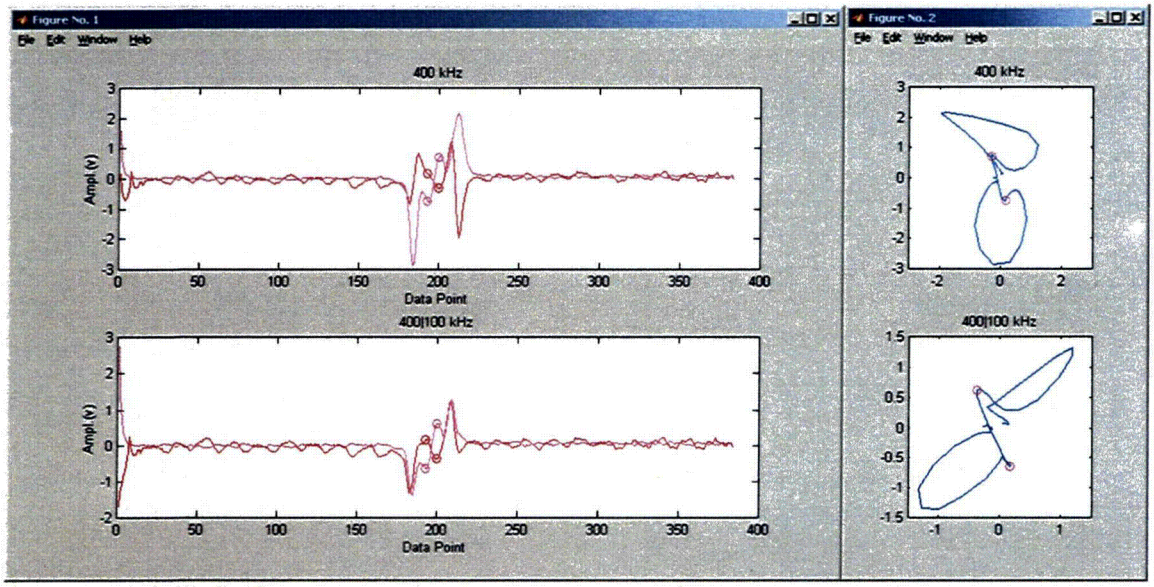

Figure 2.6 *Evaluation of bobbin coil mix results for TSP-level test section #6 with ODSCC indication. Graphics show original (top left) and processed (bottom left) traces and lissajous plot of results for TSP zone before (top right) and after (bottom right) mix.*

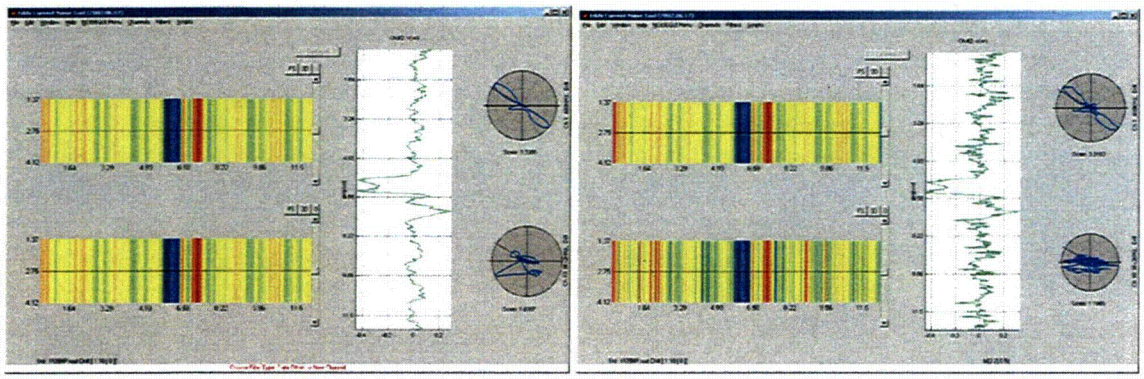

Figure 2.7 *Evaluation of noise influence on bobbin coil signal for TSP-level test section #4 with an ODSCC indication. Graphics show 400/100 kHz process channel data, also shown in Fig. 2.5, without (left) and with (right) addition of random noise. The level of noise, added equally to vertical and horizontal signal components in this case, resulted in significant distortion of the impedance plane trajectory.*

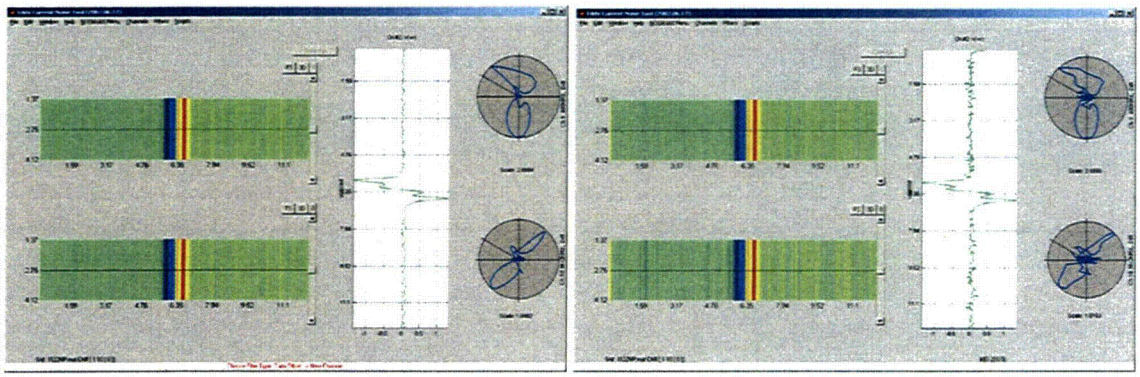

Figure 2.8 *Evaluation of noise influence on bobbin coil signal for TSP-level test section #6 with an ODSCC indication. Graphics show 400/100 kHz process channel data, also shown in Fig. 2.6, without (left) and with (right) addition of random noise. The level of noise, added equally to vertical and horizontal signal components in this case, resulted in minor distortion of the impedance plane trajectory.*

value. This value is typical for the measured baseline noise in bobbin coil data from a calibration standard tube.

A series of MATLAB™ scripts was developed to calculate the parameters defined above. Sample calculations of RMS noise and *S/N*, based on the magnitude of the vertical component of noise (V_{max}), are given next. They were obtained from bobbin coil data for a selected set of mock-up test sections. Noise in the region of interest was determined by averaging the values from three successive (non-overlapping) windows on both sides and away from the flaw signal. This is the standard practice currently used by the industry. To minimize the interference from the flaw and any extraneous signals, the noise is typically measured outside the flawed region of the tube. Figure 2.9 depicts the measurement region at a tube support intersection and the associated measurement variables. A fixed window size of 15.2 mm (0.6 in) was used for the bobbin coil data. In addition to calculations using the average value of the noise, the above indicators of noise influence were also calculated by using the maximum value of the noise from any of the windows in the region of interest. Indicators of noise level were also calculated with a ROI encompassing the zones adjacent to the ends of the flaw signal.

Figures 2.10 through 2.17 show examples of the signals resulting from adding two types of simulated noise (namely, random and periodic) to the signals from a subset of test sections from a database of 18 mock-up tubes used in these studies. The simulated signals in Figs. 2.10 through 2.17 were generated by the MATLAB™ scripts, which were developed to calculate the level of noise. Eddy current traces without and with the added noise are shown for each test case. In all cases, noise was added to the processed channel data that are commonly used for reporting of bobbin coil indications. For the SG tubing with 22.2-mm (0.875-in) diameter and 1.27-mm (0.05-in) nominal wall thickness, the 400|100 kHz differential mix is typically used during field inspections and was used as the primary screening and reporting channel for the analysis of bobbin coil data from the mock-up. For each case, the peak-to-peak voltage (V_{pp}) and the maximum rate of change (calculated from the slope of the impedance plane signal trajectory) were used to initially estimate the flaw amplitude and phase, respectively.

Figures 2.10 through 2.13 show the strip chart and lissajous displays of the recorded data from test section #1 with various levels of simulated noise. The degradation in this test section was identified as an axial ODSCC indication at a TSP intersection. A lower frequency channel was used to locate the approximate position of the TSP edges. The inner and outer markings (vertical dashed lines) that identify the ends of flaw and TSP response, respectively, are displayed on each axial trace. In the examples shown here, the total segment length that comprises the ROI for the measurement of noise consisted of either two equal segments on both sides of the outer (TSP edges) or the inner (flaw ends) markings. For this case, the measured amplitude and phase of the flaw signal from the original trace were ≈ 0.6 V and 52°, respectively. The phase angle information suggests that the flaw is deep.

In Fig. 2.10, the small level of random noise that was added equally to both the horizontal and vertical components of every other data point resulted in significant distortion of the lissajous pattern. However, the indication is still detectable from the axial trace. Figure 2.11 shows the same data with the random noise now added to every data point. A larger distortion of signal is evident in this case, and no flaw response is discernible from the lissajous pattern. Figure 2.12 shows another test case in which the noise level added to the vertical component of the data had twice the amplitude of that shown in Fig. 2.11. As expected, even more distortion of the flaw signal is produced in this case. Finally, in Fig. 2.13, in addition to a low level of random noise, periodic noise was added to the data from the same test section. A peak amplitude of 0.25 V ($V_{pp} = 0.5$ V) was used to simulate the sinusoidal noise having a periodicity of 30 data points and a phase angle of 15°. The composite noise (i.e., random and periodic component) in this case resulted in complete masking of the flaw signal.

Figures 2.14 and 2.15 show similar results on the effects of simulated noise added to test section #4, which was identified as having an ODSCC indication at the TSP intersection. The amplitude and phase of the flaw signal measured from the original trace were ≈ 0.75 V and $\approx 45^{\circ}$, respectively, suggesting a deep OD indication. Only the region outside the TSP was used for the calculation of the various noise parameters. Figure 2.14 shows the effect of random noise with a vertical amplification factor twice that of the horizontal component. Figure 2.15 shows the same test section with added random and periodic noise. All the parameters describing the simulated noise in this case are the same as those used in Fig. 2.13. Once again, significant distortion of the flaw signal occurred in both cases.

Finally, Figs. 2.16 and 2.17 show the effect of added noise to test section #14 with an ODSCC indication at the TSP intersection. Similar parameters as those in the previous test cases, provided in the figure captions, were used to simulate the two types of noise. The amplitude and phase of the indication measured from the original trace were ≈ 1.25 V and $\approx 120^{\circ}$, respectively, suggesting the presence of a shallow OD degradation. Only the region outside the TSP was used for the calculation of the various noise parameters. Because of the relatively larger amplitude of the indication in test section #14 in comparison to test section #4, the added noise resulted in less distortion of the flaw signal.

Calculated RMS noise and *S/N* values for the above test cases are listed in Table 2.1. Preliminary evaluations of the data used in the development of Table 2.1 suggest that the RMS value of the noise level calculated by the window–averaging procedure described above generally leads to reproducible values of the calculated noise parameter. In other words, the RMS value is not strongly dependent on the ROI chosen for the calculation. The use of a small window size for calculating the mean-removed RMS value helps suppress the effect of low frequency baseline variations, and the averaging over multiple increments in effect minimizes the influence of high frequency variations. Another observation is that the added noise levels that significantly distorted the flaw signal produced relatively small changes of the RMS value. Hence, the RMS value calculated by the averaging procedure may not adequately reflect the impact of higher noise. For the test cases examined so far, the vertical component of *S/N* seems to better reflect the impact of the change in noise level. The modified *S/N* calculated using Eq. 2.13 seems to be less dependent on the choice of the ROI than that given by Eq. 2.12 as evidenced by the small change in the modified S/N when the TSP was included in the ROI as compared to when the TSP was not included in the ROI. Preliminary results suggest that the use of RMS noise or the modified *S/N* provides a tradeoff between reproducibility of estimates and sensitivity to more localized variations in the level of noise.

A reliable ISI data analysis method is expected to be operator independent for detecting a flaw signal in the presence of noise. Based on the initial evaluations presented above, the measurement of noise using three successive windows on both sides of the flaw signal may not always produce repeatable results. Additional studies were subsequently carried out to investigate alternative methods that could help improve measurement repeatability for viable indicators of noise.

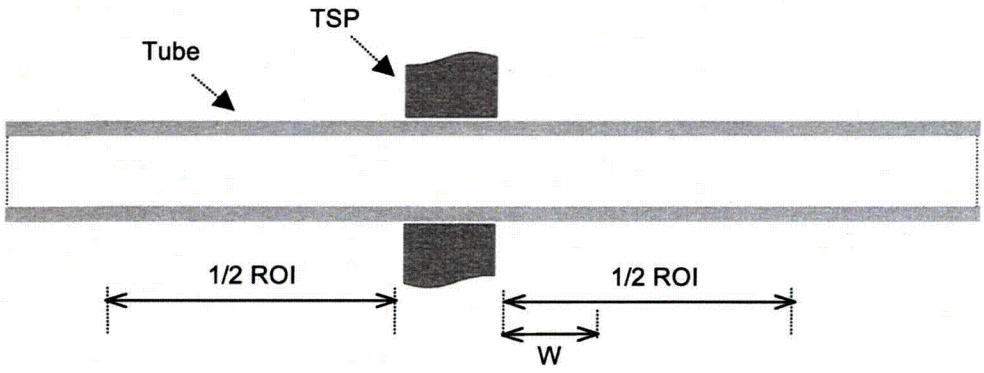

Figure 2.9 *Depiction of the measurement region and the associated variables for the measurement of noise outside a TSP intersection. The total segment length, i.e., the region of interest (ROI), is composed of two equal segments on both sides of the TSP. Also shown is the size of each measurement window, W. For standard measurement of noise, six successive measurements that the encompass ROI are averaged.*

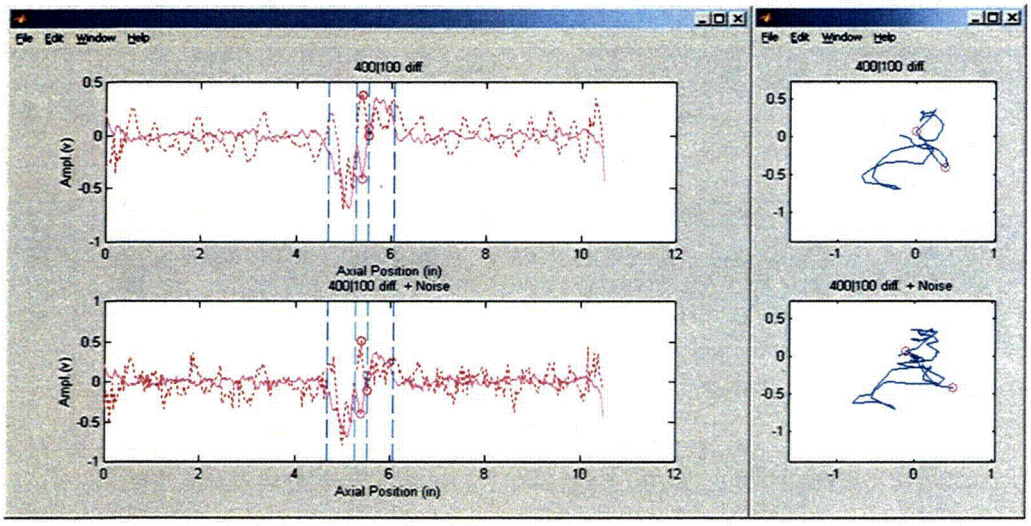

Figure 2.10 *Evaluation of the influence of noise on bobbin coil data from mock-up test section #1 with an ODSCC indication at a TSP intersection. Graphics show the processed channel data without (top) and with (bottom) the added noise. Axial trace of both the vertical (solid line) and the horizontal (dashed line) component of data are shown in each stripchart plot. Also shown are the inner and outer markings that identify the approximate location of flaw and TSP ends, respectively. Random noise with an amplification factor of 1 was added proportionally to both channels and to every other data point.*

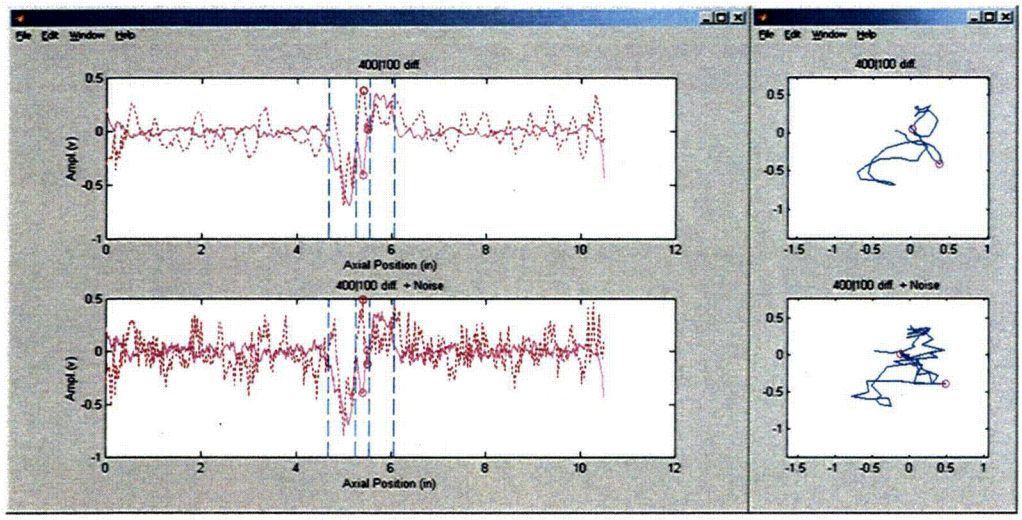

Figure 2.11 *Second evaluation of the influence of noise on bobbin coil data from mock-up test section #1 with ODSCC indication at a TSP intersection. Graphics show the processed channel data without (top) and with (bottom) the added noise. Also shown are the inner and outer markings that identify the approximate location of flaw and TSP ends, respectively. Random noise with an amplification factor of 1 was added proportionally to both channels and to every data point.*

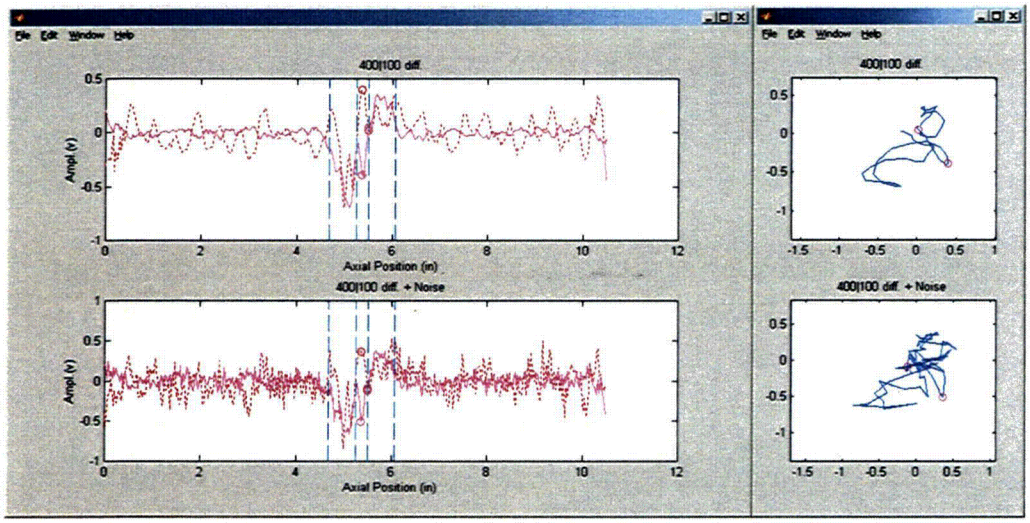

Figure 2.12 *Third evaluation of the influence of noise on bobbin coil data from mock-up test section #1 with an ODSCC indication at a TSP intersection. Graphics show the processed channel data without (top) and with (bottom) the added noise. Also shown are the inner and outer markings that identify the approximate location of flaw and TSP ends, respectively. Random noise with horizontal amplification factor of 1 and vertical amplification factor of 2 was added to every data point.*

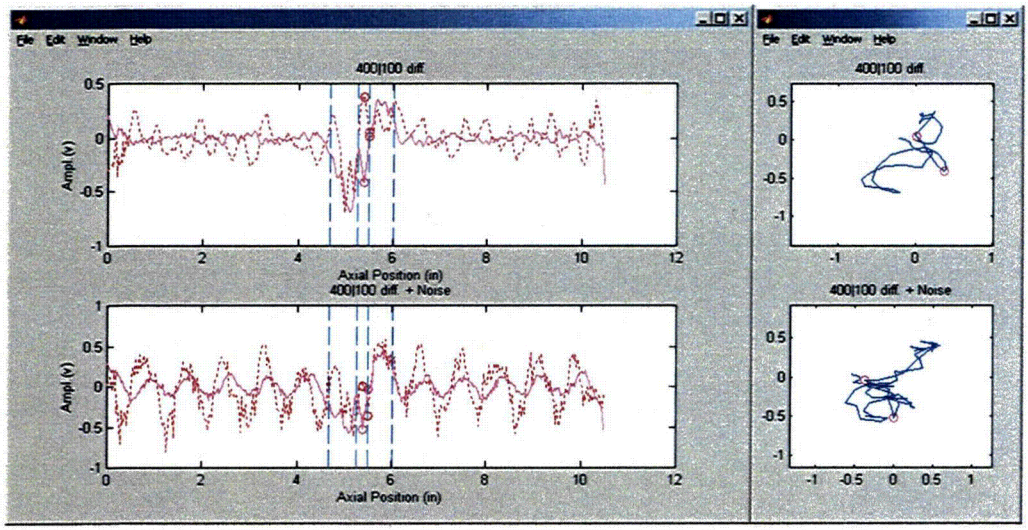

Figure 2.13 *Fourth evaluation of the influence of noise on bobbin coil data from mock-up test section #1 with an ODSCC indication at a TSP intersection. Graphics show the processed channel data without (top) and with (bottom) the added noise. Also shown are the inner and outer markings that identify the approximate location of flaw and TSP ends, respectively. Composite noise consisted of a small random component, as that in Fig. 2.10, and a periodic component with amplitude of 0.25 V (V_{pp} = 0.5 V) and phase of 15°.*

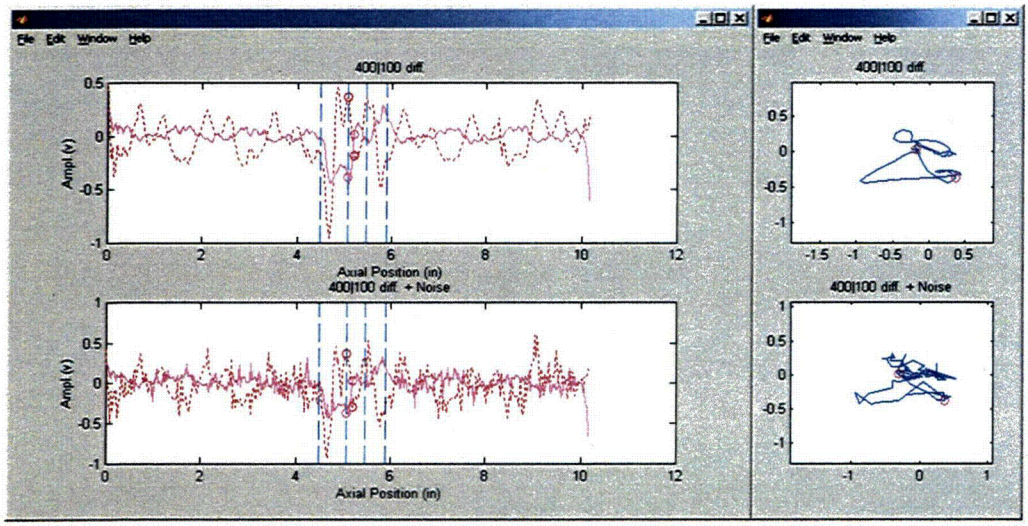

Figure 2.14 *Evaluation of the influence of noise on bobbin coil data from mock-up test section #4 with an ODSCC indication at a TSP intersection. Graphics show the processed channel data without (top) and with (bottom) the added noise. Also shown are the inner and outer markings that identify the approximate location of flaw and TSP ends, respectively. Random noise with horizontal amplification factor of 1 and vertical amplification factor of 2 was added to every other data point.*

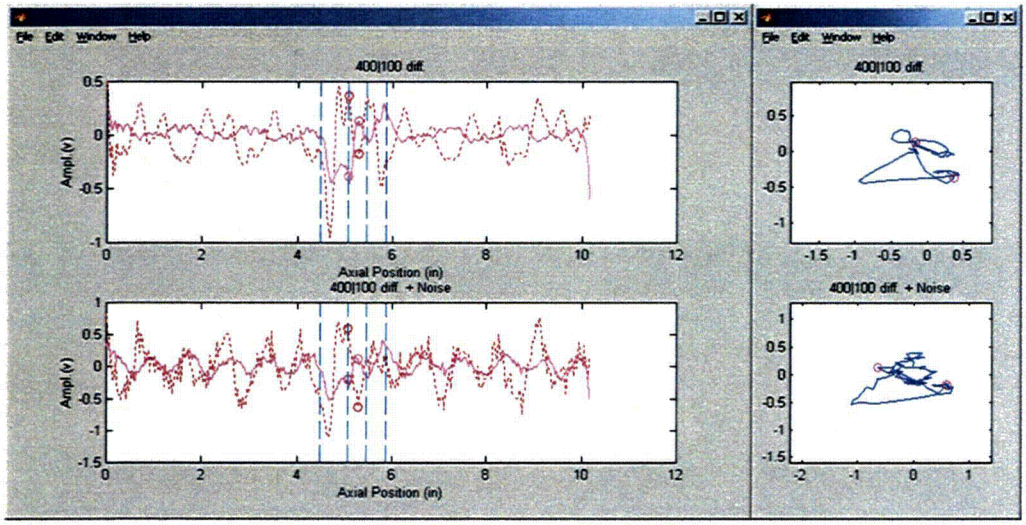

Figure 2.15 *Second evaluation of the influence of noise on bobbin coil data from mock-up test section #4 with an ODSCC indication at a TSP intersection. Graphics show the processed channel data without (top) and with (bottom) the added noise. Also shown are the inner and outer markings that identify the approximate location of flaw and TSP ends, respectively. Composite noise consisted of a small random component, as that in Fig. 2.10, and a periodic component with amplitude of 0.25 V (V_{pp} = 0.5 V) and phase of 15°.*

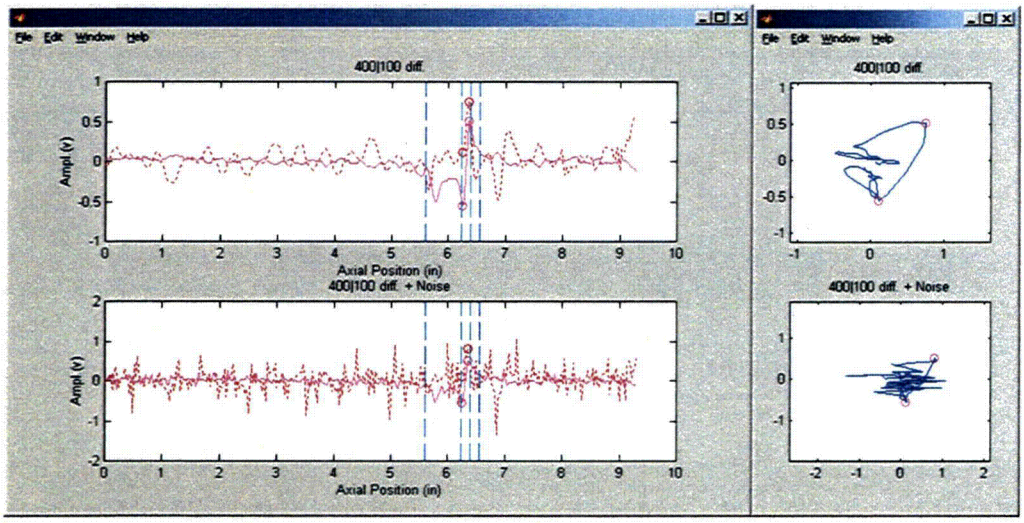

Figure 2.16 *Evaluation of the influence of noise on bobbin coil data from mock-up test section #14 with an ODSCC indication at a TSP intersection. Graphics show the processed channel data without (top) and with (bottom) the added noise. Also shown are the inner and outer markings that identify the approximate location of flaw and TSP ends, respectively. Random noise with an amplification factor of 2 was added proportionally to both channels and to every other data point.*

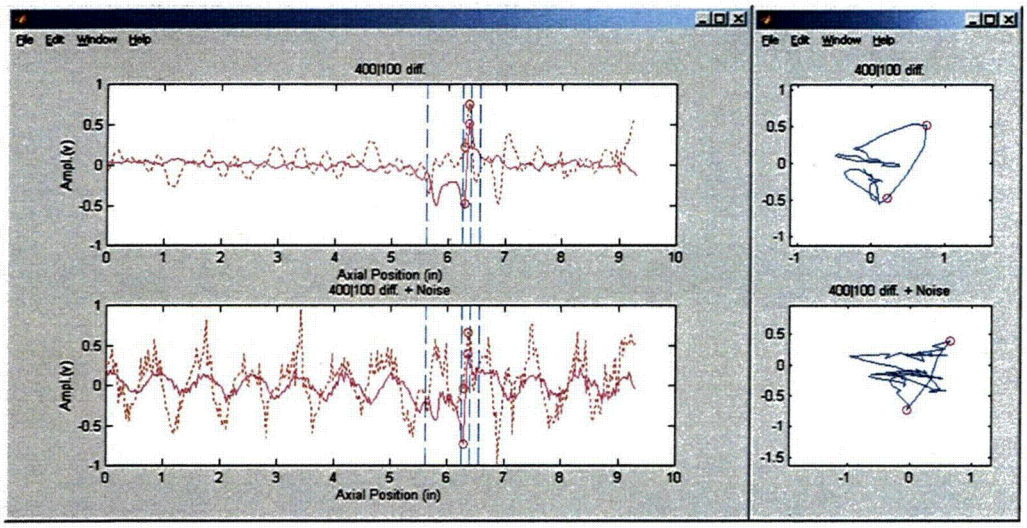

Figure 2.17 *Second evaluation of the influence of noise on bobbin coil data from mock-up test section #14 with an ODSCC indication at a TSP intersection. Graphics show the processed channel data without (top) and with (bottom) the added noise. Also shown are the inner and outer markings that identify the approximate location of flaw and TSP ends, respectively. Composite noise consisted of a small random component using the same parameters as those in Fig. 2.10 and a periodic component with amplitude of 0.25 V (V_{pp} = 0.5 V) and phase of 15°.*

Table 2.1 Calculated values of signal and noise without and with various levels of simulated noise for the test sections shown in Figs. 2.10 to 2.17.

	Without simulated noise				With simulated noise			
	N^{h}_{RMS}	N^{v}_{RMS}	$\left(S/N\right)^{v}$	$\left(S/(N+N_c)\right)^{v}$	N^{h}_{RMS}	N^{v}_{RMS}	$\left(S/N\right)^{v}$	$\left(S/(N+N_c)\right)^{v}$
Fig. 2.10 (TSP not included)	0.10	0.03	4.10	2.17	0.12	0.04	2.40	1.52
Fig. 2.10 (TSP included)	0.11	0.06	2.40	1.57	0.13	0.07	1.85	1.28
Fig. 2.11 (TSP not included)	0.10	0.03	4.10	2.17	0.15	0.05	2.30	1.51
Fig. 2.11 (TSP included)	0.11	0.06	2.40	1.57	0.16	0.07	1.74	1.23
Fig. 2.12 (TSP not included)	0.10	0.03	4.10	2.17	0.16	0.07	1.68	1.24
Fig. 2.12 (TSP included)	0.11	0.06	2.40	1.57	0.16	0.10	1.34	1.05
Fig. 2.13 (TSP not included)	0.10	0.03	4.10	2.17	0.27	0.09	1.60	1.21
Fig. 2.14 (TSP not included)	0.10	0.03	5.42	2.80	0.15	0.09	1.36	1.08
Fig. 2.15 (TSP not included)	0.10	0.03	5.42	2.80	0.29	0.08	1.55	1.17
Fig. 2.16 (TSP not included)	0.10	0.03	9.73	5.14	0.27	0.07	3.85	2.83
Fig. 2.17 (TSP not included)	0.10	0.03	9.73	5.14	0.28	0.11	2.98	2.35

2.2.4 Measurement Repeatability

To improve repeatability and to further reduce the dependency of the measurements on position, a sliding window approach for evaluating the measures of noise was examined. All noise-related indices were calculated for every data point (i.e., one-point increments) within the ROI. In reference to Fig. 2.9, the last measurement position in the free-span region of the tube was designated as the point where the center of the sliding window coincided with the edge of the ROI. As described earlier in reference to Fig. 2.10, the inner and outer markings (vertical dashed lines) that identify the ends of the flaw and TSP signals, respectively, are displayed on each stripchart plot. The total segment length that comprises the ROI for the measurement of noise consisted either of two equal segments on both sides of the outer (TSP edges as depicted in Fig. 2.9) or the inner (flaw ends) markings. Measurements made outside the TSP are expected to better represent the baseline noise, and those measured immediately outside the flaw signal are expected to better represent the localized noise level that more directly affects the detection of a particular indication.

To assess the effect of noise on both detection and sizing capability, calculations based on both V_{max} and V_{pp} measurements are presented. Measurement based on V_{max} is expected to better indicate the capability of the EC inspection technique to detect a signal in the presence of noise, and that based on V_{pp} to better indicate the reliability of sizing results. As mentioned in Sec. 2.2.3, a series of MATLAB™ scripts was developed to perform the computations. In comparison with the standard approach for calculating the RMS noise, this method allows for incremental measurements over a larger number of overlapping windows and thus helps reduce measurement variability. The variance of noise over the ROI was used as the criterion for evaluating the effect of segment (i.e., axial extent of the ROI) and measurement window length on indices of noise level. The ranges of segment and window lengths were chosen from the observed correlation between data points within the ROI (i.e., in accordance with the coil coverage) and the proximity to the flaw signal. The distance between two points on opposite ends of the probe response (i.e., interaction zone) where the peak signal amplitude attenuates to nearly the same level as the baseline was used to determine the effective coil coverage. This distance is expected to vary slightly as a function of excitation frequency within the usable range.

For a differential bobbin probe, the coil coverage (i.e., field spread) at the highest test frequency was estimated to be around 15.2 mm (0.6 in), based on the probe response to a 100% throughwall (TW) drilled hole on a calibration standard tube. For the test cases here, the window length was varied between 7.6 mm (0.3 in) and 30.5 mm (1.2 in). In addition, the segment length was varied between 15.2 mm (0.6 in) and 70 mm (2.4 in) on both sides of the flaw signal. All noise indices were calculated by using the mean value of noise over all measurement windows within the ROI. While the average value is not expected to provide the most conservative estimate of noise level, this approach was adopted to help minimize the effect of baseline fluctuations.

The expressions for calculation of RMS and *S/N* were given in the previous section. The voltage *S/N* here is presented in decibel (dB) units,

$$\left(S/N \right)_{dB} = 20\, log\left(S/N \right) \tag{2.14}$$

This conversion increases the dynamic range at small *S/N* values. For large *S/N* values, where the effect of moderate changes in the level of noise on the distortion of the flaw signal is minimal, the slope of the logarithmic curve will be small. As the *S/N* approaches the lower limits of detection (e.g., $S/N < 2$), the logarithmic relationship will result in a sharp drop in the $(S/N)_{dB}$ value for small increases in the level of

noise. This drop is the expected behavior when dealing with weak EC indications, where the uncertainty in determining *S/N* and, in turn, detection capability is large.

For the studies here, simulated random and periodic noise were added to the bobbin coil data from two TSP test sections of the mock-up. Figure 2.18 shows the EC data for test section #1 containing a deep ODSCC indication (based on the phase angle information) at the TSP intersection. Processed channel data (400|100 kHz mix) are displayed for the same length of the tube, without and with the two types of simulated noise. Variations of several noise- and signal-related parameters as a function of segment length for a fixed window length of 15.2 mm (0.6 in) are shown in Fig. 2.19. In reference to Fig. 2.18, the ROI segments on both sides of the flaw signal are outside the TSP (i.e., it does not encompass the probe response from TSP). Figure 2.19(a) is a plot of the variance of the vertical component of noise (V_{max}) as a function of segment length, calculated with the mean value of all the increments within each segment. The slope of the variance curve decreases as the segment length is increased. This behavior is expected because the variance is calculated by successively including a larger number of data points. The average value of V_{max} noise as a function of segment length is displayed in Fig. 2.19(b). The estimates in this case do not fluctuate for segment lengths greater than $\approx$38 mm (1.5 in). Figure 2.19(c) shows the calculated values for both the vertical component and total RMS noise. Both components remain relatively constant over the entire range. In addition, as observed in the previous approach, the RMS value of the vertical component of noise, often used as an indicator of detection capability, shows only a small increase as a result of the added random noise. Finally, Fig. 2.19(d) shows variation of the mean *S/N* as a function of segment length. Note that the *S/N* here is inversely related to the V_{max} data shown in Fig. 2.19(b). Although calculated values in this case suggest that the flaw signal may still be detectable in the presence of added random noise, the results also show significant degradation of the *S/N* ($\approx$9 dB drop) due to addition of composite noise, which significantly reduces the probability of detection (POD) for this particular indication.

Figure 2.20 shows the results for the same test section as in Fig. 2.19, except that the parameter varied in this case is the length of the sliding measurement window. For all cases here, the segment length on both sides of the indication was kept at 45.7 mm (1.8 in). Once again, as the window length is increased, the slope of curves drops off for all indicators. The variation of the signal and noise parameters with window length is similar to that observed in Fig. 2.19 for segment length. Examination of the data in Figs. 2.19 and 2.20 suggests that the *S/N* will not fluctuate much if a window length around 20.3 mm (0.8 in) and a segment length >38.1 mm (1.5 in) are used. Therefore, these values are expected to produce acceptable error bounds when estimating the level of noise or *S/N* based on the V_{max} component.

Figures 2.21 and 2.22 display the results for the same parameters used in Fig. 2.19 and 2.20, but a different region is used for calculation of noise. The ROI in this case encompassed the TSP intersection and thus the noise in close proximity to the indications. The inner markings that identify the ends of the flaw signal are shown in Fig. 2.18. All indicators in this case show increased variation in comparison to the previous test case. Both the RMS noise and mean V_{max} values shown in Figs. 2.21(b)-(c) and 2.22(b)-(c) changed notably in comparison to those shown in Figs. 2.19 and 2.20. Once again, examination of the RMS noise and *S/N* suggests that similar window and segment lengths, as in the previous case, may be selected to obtain acceptable measurement accuracy. Data shown in Fig. 2.22(d) suggest that the measured noise level becomes relatively independent of window length at $\approx$20.3 mm (0.8 in). The results also indicate that inclusion of the TSP in the ROI can significantly affect the measured level of noise. Thus, neglecting to include the TSP in the noise calculation could give a misleading estimate of the detectability of the flaw.

Figure 2.23 shows the EC data for test section #4 without and with simulated random and composite noise. The tube in this case also contained a deep ODSCC indication at the TSP intersection. Figures 2.24-2.27 display the results of parametric calculations, obtained by varying the segment and window length as

well as selecting different regions of interest for noise evaluations. In all cases, observed trends are similar to those seen in the previous test case. In reference to Fig. 2.23(b), roughly doubling the vertical component of random noise, compared to that in Fig. 2.18(b), resulted in a significant change in the V_{max} and *S/N* values shown in Figs. 2.24 and 2.25, with a small change in the RMS values of the vertical component of noise. Similar results are seen in Figs. 2.26 and 2.27, where the ROI for calculation of noise included the TSP intersection. However, the *S/N* values suggest that both types of noise can result in the flaw going undetected. Once again, results here suggest that a window length around 20.3 mm (0.8 in) and a segment length >38.1 mm (1.5 in) should provide repeatable measurements of the *S/N* value.

Although this study is limited in scope, some conclusions that can be drawn may have fairly general applicability. First, the RMS value of the vertical component of noise, which can be determined with good repeatability (i.e., it is relatively insensitive to small variations in measurement parameters), shows little sensitivity to localized changes in the level of noise. The total RMS value (i.e., both vertical and horizontal component of noise), which follows similar trends, better reflects the effect of the added noise. However, the total RMS value may not be an appropriate measure of detection capability because of the dominant influence of the horizontal component of noise on the value. Second, the V_{max} component of noise, which is used for calculating *S/N*, seems to be a useful indicator of the ability to detect flaw signals in the presence of noise. Calculation of V_{max}, however, can be strongly dependent on the measurement parameters. Third, by selecting an ROI that extends too far from the flaw signal, one might be neglecting localized effects in the vicinity of the indication that may more truly represent the influence of noise. Yet, although smaller segment lengths may better represent the true level of noise in the flaw vicinity, they can lead to larger fluctuations in the estimates. Choosing sections which exclude the immediate vicinity of a flaw (e.g., TSP response) leads to more repeatable measurements of noise. Excluding this region, however, gives a less accurate representation of the noise that affects detection capability. Fourth, values for segment and window length are given that provide repeatable measurements. These values should also produce acceptable measurement variability when the immediate vicinity of the flaw signal is selected as the ROI. Finally, an *S/N* value that incorporates the horizontal component of noise (discussed in the next few paragraphs) is expected to show larger decreases as noise increases than one based on just the vertical component of noise. This effect suggests that a low level of noise that may not challenge detection of flaw signals could have a profound effect on sizing. For example, in the lissajous patterns in Figs. 2.18 and 2.23, the phase angle information is significantly distorted as a result of the added levels of noise.

As noted previously, the detection of an EC flaw signal is more closely related to the component of noise that contributes to the vertical channel data. Sizing requires consideration of the phase angle and, hence, both components of the signal and the noise. Thus, both the horizontal (H_{max}) and the vertical (V_{max}) component of signal and noise must be measured to assess the effect of noise on detection and sizing capability. Many sources of unwanted signals in EC inspection interfere more strongly with the horizontal component of the probe response. The measurement procedure for both components of noise and the *S/N* was given in the previous section. The peak-to-peak amplitude (V_{pp}) of noise is defined as

$$V_{pp} = \sqrt{H_{max}^2 + V_{max}^2} \tag{2.15}$$

Since V_{pp} often closely follows the horizontal component of noise in the useful range of frequencies for detection of flaws, it was used to characterize the noise rather than H_{max}. As before, both the length of the measurement window and the ROI were varied over a prescribed range. The criteria for selection of the parameters associated with indicators of noise influence used in this study were described in the previous section of this report.

In Fig. 2.28, several indicators of noise are shown as a function of segment length computed with a fixed window length of 15.2 mm (0.6 in). Results are shown for both random noise and a composite noise signal that consisted of the random component and a periodic component with amplitude of 0.25 V (V_{pp} = 0.5 V) and phase of 15°. In reference to Fig. 2.18, the ROI on both sides of the flaw signal starts and extends away from the TSP ends, which was marked by using the coil response at a lower test frequency. Figure 2.28(a) is a plot of the variance of the magnitude of the noise (i.e., V_{pp}) as a function of segment length, calculated by using the mean value of all the window increments within each segment. The average value of the peak-to-peak noise as a function of segment length is displayed in Fig. 2.28(b). Figure 2.28(c) shows the calculated values for both the vertical component and total RMS noise. (For the sake of completeness, the calculated RMS values shown in Figs. 2.19-2.22 and 2.24-2.27 are replicated in Figs. 2.28-2.35.) Finally, Fig. 2.28(d) shows the variation of *S/N* as a function of segment length. All indicators in this case show similar trends, suggesting a relatively small influence of the random noise and a larger influence of the composite noise. In comparison with the earlier calculations based on the V_{max} component of the signal and noise, the *S/N* values based on the V_{pp} measurement shown in Fig. 2.28(d) indicate more significant degradation (< -2 dB) of the signal as a result of added composite noise. The impact of this noise on the ability to detect and characterize the flaw is evident from the excessive distortion of the impedance plane response shown in Fig. 2.18(c). As with the previous results, these estimates remain relatively unchanged for segment lengths larger than ≈ 38 mm (1.5 in).

Figure 2.29 shows the results for the case when the parameter varied is the length of the sliding measurement window. For all cases here, the segment length on both sides of the indication was kept at 45.7 mm (1.8 in). Once again, the slope of the curves for all indicators levels off as the window length is increased. The trends in this case are similar to those in Fig. 2.28. Examination of the results in Figs. 2.28 and 2.29 suggests that the fluctuation of *S/N* will be minimal for a window length of around 20 mm (≈ 0.8 in) and a segment length greater than 38 mm (≈ 1.5 in). Therefore, for the case where the ROI is selected away from the flaw signal (i.e., outside the TSP), these values are expected to produce acceptable error bounds when estimating the level of noise based on V_{pp} measurements.

Figures 2.30 and 2.31 display the results for the same parameters as those used in Fig. 2.28 and 2.29, but use a different region for the calculation of noise. The region of interest in this case encompasses the entire TSP intersection. The inner markings that identify the ends of the flaw signal are shown in Fig. 2.18. All indicators in this case show increased variation as a function of both the segment and window length. Both the mean V_{pp} and RMS values shown in Figs. 2.30(b)-(c) and 2.31(b)-(c) increased in comparison with those shown in Figs. 2.28 and 2.29. However, the overall trends in terms of variation with window and segment length are similar for these two cases. Once again, examination of the RMS and *S/N* value suggests that a window and segment length similar to that in the previous case, where the region of interest was outside the TSP intersection, gives acceptable measurement accuracy. In all cases, *S/N* values indicate that the simulated composite noise here would result in significant degradation of detection and sizing capability.

As previously discussed, Fig. 2.23 shows EC data for test section #4 with and without simulated random and periodic noise. The tube in this case also contained a deep ODSCC indication at the TSP intersection. Figures 2.32-2.35 display the results of parametric evaluations based on V_{pp} measurements as a function of the segment and window length, as well as for different regions of interest for noise measurement. In all cases, observed trends are similar to those seen in the previous test case. Roughly doubling the vertical component of random noise, compared to that in Fig. 2.18(b), resulted in a significant change in the *S/N* values shown in Figs. 2.32 and 2.33, but only minor changes in the total RMS values of the composite noise. Another interesting observation is that, while the mean V_{pp} value in all cases is greater for the composite noise than for the random noise, the *S/N* values show the reverse trend. In this particular case, the simulated noise added constructively to the horizontal component of noise, thus effectively increasing the magnitude of the

flaw signal. As stated earlier, constructive and destructive interference by noise can have a profound effect on the detection and sizing of weak signals. Similar results are seen in Figs. 2.34 and 2.35, where the ROI for calculation of noise included the TSP intersection. In addition to the overall reduction of *S/N* value for the original trace, the results suggest that both types of noise will result in significant degradation of the ability to detect and estimate the size of the flaw. Once again, results here suggest that a window length around 20 mm ($\approx$ 0.8 in) and a segment length greater than 38 mm ($\approx$ 1.5 in) should provide repeatable measurements of *S/N*.

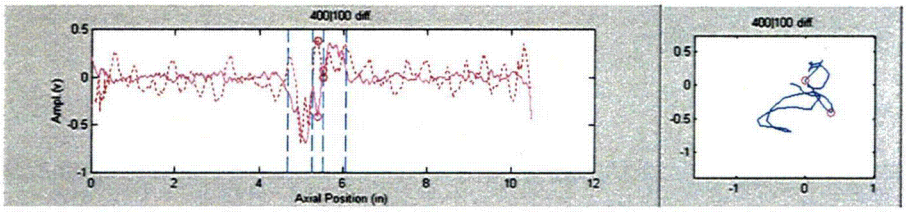

(a)

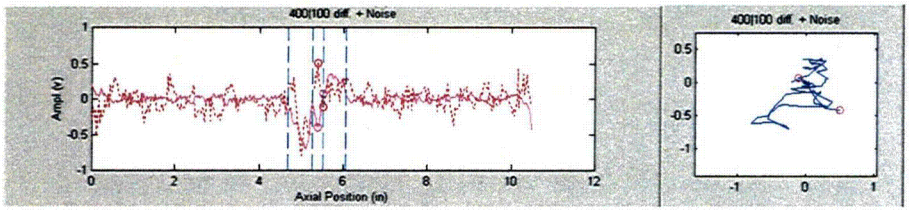

(b)

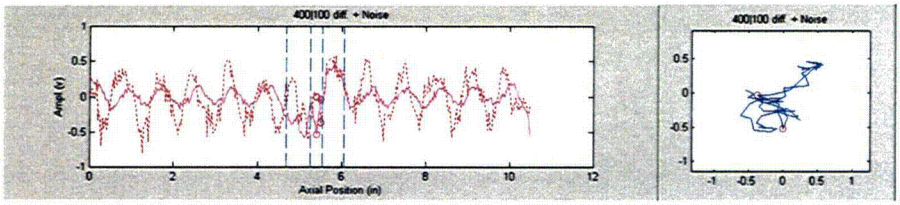

(c)

Figure 2.18 *Evaluation of the influence of random and periodic noise on bobbin coil data from mock-up test section #1 with an ODSCC indication at a TSP intersection. Graphics show the mix channel data (a) without added noise, (b) with added random noise, and (c) with added composite noise. Also shown are the inner and outer markings that identify the approximate location of flaw and TSP ends, respectively. Random noise with an amplification factor of 1 was added proportionally to both channels and to every other data point. Composite noise consisted of a small random component, as shown in (b), and a periodic component with amplitude of 0.25 V (V_{pp} = 0.5 V) and phase of 15°. In all cases, the strip chart shows both the vertical (solid line) and horizontal (dotted line) component of data.*

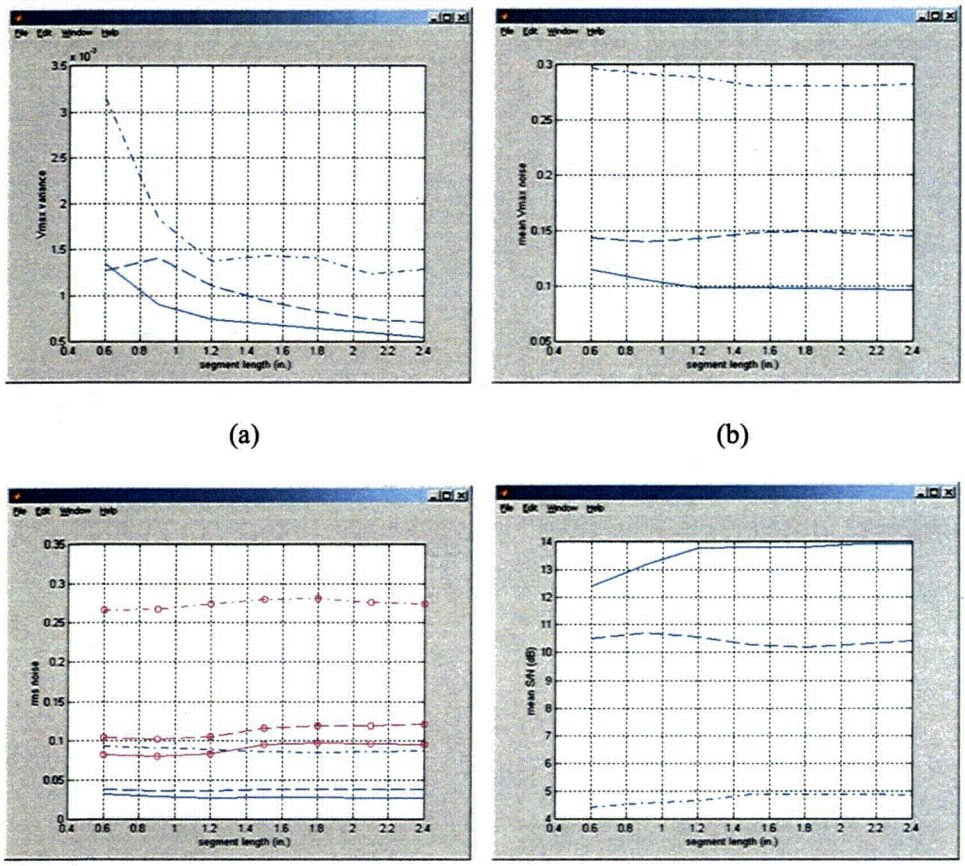

(a) (b)

(c) (d)

Figure 2.19 *First parametric evaluation of the influence of noise on bobbin coil data from mock-up test section of Fig. 2.18. Graphs show (a) variance of vertical component of noise (V_{max}), (b) mean value of V_{max}, (c) vertical component and total (circles) RMS noise, and (d) mean value of S/N in dB, all as a function of segment length. Results are shown for processed channel data without (solid curves) and with random (dashed curves) and composite (dash-dot curves) noise. A fixed window length of 15.2 mm (0.6 in) was used in all cases. The region of interest started outside the TSP edge (outer markings in Fig. 2.18) on both sides of the indication.*

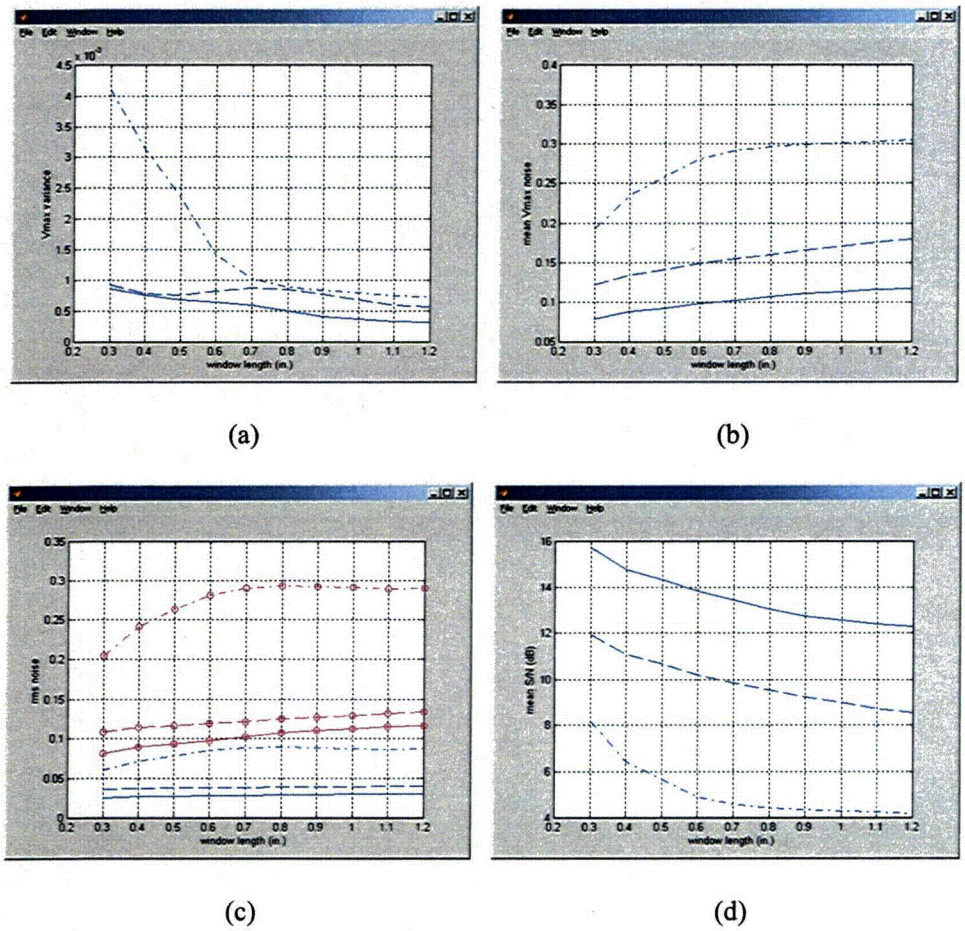

Figure 2.20 *Second parametric evaluation of the influence of noise on bobbin coil data from mock-up test section of Fig. 2.18. Graphs show (a) variance of vertical component of noise (V_{max}), (b) mean value of V_{max}, (c) vertical component and total (circles) RMS noise, and (d) mean value of S/N in dB, all as a function of window length. Results are shown for processed channel data without (solid curves) and with random (dashed curves) and composite (dash-dot curves) noise. A fixed segment length of 45.7 mm (1.8 in) was used in all cases. The region of interest started outside the TSP edge (outer markings in Fig. 2.18) on both sides of the indication.*

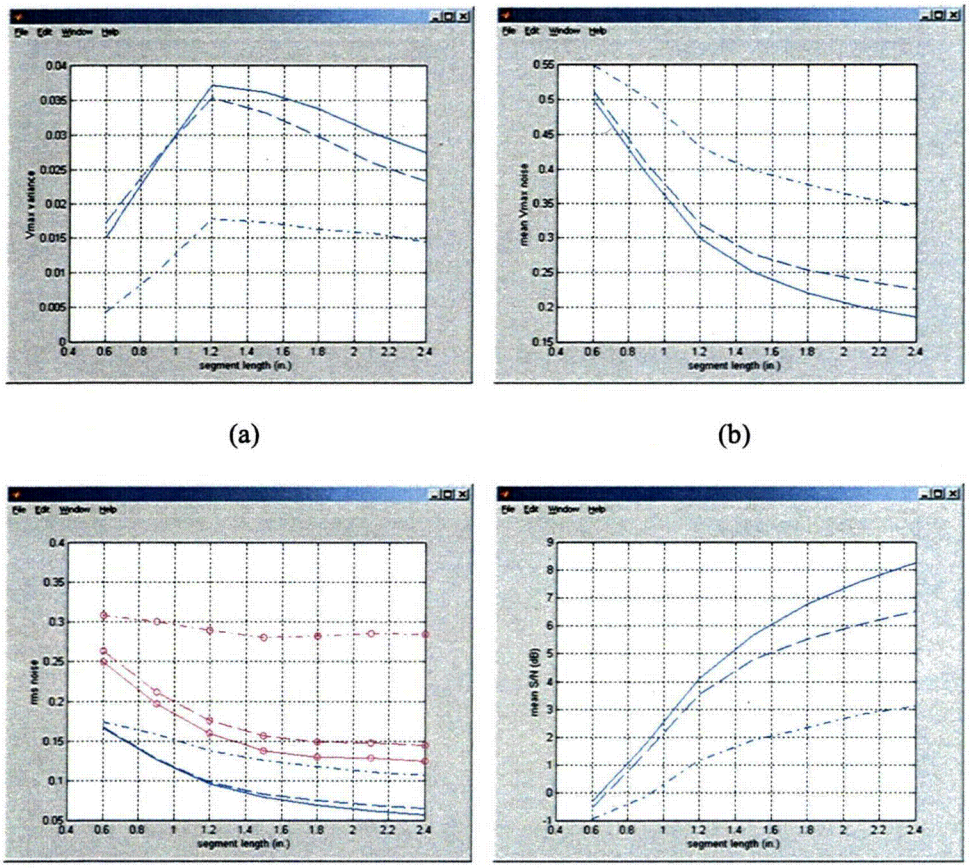

Figure 2.21 *Third parametric evaluation of the influence of noise on bobbin coil data from mock-up test section of Fig. 2.18. Graphs show (a) variance of vertical component of noise (V_{max}), (b) mean value of V_{max}, (c) vertical component and total (circles) RMS noise, and (d) mean value of S/N in dB, all as a function of segment length. Results are shown for processed channel data without (solid curves) and with random (dashed curves) and composite (dash-dot curves) noise. A fixed window length of 15.2 mm (0.6 in) was used in all cases. The region of interest started outside the flaw signal (inner markings in Fig. 2.18) on both sides of the indication.*

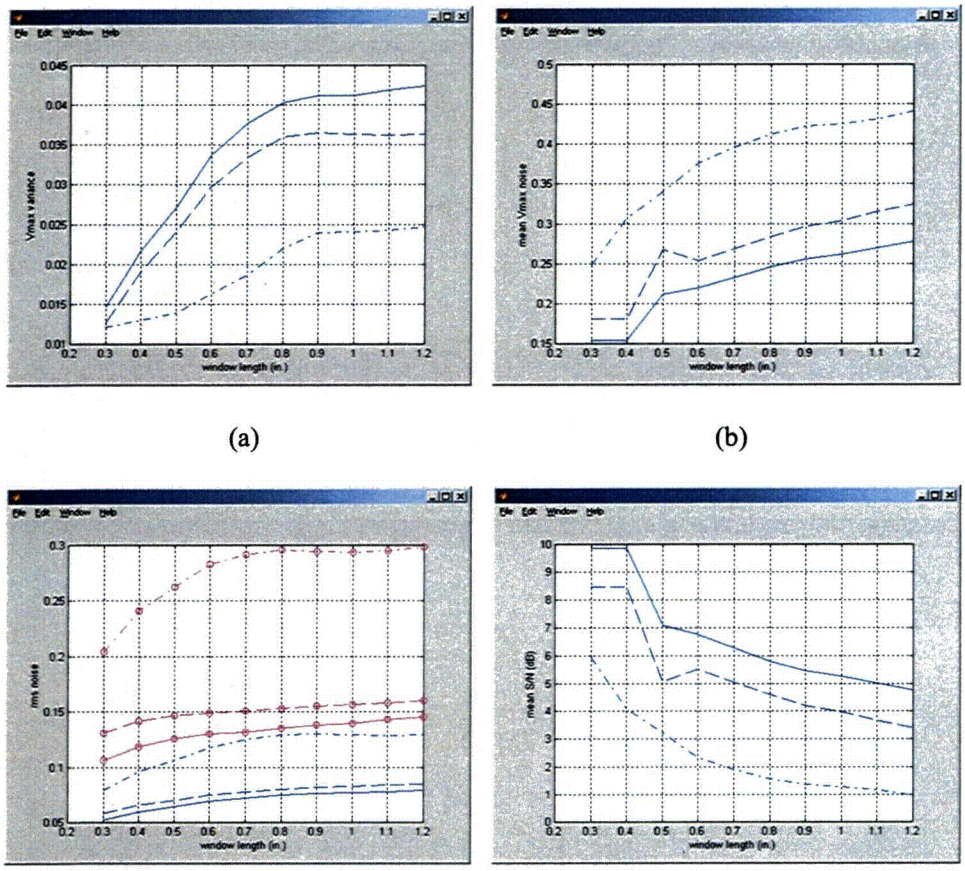

Figure 2.22 *Fourth parametric evaluation of the influence of noise on bobbin coil data from mock-up test section of Fig. 2.18. Graphs show (a) variance of vertical component of noise (V_{max}), (b) mean value of V_{max}, (c) vertical component and total (circles) RMS noise, and (d) mean value of S/N in dB, all as a function of window length. Results are shown for processed channel data without (solid curves) and with random (dashed curves) and composite (dash-dot curves) noise. A fixed segment length of 45.7 mm (1.8 in) was used in all cases. The region of interest started outside the flaw signal (inner markings in Fig. 2.18) on both sides of the indication.*

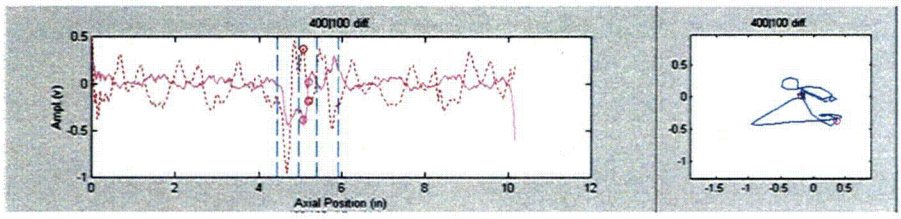

(a)

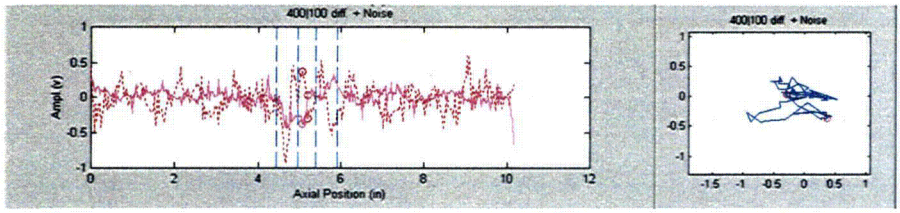

(b)

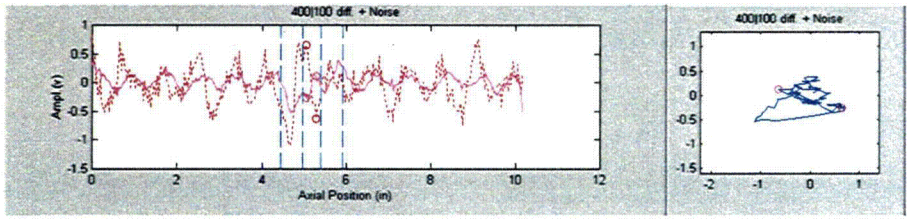

(c)

Figure 2.23 *Evaluation of the influence of random and periodic noise on bobbin coil data from mock-up test section #4 with an ODSCC indication at a TSP intersection. Graphics show the mix channel data (a) without added noise, (b) with added random noise, and (c) with added composite noise. Also shown are the inner and outer markings that identify the approximate location of flaw and TSP ends, respectively. Random noise with an amplification factor of 1 for the horizontal and 2 for the vertical component was added proportionally to both channels and to every other data point. Composite noise consisted of a small random component, as shown in (b), and a periodic component with amplitude of 0.25 V (V_{pp} = 0.5 V) and phase of 15°. In all cases, the strip chart shows the vertical (solid line) and horizontal (dotted line) component of data.*

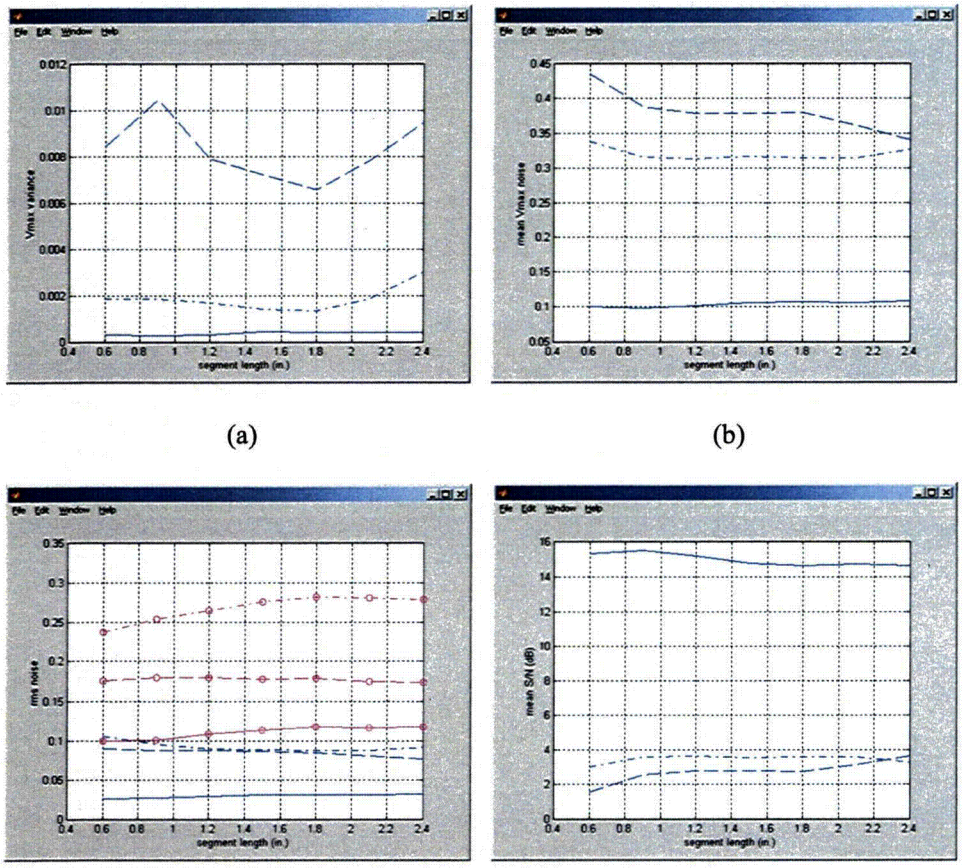

(a) (b)

(c) (d)

Figure 2.24 *Parametric evaluation of the influence of noise on bobbin coil data from mock-up test section of Fig. 2.23. Graphs show (a) variance of vertical component of noise (V_{max}), (b) mean value of V_{max}, (c) vertical component and total (circles) RMS noise, and (d) mean value of S/N in dB, all as a function of segment length. Results are shown for processed channel data without (solid curves) and with random (dashed curves) and composite (dash-dot curves) noise. A fixed window length of 15.2 mm (0.6 in) was used in all cases. The region of interest started outside the TSP edge (outer markings in Fig. 2.23) on both sides of the indication.*

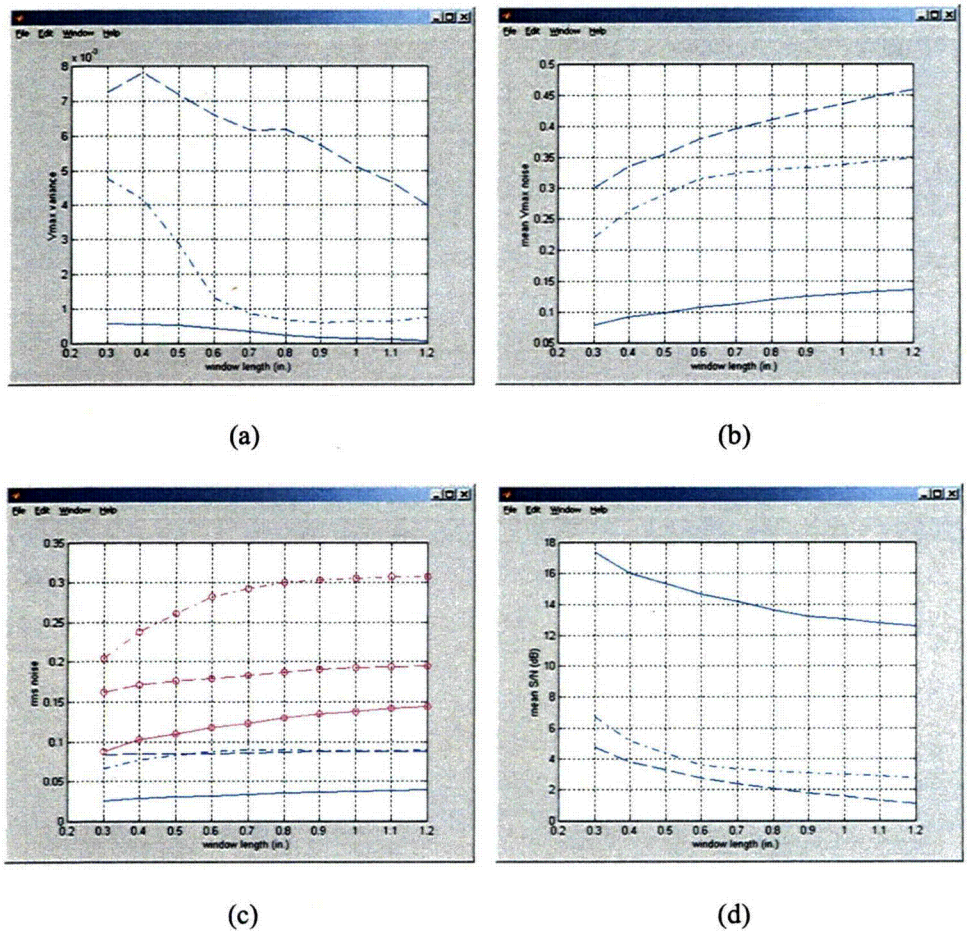

Figure 2.25 *Second parametric evaluation of the influence of noise on bobbin coil data from mock-up test section of Fig. 2.23. Graphs show (a) variance of vertical component of noise (V_{max}), (b) mean value of V_{max}, (c) vertical component and total (circles) RMS noise, and (d) mean value of S/N in dB, all as a function of window length. Results are shown for processed channel data without (solid curves) and with random (dashed curves) and composite (dash-dot curves) noise. A fixed segment length of 45.7 mm (1.8 in) was used in all cases. The region of interest started outside the TSP edge (outer markings in Fig. 2.23) on both sides of the indication.*

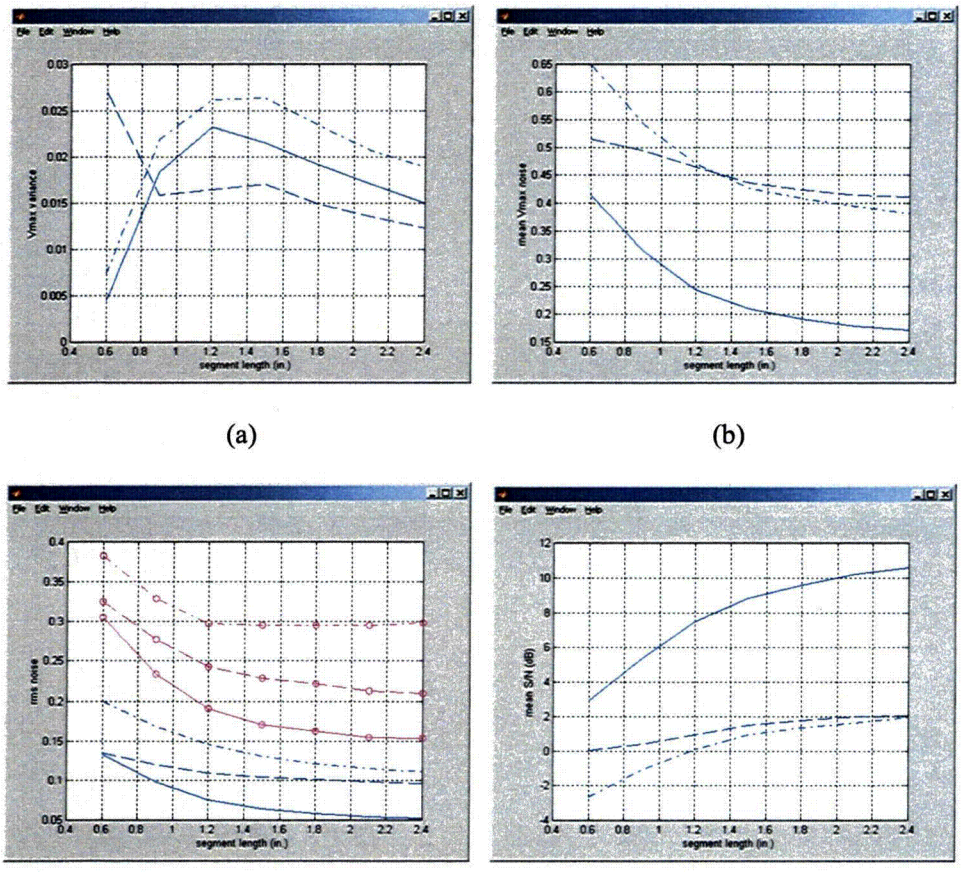

(a) (b)

(c) (d)

Figure 2.26 *Third parametric evaluation of the influence of noise on bobbin coil data from mock-up test section of Fig. 2.23. Graphs show (a) variance of vertical component of noise (V_{max}), (b) mean value of V_{max}, (c) vertical component and total (circles) RMS noise, and (d) mean value of S/N in dB, all as a function of segment length. Results are shown for processed channel data without (solid curves) and with random (dashed curves) and composite (dash-dot curves) noise. A fixed window length of 15.2 mm (0.6 in) was used in all cases. The region of interest started outside the flaw signal (inner markings in Fig. 2.23) on both sides of the indication.*

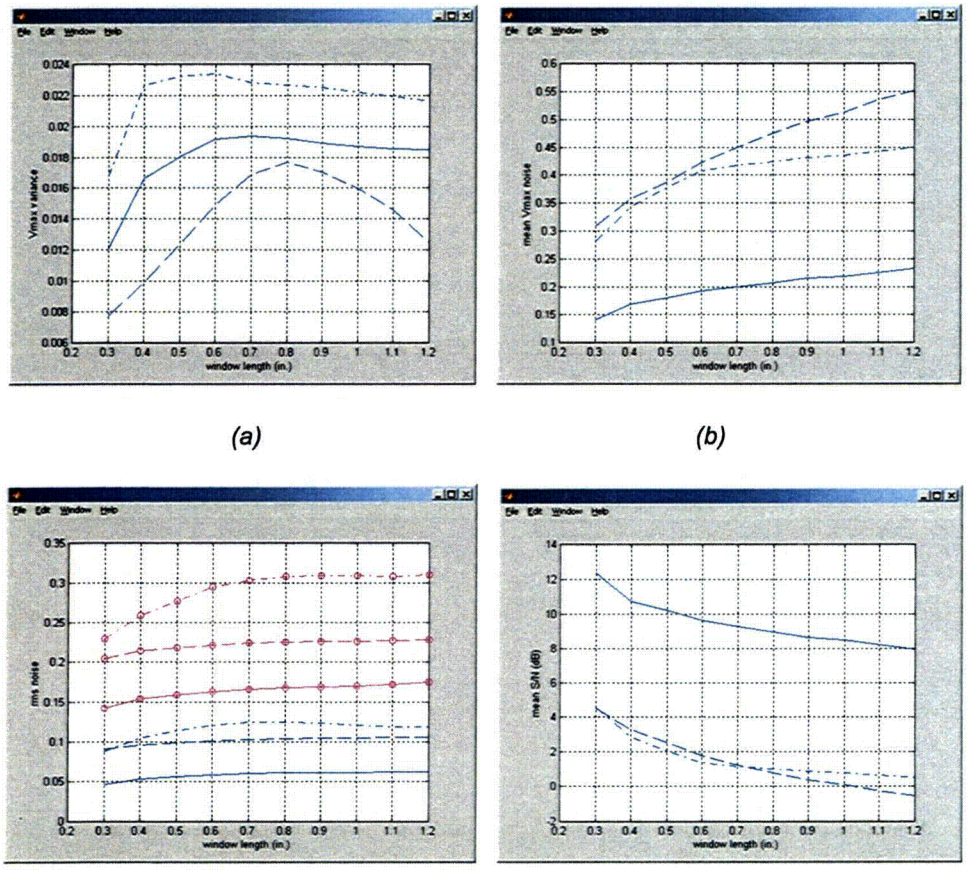

Figure 2.27 *Fourth parametric evaluation of the influence of noise on bobbin coil data from mock-up test section of Fig. 2.23. Graphs show (a) variance of vertical component of noise (V_{max}), (b) mean value of V_{max}, (c) vertical component and total (circles) RMS noise, and (d) mean value of S/N in dB, all as a function of window length. Results are shown for processed channel data without (solid curves) and with random (dashed curves) and composite (dash-dot curves) noise. A fixed segment length of 45.7 mm (1.8 in) was used in all cases. The region of interest started outside the flaw signal (inner markings in Fig. 2.23) on both sides of the indication.*

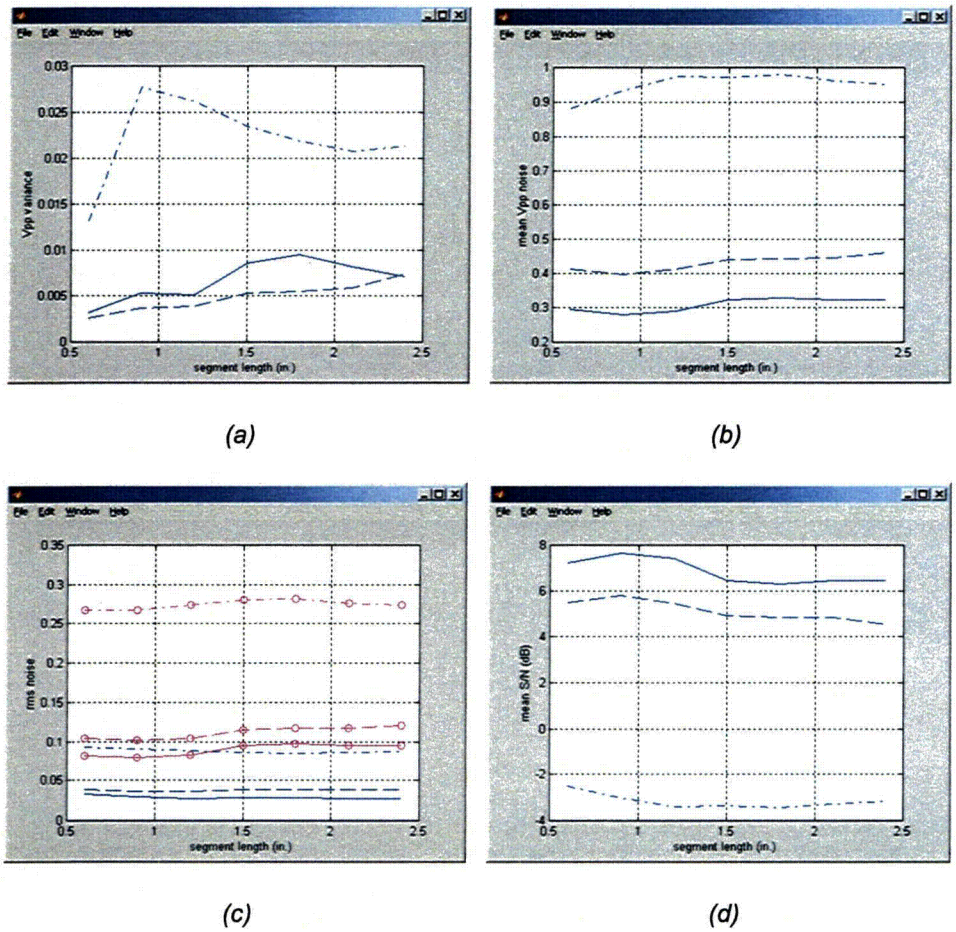

Figure 2.28 *Fifth parametric evaluation of the influence of noise on bobbin coil data from mock-up test section of Fig. 2.18. Graphs show (a) variance of peak-to-peak (V_{pp}) noise, (b) mean value of V_{pp} noise, (c) vertical component and total (circles) RMS noise, and (d) mean value of S/N in dB, all as a function of segment length. Results are shown for processed channel data without (solid curves) and with random (dashed curves) and composite (dash-dot curves) noise. A fixed window length of ≈ 15 mm (0.6 in) was used in all cases. The region of interest started outside the TSP edge (outer markings in Fig. 2.18) on both sides of the indication.*

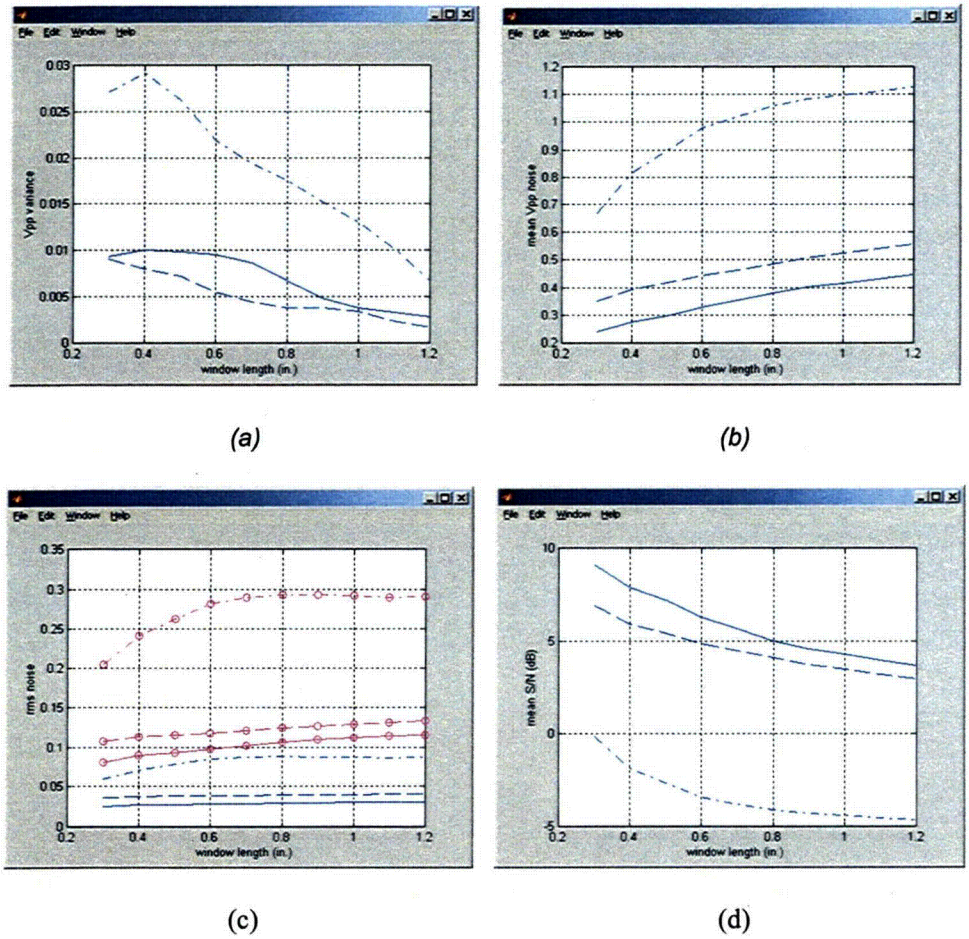

Figure 2.29 *Sixth parametric evaluation of the influence of noise on bobbin coil data from mock-up test section of Fig. 2.18. Graphs show (a) variance of peak-to-peak (V_{pp}) noise, (b) mean value of V_{pp} noise, (c) vertical component and total (circles) RMS noise, and (d) mean value of S/N in dB, all as a function of window length. Results are shown for processed channel data without (solid curves) and with random (dashed curves) and composite (dash-dot curves) noise. A fixed segment length of ≈ 46 mm (1.8 in) was used in all cases. The region of interest started outside the TSP edge (outer markings in Fig. 2.18) on both sides of the indication.*

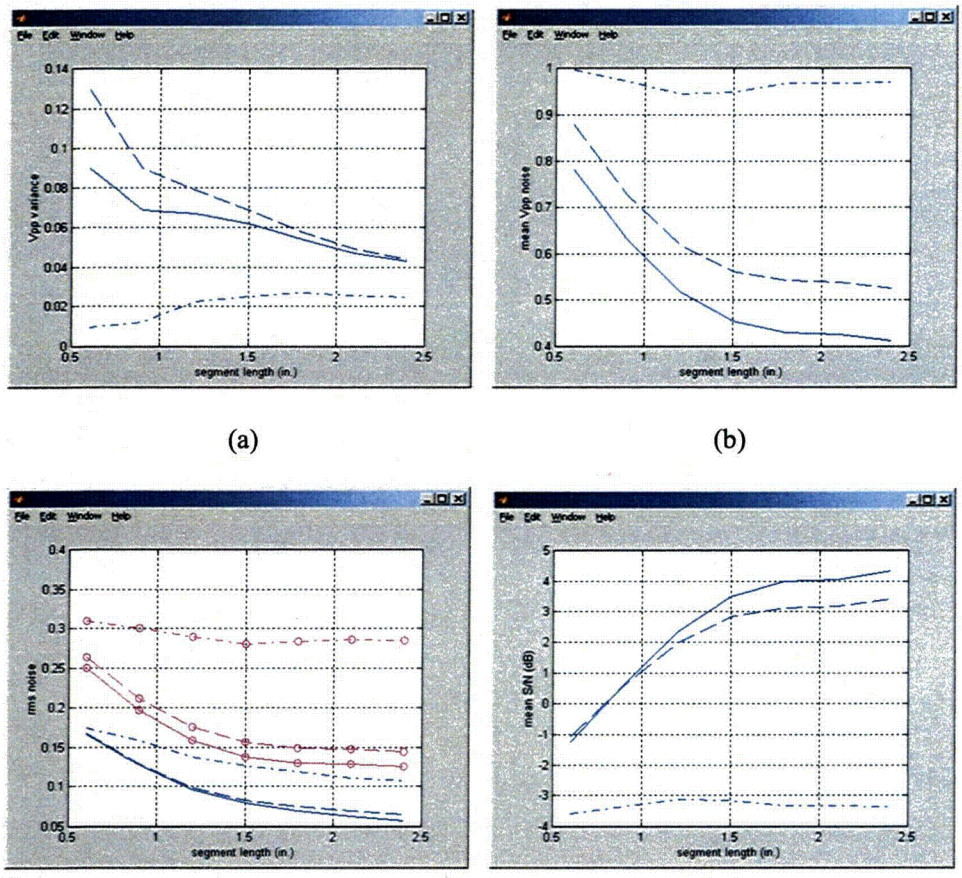

Figure 2.30 *Seventh parametric evaluation of the influence of noise on bobbin coil data from mock-up test section of Fig. 2.18. Graphs show (a) variance of peak-to-peak (V_{pp}) noise, (b) mean value of V_{pp} noise, (c) vertical component and total (circles) RMS noise, and (d) mean value of S/N in dB, all as a function of segment length. Results are shown for processed channel data without (solid curves) and with random (dashed curves) and composite (dash-dot curves) noise. A fixed window length of ≈ 15 mm (0.6 in) was used in all cases. The region of interest started outside the flaw signal (inner markings in Fig. 2.18) on both sides of the indication.*

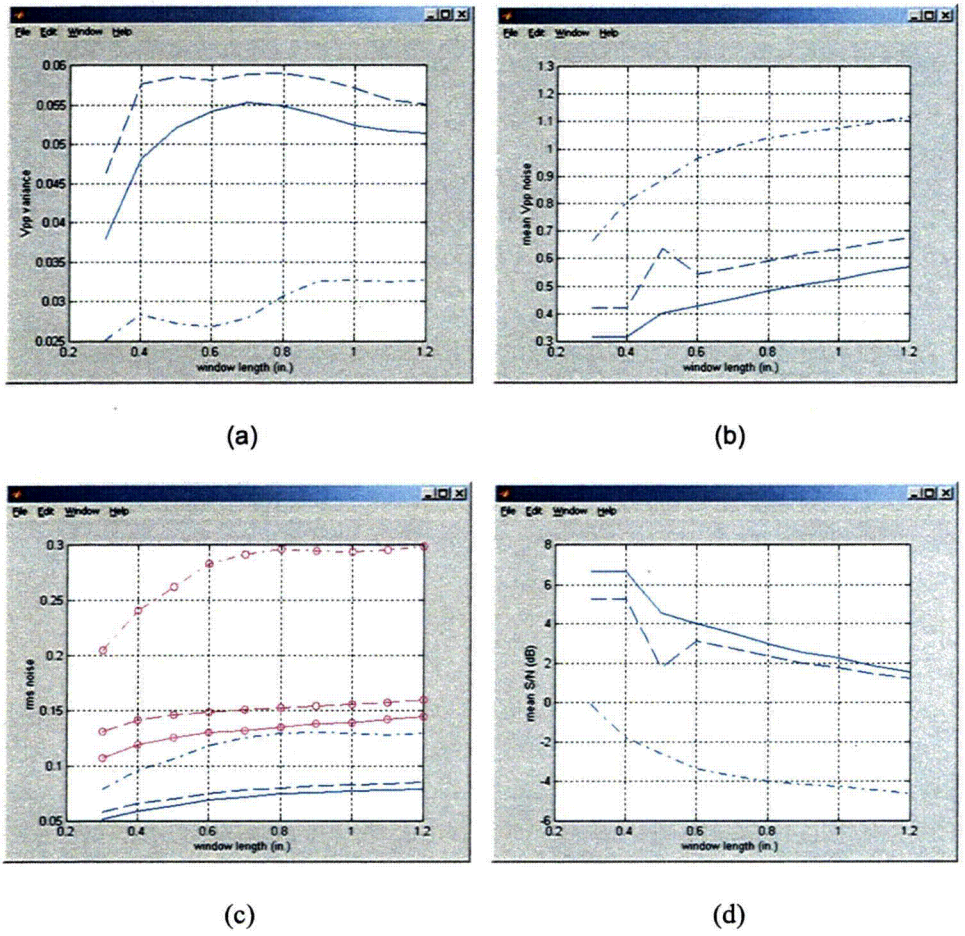

Figure 2.31 *Eighth parametric evaluation of the influence of noise on bobbin coil data from mock-up test section of Fig. 2.18. Graphs show (a) variance of peak-to-peak (V_{pp}) noise, (b) mean value of V_{pp} noise, (c) vertical component and total (circles) RMS noise, and (d) mean value of S/N in dB, all as a function of window length. Results are shown for processed channel data without (solid curves) and with random (dashed curves) and composite (dash-dot curves) noise. A fixed segment length of ≈ 46 mm (1.8 in) was used in all cases. The region of interest started outside the flaw signal (inner markings in Fig. 2.18) on both sides of the indication.*

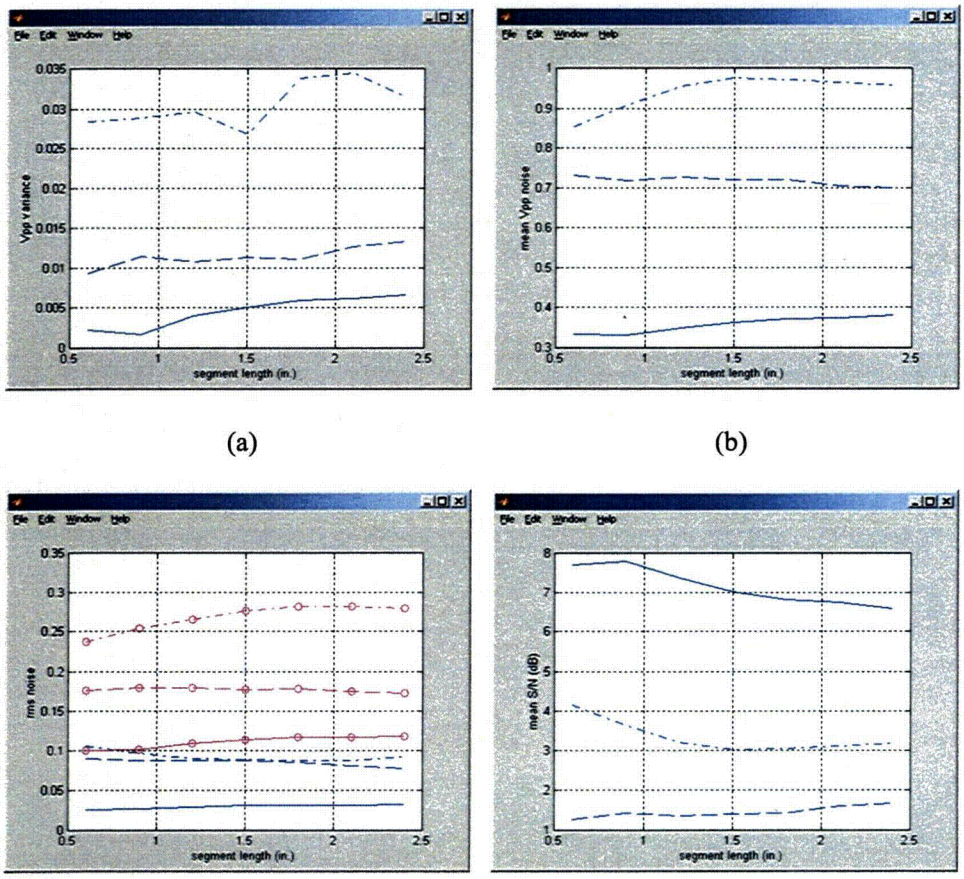

Figure 2.32 *Parametric evaluation of the influence of noise on bobbin coil data from mock-up test section of Fig. 2.23. Graphs show (a) variance of peak-to-peak (V_{pp}) noise, (b) mean value of V_{pp} noise, (c) vertical component and total (circles) RMS noise, and (d) mean value of S/N in dB, all as a function of segment length. Results are shown for processed channel data without (solid curves) and with random (dashed curves) and composite (dash-dot curves) noise. A fixed window length of ≈ 15 mm (0.6 in) was used in all cases. The region of interest started outside the TSP edge (outer markings in Fig. 2.23) on both sides of the indication.*

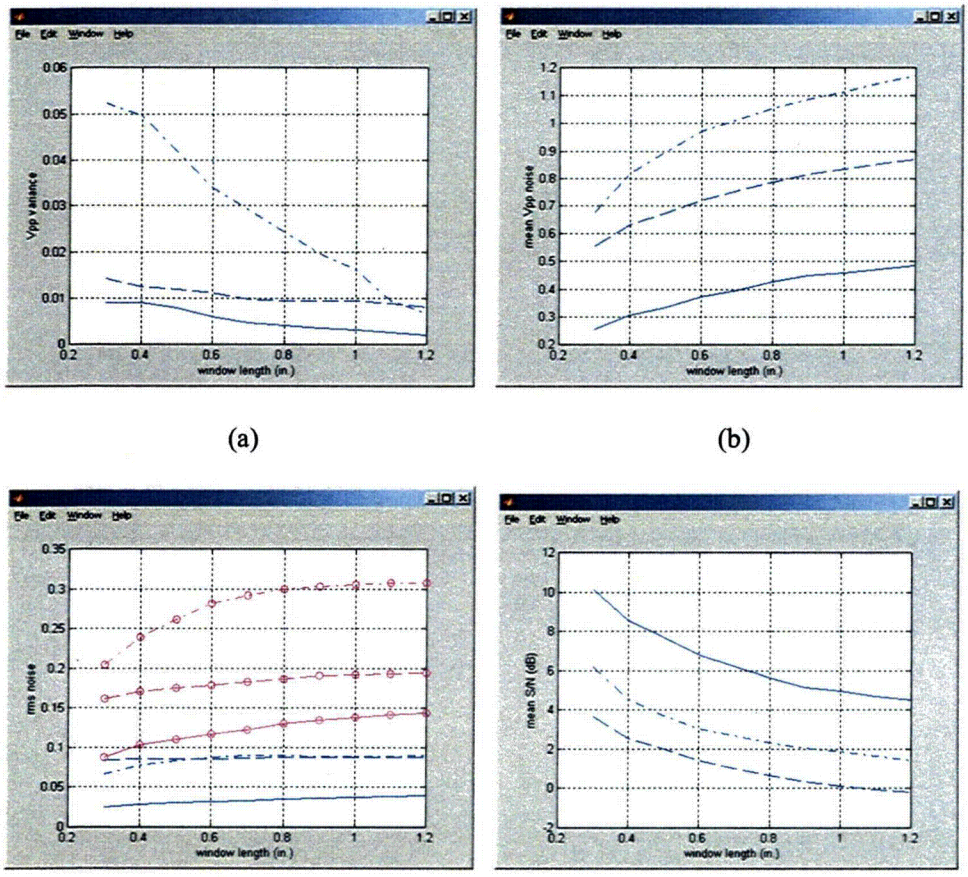

Figure 2.33 *Second parametric evaluation of the influence of noise on bobbin coil data from mock-up test section of Fig. 2.23. Graphs show (a) variance of peak-to-peak (V_{pp}) noise, (b) mean value of V_{pp} noise, (c) vertical component and total (circles) RMS noise, and (d) mean value of S/N in dB, all as a function of window length. Results are shown for processed channel data without (solid curves) and with random (dashed curves) and composite (dash-dot curves) noise. A fixed segment length of ≈ 46 mm (1.8 in) was used in all cases. The region of interest started outside the TSP edge (outer markings in Fig. 2.23) on both sides of the indication.*

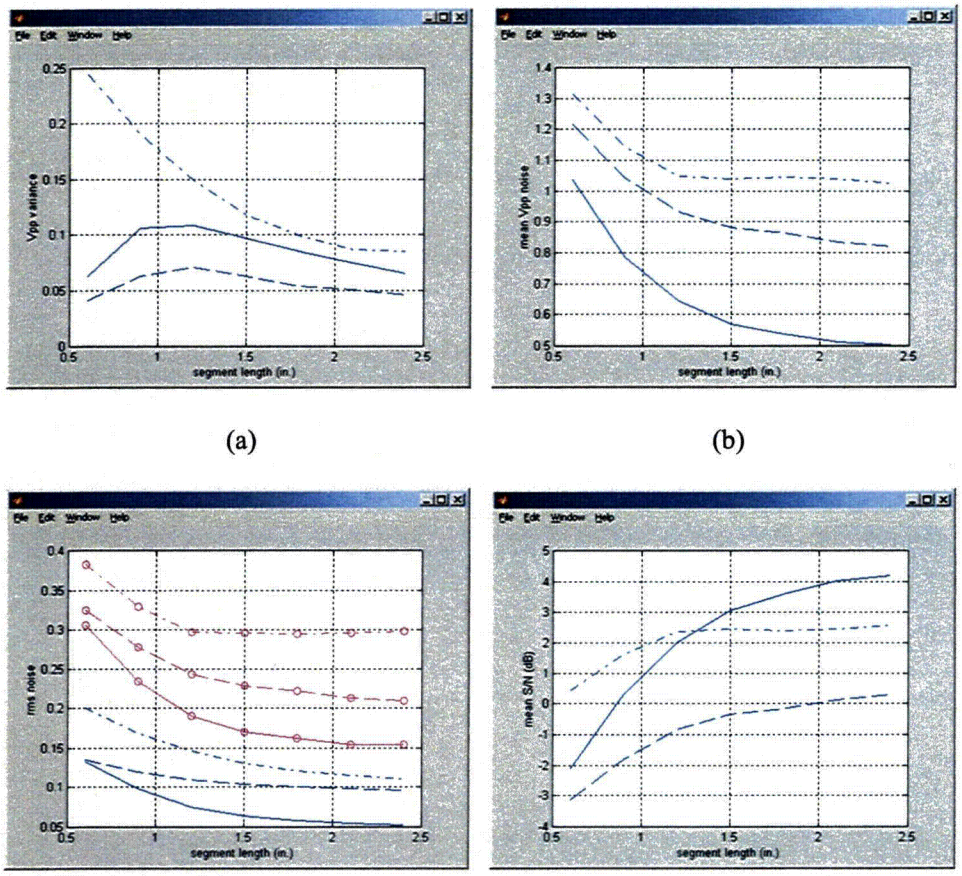

Figure 2.34 *Third parametric evaluation of the influence of noise on bobbin coil data from mock-up test section of Fig. 2.23. Graphs show (a) variance of peak-to-peak (V_{pp}) noise, (b) mean value of V_{pp} noise, (c) vertical component and total (circles) RMS noise, and (d) mean value of S/N in dB, all as a function of segment length. Results are shown for processed channel data without (solid curves) and with random (dashed curves) and composite (dash-dot curves) noise. A fixed window length of ≈ 15 mm (0.6 in) was used in all cases. The region of interest started outside the flaw signal (inner markings in Fig. 2.23) on both sides of the indication.*

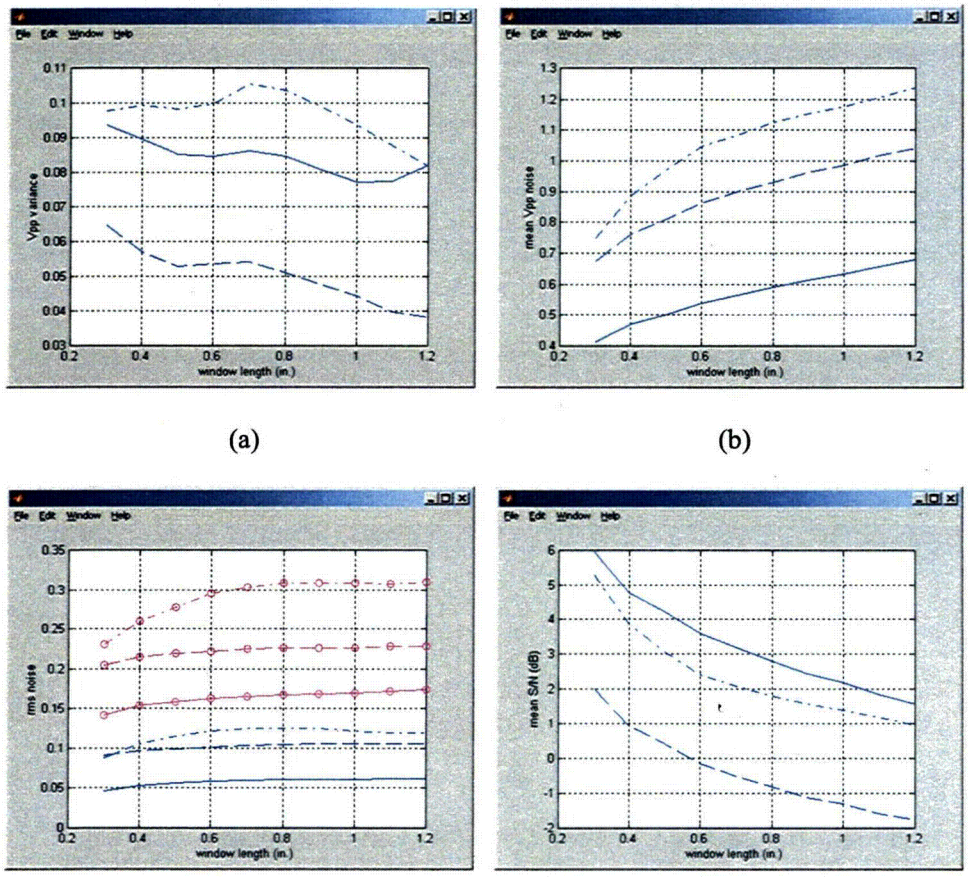

Figure 2.35 *Fourth parametric evaluation of the influence of noise on bobbin coil data from mock-up test section of Fig. 2.23. Graphs show (a) variance of peak-to-peak (V_{pp}) noise, (b) mean value of V_{pp} noise, (c) vertical component and total (circles) RMS noise, and (d) mean value of S/N in dB, all as a function of window length. Results are shown for processed channel data without (solid curves) and with random (dashed curves) and composite (dash-dot curves) noise. A fixed segment length of ≈ 46 mm (1.8 in) was used in all cases. The region of interest started outside the flaw signal (inner markings in Fig. 2.23) on both sides of the indication.*

2.2.5 Assessment of Noise Level in Rotating Probe Data

The equations for the measurement of noise level in bobbin probe data were modified to calculate corresponding indicators of noise in rotating probe data. A series of algorithms was developed to extend the analyses performed on bobbin probe data to EC data acquired with rotating probes. The objective of the work was to determine whether these measurement procedures could better reflect the influence of noise on detection and sizing with rotating probes. The effect of each measurement variable (i.e., window size and ROI) on calculation of the noise level in rotating probe data is discussed.

Conventional procedures for noise measurement treat bobbin coil data, a spatially one-dimensional (1-D) signal, and rotating probe data, a spatially two-dimensional (2-D) signal, in a similar manner. Localized noise can have a 2-D spatial distribution that interferes with rotating probe signals in ways that cannot always be accurately represented by a 1-D measurement of the noise. Several algorithms have been incorporated into the MATLAB-based GUI to allow measurement of various indicators of noise level (e.g., RMS noise and *S/N* using the maximum vertical component or peak-to-peak measurements) from the rotating probe data in both the axial and circumferential directions. Because the dimensions of the measurement window can be selected arbitrarily, the contribution from a particular component of the noise can be better isolated. The routines also allow removal of signals from any given test section so that noise can be measured at the same axial position as the flaw. As before, a sliding window approach is used to help assess the effect of each parameter on the measurement results and to provide more precise information on the spatial variability of the noise level along the tube.

Expressions for calculating various signal and noise components from 1-D EC data were presented in Sects. 2.2.3 and 2.2.4. These expressions have been extended to the 2-D case in which both the measurement window and the ROI extend in the axial and circumferential directions. For example, as an extension of Eq. 2.9 the RMS components of the noise for the 2-D case can be determined by

$$N_{RMS}^{h,v} = \sqrt{\frac{1}{n}\frac{1}{m}\sum_{i=1}^{n}\sum_{j=1}^{m}\left(N_{i,j}^{h,v} - \bar{N}_{i,j}^{h,v}\right)^2} \tag{2.16}$$

and

$$\bar{N}^{h,v} = \frac{1}{n}\frac{1}{m}\sum_{i=1}^{n}\sum_{j=1}^{m} N_{i,j}^{h,v} \tag{2.17}$$

where the superscripts h and v denote the horizontal or vertical component of noise, respectively, and i and j denote the indices of data points along the axial and circumferential directions. The total RMS value in the ROI may then be calculated from

$$N_{RMS}^{T} = \sqrt{\left(N_{RMS}^{h}\right)^2 + \left(N_{RMS}^{v}\right)^2} \tag{2.18}$$

Rotating-probe inspection data collected on several flawed and unflawed laboratory specimens that include tube geometry changes and external support structures were used in our investigations. For the initial validation studies, 2-D results were compared with 1-D measurements of noise over approximately the same region of the tube. Figure 2.36 shows different views of the rotating probe data (0.115-in. pancake coil) from

a laboratory-degraded specimen with axial ODSCC indications at a TSP intersection. The figure shows image, isometric, strip-chart, and lissajous plots of the original and composite data with random and periodic components. Figure 2.37 displays an axial profile of the noise level determined by 1-D and 2-D measurement methods over the non-flawed section of the tube shown in Fig. 2.36(a).

In accordance with conventional 1-D measurement procedures, the region of interest in this case consisted of two ≈ 23-mm (0.9-in)-long sections on both sides of the TSP intersection in the free-span region of the tube. The 1-D case used a 7.6-mm (0.3-in) wide window, which corresponds to >800 data points within each measurement window. For the 2-D case (i.e., rotating probe data arranged in matrix format with columns representing the width and the rows representing the height), the measurement window had a width (axial extent) of 7.6 mm (0.3 in) and a height (circumferential extent) of 360°. Based on the mean value of noise over the region of interest, the results in Fig. 2.37 show good agreement between the two measurement methods.

A series of calculations was subsequently carried out to examine the effect of window size on the measurement of noise away from the flaw (i.e., in free span). Both window height and width were varied over a relatively wide range, spanning the expected values for the coil coverage in the axial and circumferential directions. For the 2-D calculations here, the noise level at each axial position is the maximum value of all the sectors around the tube's circumference. As before, the noise level over the region of interest is the average of all measurement points along the tube axis.

Figure 2.38 shows a series of plots in which either the window height or width was varied, while the other parameter was held constant. In all cases, the region of interest consisted of two 25.4-mm (1.0-in)-long segments on both sides of the intersection. Each graph shows the measurement results without and with two types of simulated noise containing random and periodic components. Figures 2.38(a) and (b) show the variation of the vertical maximum amplitude (V_{max}) and RMS (V_{rms}) value of noise, respectively, as a function of window height for a fixed 7.6-mm (0.3-in) window width. In both cases, the results show little change in the level of noise for sectors >90°. Figures 2.38(c) and (d) show the variation of the same indicators as a function of window width for a fixed window height of 360°. The mean V_{max} values in this case show a minor increase in the level of noise for window widths >5.0 mm (0.2 in). The vertical component of the RMS noise, however, shows essentially no dependence on the width of the measurement window. Analogous to the 1-D calculation of noise, this effect occurs because of the relatively large number of data points around the tube circumference that are used for estimation of the RMS value. Although both indicators in this case show similar trends in variation of the noise level as a function of window size, the mean V_{max} value provides a more direct indication of the severity of the localized noise influence.

The calculated results shown in Fig. 2.39 are based on the peak-to-peak and the total RMS noise in accordance with Eq. 2.18, which takes into account contributions from the horizontal and the vertical component. The trends in this case are similar to those in Fig. 2.38. As with earlier observations, the higher level of total noise that is dominated primarily by its horizontal component is expected to have a more profound effect on the sizing results.

These test cases deal exclusively with estimation of noise in the free-span region of the tube. With large measurement windows, such calculations provide information primarily about the global level of noise. This kind of information is important in assessing overall EC data quality. However, in many practical applications such as performance demonstrations on detection and sizing capability, it is important to determine the level of noise close to the location of the flaw. Such information can be extracted from 2-D EC data collected with rotating or array probes. Figure 2.40 shows intermediate stages of the process for calculation of the noise level over a region of interest that includes the flaw signal. Figure 2.40(a) shows the

original strip chart and image display of rotating probe data for the same specimen shown in Fig. 2.36. Figure 2.40(b) shows the same section of tube after the flaw signal has been eliminated from the TSP intersection. Figures 2.40(c) and (d) display the V_{max} and V_{rms} profiles over a 63.5-mm (2.5-in) section of the tube, determined with windows of different size. The window dimensions in this case were selected such that the measurements along the tube axis would represent the level of noise primarily in the circumferential and the axial direction, respectively. As expected, in both cases the maximum values occur at the edge of the tube support plate.

Three additional test sections of the mock-up that had discontinuities associated with tube dimensional changes and external support structures were examined. The noise level over the region of interest was measured with a window size selected based on the parametric evaluations. For the test cases here, the window dimensions were set so that the noise level is measured along either the axial or the circumferential direction. To examine the spatial distribution of noise, the calculated values were plotted as a function of position along the tube axis. Figure 2.41 shows the rotating probe data obtained with a 2.92-mm (0.115-in) pancake coil and collected from a dented TSP intersection. Image, isometric, strip-chart, and lissajous plots of the original data are displayed in Fig. 2.41(a). Figure 2.41(b) shows the signal elimination stage of the process in which the dent was removed from the TSP intersection. Figures 2.41(c) and (d) display the axial profile of the noise that was measured along the circumferential and axial direction, respectively. The region of interest in this case covered roughly a 63.5-mm (2.5-in)-long section of the tube, centered approximately at the middle of the TSP. For the window dimensions selected here, the V_{max} and V_{rms} values show similar trends in terms of the spatial distribution of noise. The average values for the axial and circumferential component of noise outside the TSP edge (i.e., free-span region) are quite close and are in agreement with the earlier calculations. Except for a narrow section at one edge of the TSP, noise measured along the circumferential direction shows little variation over the region of interest. This is because the interference from the axially symmetric and relatively smooth TSP response is rather small along the circumferential direction. The axial profile of the noise measured along the tube axis, shown in Fig. 2.41(d), has two large peaks at the edges of the TSP. Analogously, the results show that the effect of an unwanted discontinuity (e.g., TSP) on a circumferential flaw signal would be conservatively estimated by measuring the noise along the axial direction.

Measurement of noise at the tube-sheet (TS) elevation was studied for two test sections with different levels of noise. Both test sections exhibited a substantial level of inner-diameter-originated noise. Figures 2.42 and 2.43 show the probe response as well as variation of the V_{max} and V_{rms} components of noise along the tube axis, measured independently along the axial and the circumferential direction. Similar trends as those observed in Fig. 2.41 can also be seen in this case. The calculated noise level for the test section in Fig. 2.42 has approximately the same mean value above and below the roll transition. In contrast, there is a substantial difference between the level of noise in the expanded and unexpanded sections of the tube shown in Fig. 2.43. Therefore, while the average value over the region of interest for the first TS test section could produce an acceptable measure of the noise level, combining the two segments comprising the entire ROI did not provide a meaningful estimate for the second TS test section. That is, for the data shown in Fig. 2.43, the significant variation in the spatial distribution and orientation of noise within the TS region is not reflected by the average value over the entire region of interest. Because the detection capability is influenced by both the global and local level of noise, these calculations clearly demonstrate the importance of measuring the spatial distribution of noise. Ultimately, the noise level in rotating probe data can be more realistically assessed by first suppressing the interference from unwanted signals (e.g., TSP response) within the ROI. Further studies in this area will help to better define the influence of various parameters on the measurement of noise in spatially two-dimensional EC inspection data.

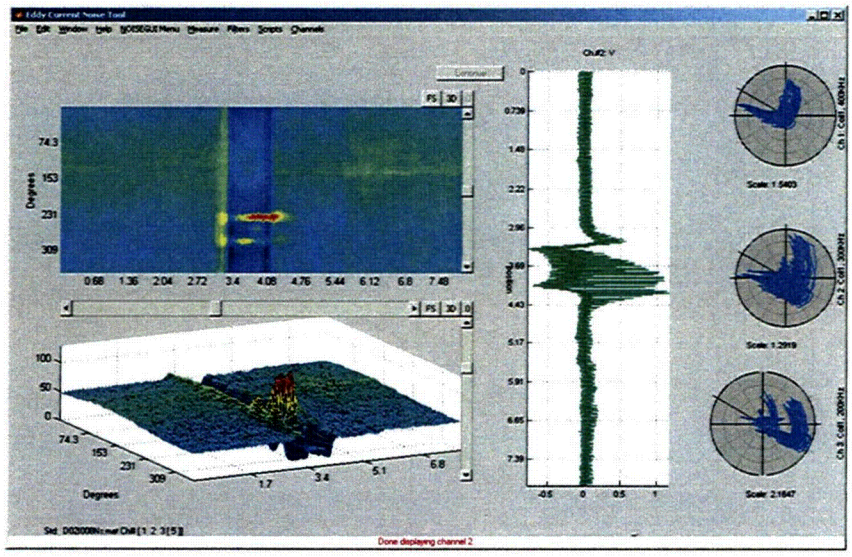

(a)

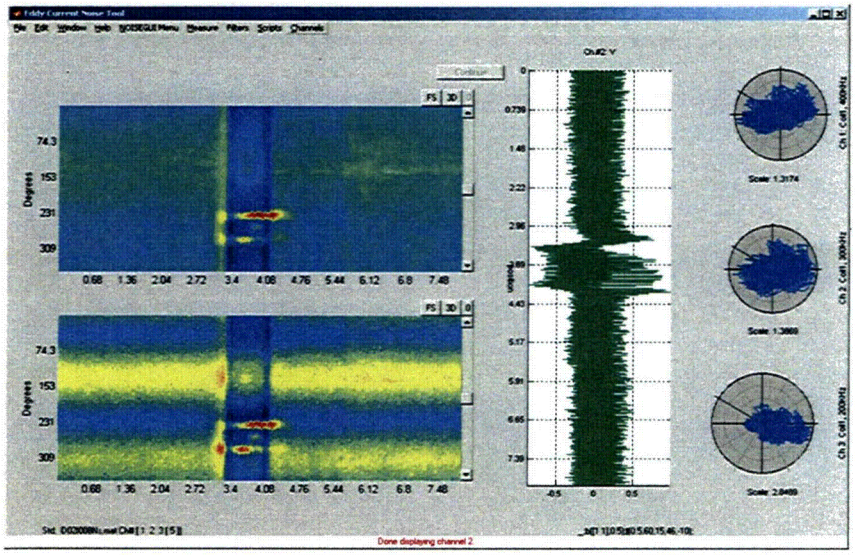

(b)

Figure 2.36 Evaluation of the influence of noise on rotating probe data from mock-up test section with an ODSCC indication at a TSP intersection. Graphics show the processed channel data (a) without and (b) with added composite (random and periodic) noise. Random noise with an amplification factor of 1 was added proportionally to both channels and to every other data point. The periodic component has amplitude of 0.25 V (V_{pp} = 0.5 V) and phase of 15°.

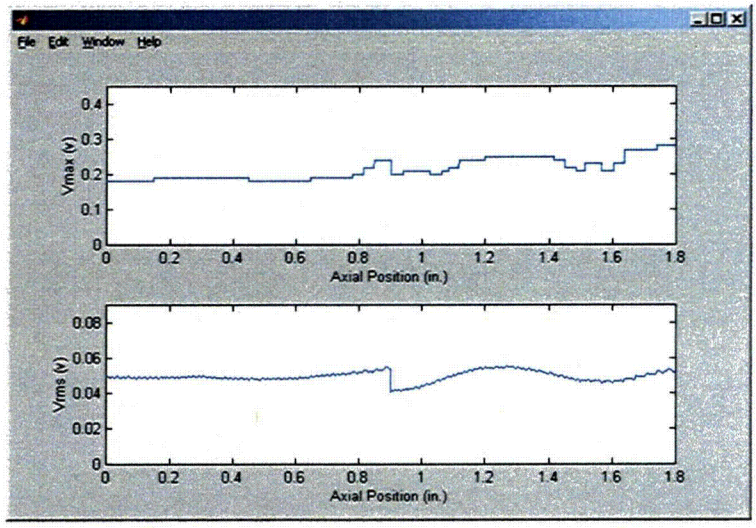

(a)

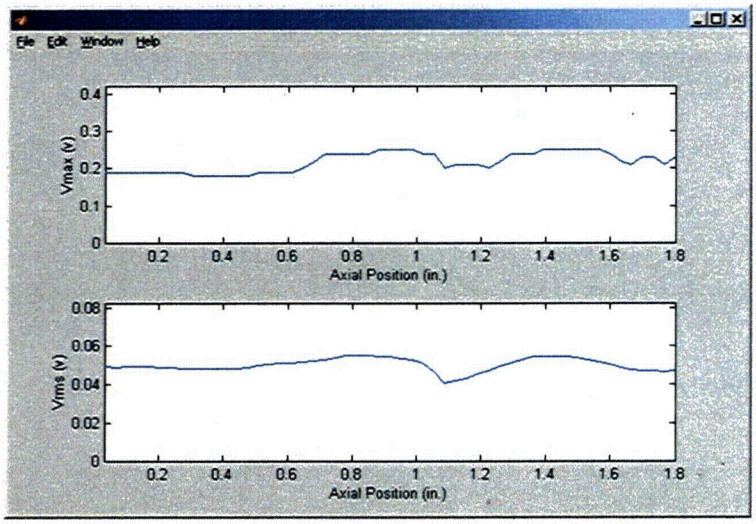

(b)

Figure 2.37 *Measurement of maximum amplitude (V_{max}) and RMS (V_{rms}) noise based on the vertical component of data along the tube axis for the specimen shown in Fig. 2.36(a). Graphs show the results using (a) 1-D and (b) 2-D measurement method. A measurement window length of 7.6 mm (0.3 in) was used for 1-D calculations. A measurement window of 7.6-mm (0.3-in) width and 360° height was used for 2-D calculations. The region of interest is two ≈ 23-mm (0.9-in)-long free-span sections on both sides and away from the TSP edges.*

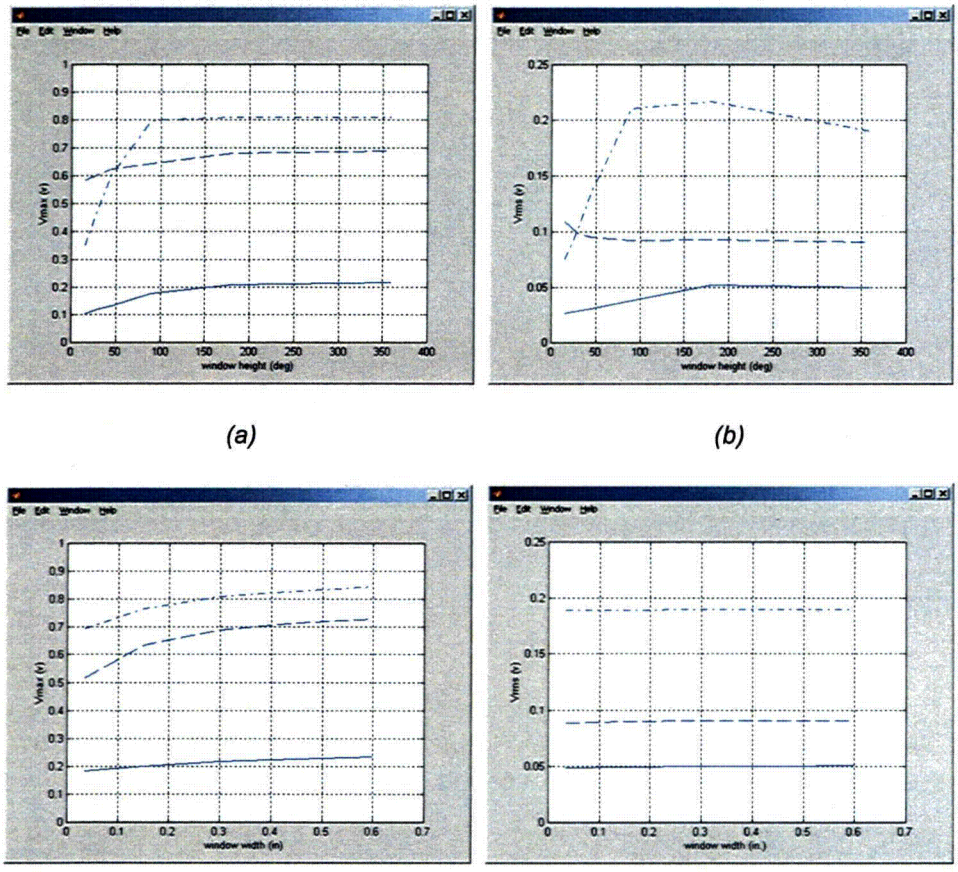

Figure 2.38 Parametric evaluation of noise influence on rotating probe data from mock-up test section of Fig. 2.36(b). Graphs show (a) mean V_{max} and (b) V_{rms} noise as a function of window height for a fixed window width of 7.6 mm (0.3 in), and (c) mean V_{max} and (d) V_{rms} as a function of window width for a fixed window height of 360°. Results are shown for 2.92-mm (0.115-in)-diameter pancake at 300 kHz without (solid curves) and with random (dashed curves) and composite (dash-dot curves) noise. The region of interest is two 25.4-mm (1.0-in)-long free-span sections on both sides and away from the TSP edges.

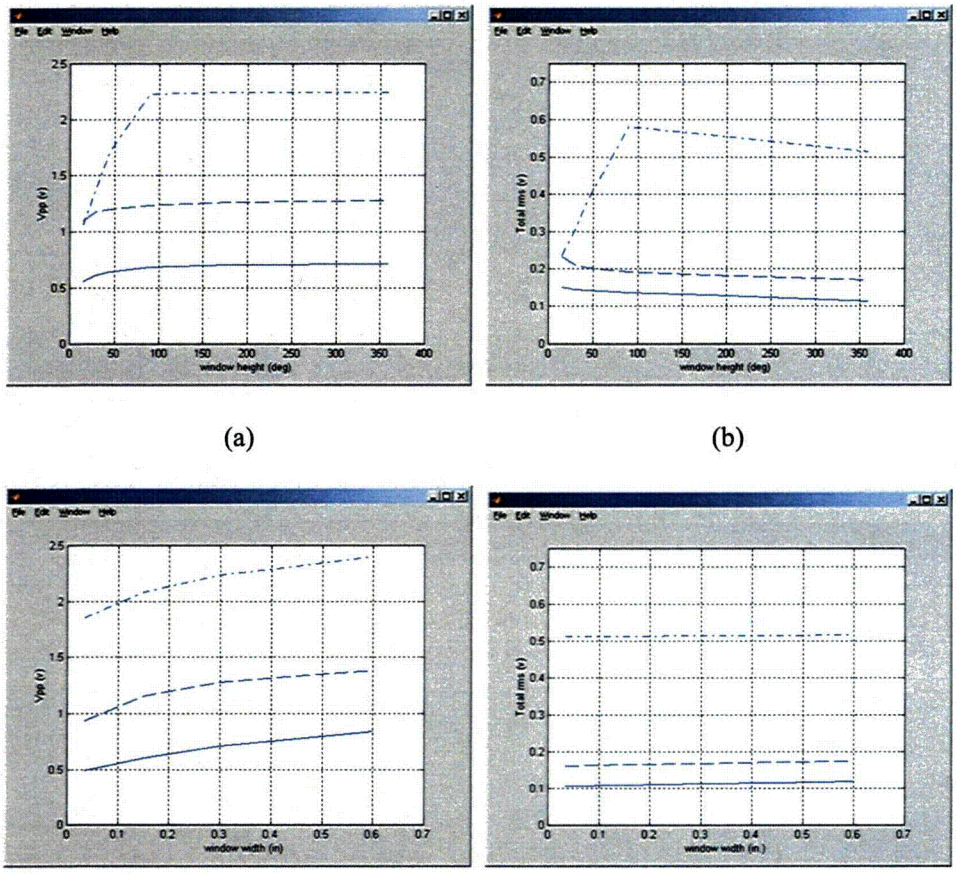

Figure 2.39 *Second parametric evaluation of noise influence on rotating probe data from mock-up test section of Fig. 2.36(b). Graphs show (a) mean V_{pp} and (b) total RMS noise that include contributions from horizontal and vertical components as a function of window height for a fixed window width of 7.6 mm (0.3 in), and (c) mean V_{pp} and (d) total RMS noise as a function of window width for a fixed window height of 360°. Results are for 2.92-mm (0.115-in)-diameter pancake at 300 kHz without (solid curves) and with random (dashed curves) and composite (dash-dot curves) noise. The region of interest is two 25.4-mm (1.0-in)-long free-span sections on both sides and away from the TSP edges.*

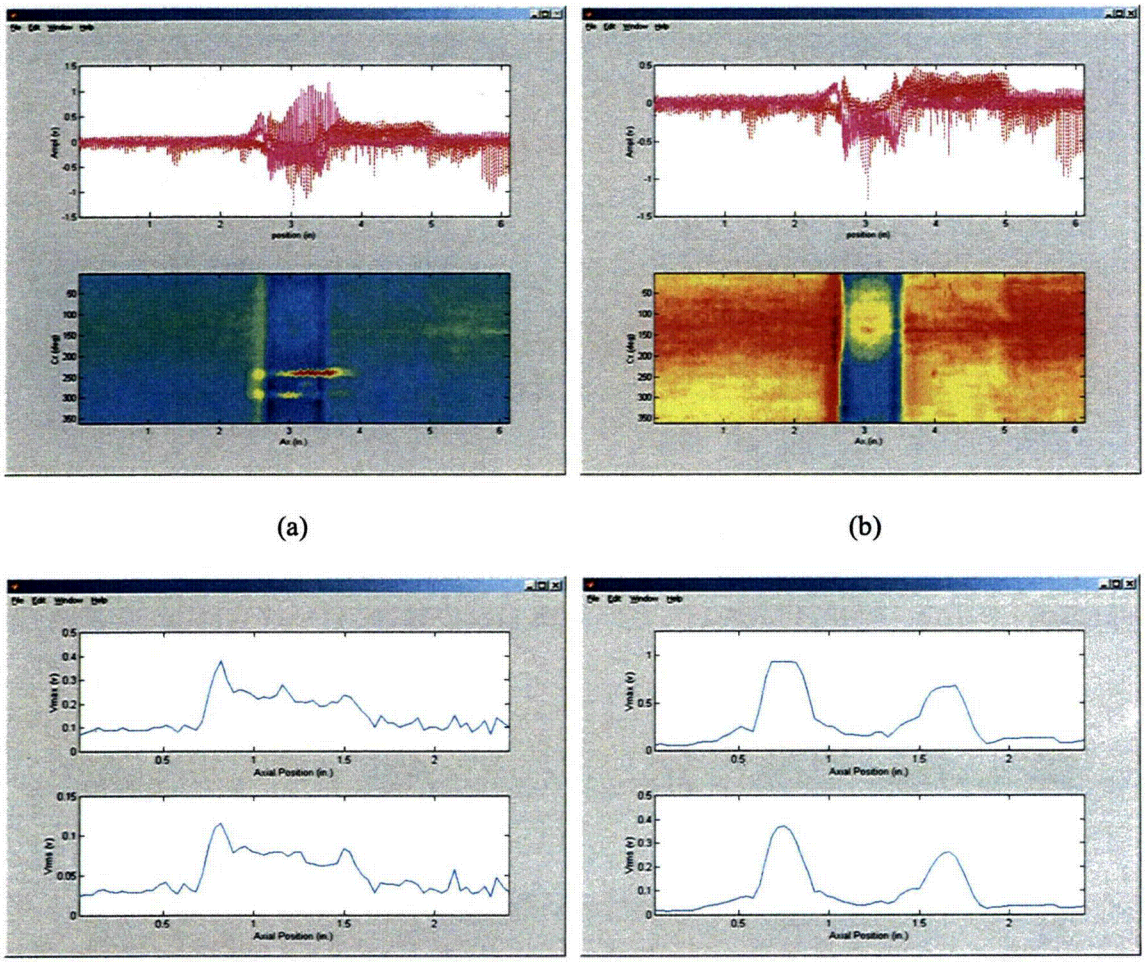

Figure 2.40 *Measurement of noise at the same location as the flaw. Graphics display the intermediate stages of the process (a) before and (b) after elimination of the flaw signal from the TSP intersection with ODSCC indications. Also shown are V_{max} and V_{rms} noise along the tube axis using (c) 0.9-mm (0.035-in) window width and 45° window height and (d) 7.6-mm (0.3-in) window width and 5° window height. The region of interest is a 63.5-mm (2.5-in)-long section of tube centered approximately at the middle of the TSP.*

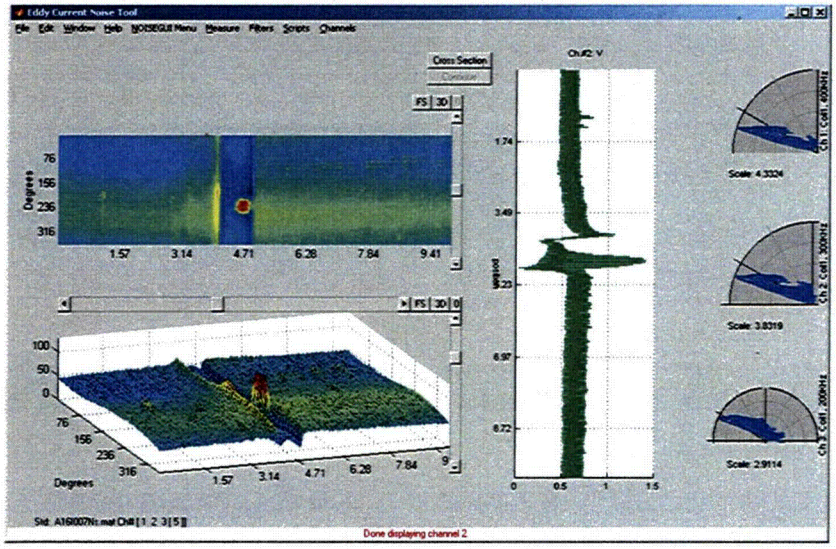

a)

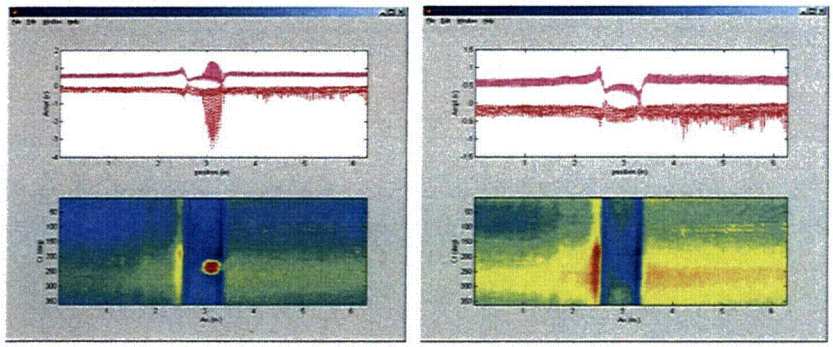

(b)

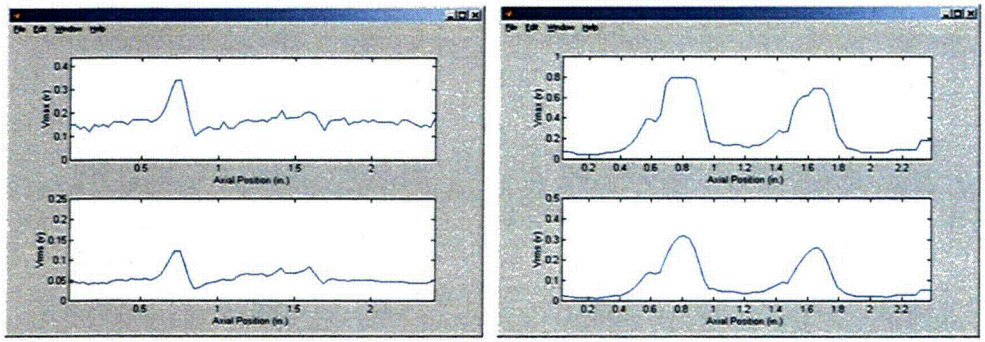

(c) (d)

Figure 2.41 *Measurement of noise in rotating probe data from mock-up test section with dent at TSP intersection. Graphics show (a) original data displayed by GUI in various formats and (b) intermediate stages of the process before and after elimination of dent signal from TSP. Also shown are V_{max} and V_{rms} noise along the tube axis using (c) 0.9-mm (0.035-in) window width and 90° window height and (d) 7.6-mm (0.3-in) window width and 4° window height. The region of interest is a 63.5-mm (2.5-in)-long section of tube centered approximately at the middle of the TSP.*

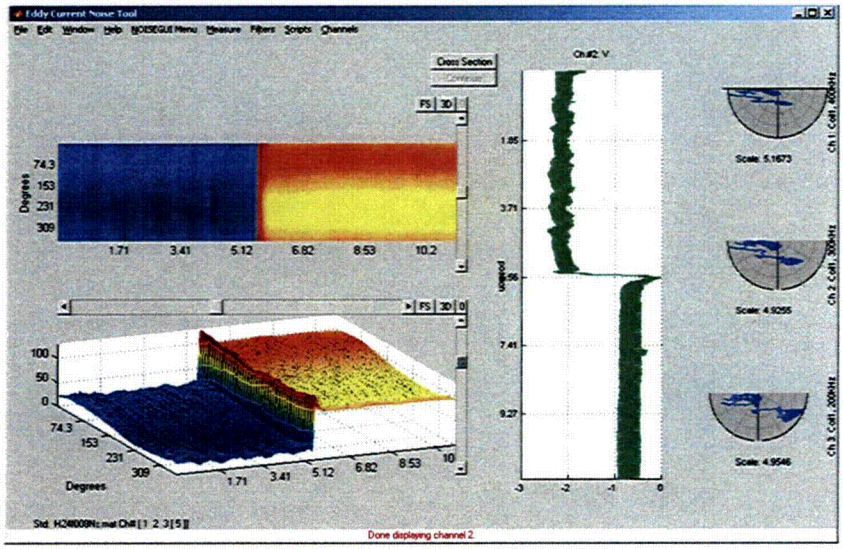

(a)

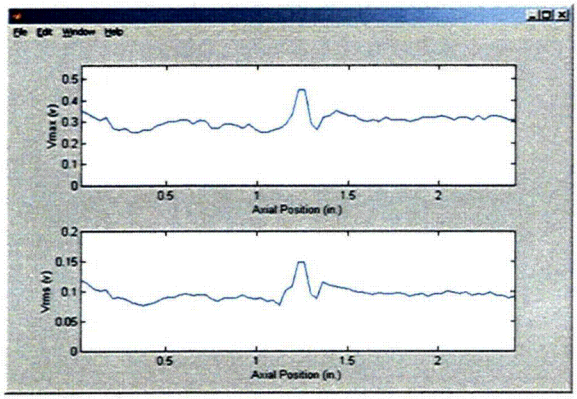

(b)

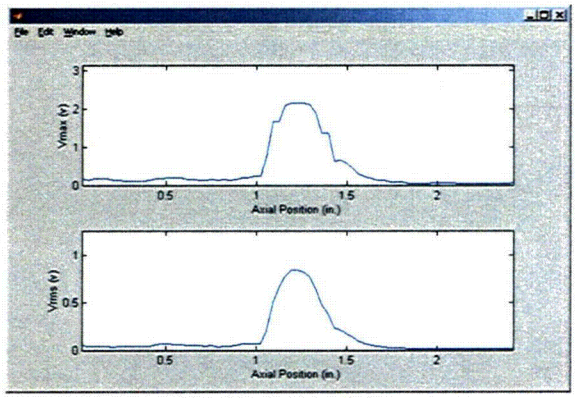

(c)

Figure 2.42 *Measurement of noise in rotating probe data from flaw-free mock-up TS test section. Graphics show (a) original data displayed by GUI in various formats. Also shown are V_{max} and V_{rms} noise along the tube axis using (b) 0.9-mm (0.035-in) window width and 90° window height and (c) 7.6-mm (0.3-in) window width and 4° window height. The region of interest is a 63.5-mm (2.5-in)-long section of tube centered approximately at the middle of the roll transition.*

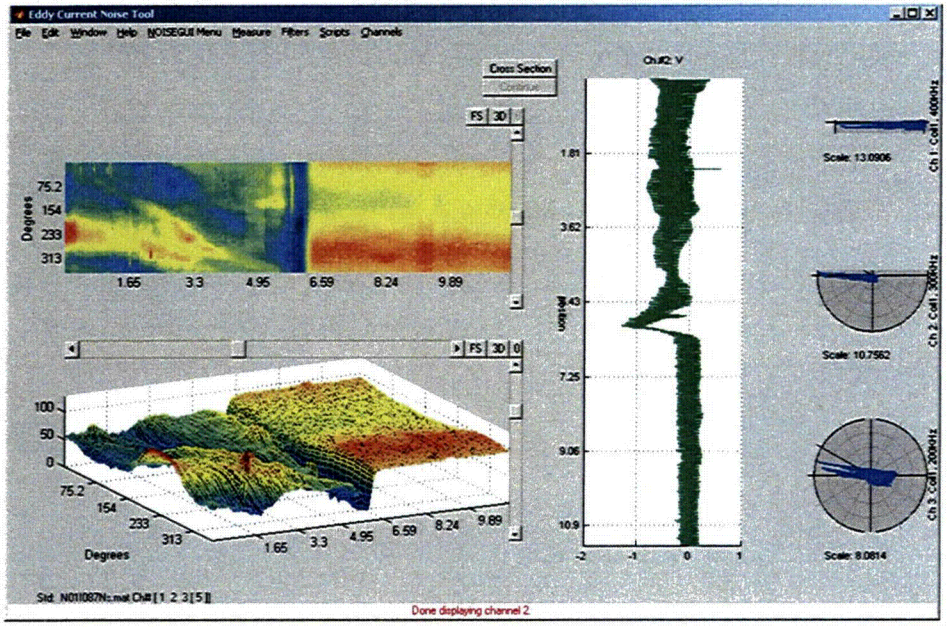

(a)

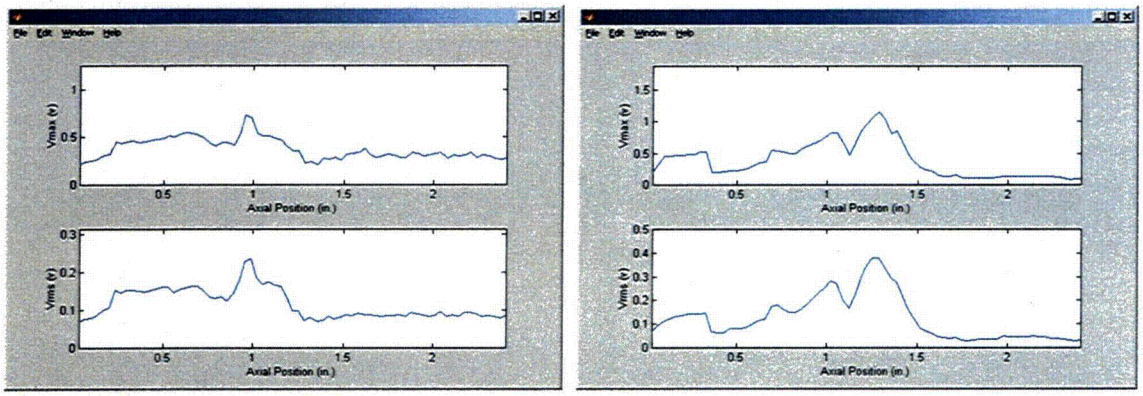

(b) (c)

Figure 2.43 Measurement of noise in rotating probe data from mock-up TS test section with large difference in level of noise above and below the roll transition region. Graphics show (a) original data displayed by GUI in various formats. Also shown are V_{max} and V_{rms} noise along the tube axis using (b) 0.9-mm (0.035-in) window width and 90° window height and (c) 7.6-mm (0.3-in) window width and 4° window height. The region of interest is a 63.5-mm (2.5-in)-long section of tube centered approximately at the middle of the roll transition.

3 Influence of Eddy Current Noise on Detection of Mock-up Flaws

Calculations were performed to assess the noise level in bobbin coil data collected from the SG tube bundle mock-up at Argonne. The goal of this investigation was to identify methods for measuring the noise associated with several flawed regions of tubing. This information could then be used to adjust the POD for the flaws in the mock-up to account for different levels of noise.

3.1 Assessment of Noise Level

The viability of statistical (e.g., RMS and mean value) and direct measures (e.g., *S/N* based on V_{max} or V_{pp} measurement) of noise level was examined in the previous sections of this report. Based on the results of these investigations, several measures of noise were chosen to quantify the level of EC noise in the data acquired from the tube bundle mock-up.[7] The essential factors in selecting these parameters included a) reproducibility of the measurement results, b) responsiveness to local and global variations in the level of noise, and c) correlation with detection probability. Bobbin probe data from a subset of mock-up test sections were selected for analysis. The procedures and the results on the assessment of noise level based on this database are discussed next.

3.1.1 Data Selection Criteria

Bobbin-coil inspection data from a subset of test sections from the tube bundle mock-up have been identified for analyses associated with the assessment of noise level. Eighteen test sections were initially included for this purpose. Except for three free-span test sections, all degradations were located at TSP intersections. Candidate tubes were selected primarily on the basis of the previous assessments of the POD curves. These POD curves for various flaw categories in the mock-up were obtained by using the data analysis results from eleven teams of analysts who participated in the round-robin exercise as discussed in Reference 7. Each team consisted of at least three analysts (i.e., a primary, a secondary, and a resolution analyst). Only those test sections for which at least one analyst team or a number of individual analysts from different teams missed the flaw, which suggests a borderline indication, were included in the database. This selection criterion was based on the assumption that the effect of noise on detection probability would be less pronounced on data points located at the extreme ends of the POD curve (i.e., high and low *S/N*), which typically include flaw signals that exhibit a very large or small amplitude response. Thus, it is necessary to examine only the limiting flaws to assess the POD. With that in mind, one test section was later excluded from the database because, following the analyses, it was decided that the reason for missing that particular flaw was not the level of EC noise. Data from this test section along with further explanation of the exclusion criteria are provided below. It should also be noted that the limited data used in the assessments here may not constitute a statistically significant database.

3.1.2 Calibration Procedure for Bobbin Coil Data

Calibration and analyses of EC data were all performed off-line using software-based tools developed at Argonne. These tools along with sample calculations are described in Sec. 2.2. For the calibration of bobbin coil data, a procedure similar to that implemented during field inspections was followed. Measurements at all locations along the tube were made on data from the 400|100 kHz differential mix channel. Sample calculations and verification of the least-squares-based mix results are given in Sec. 2.2.2. For amplitude

calibration, the peak-to-peak value of the signal from the four flat-bottom holes (FBH) in the ASME standard was set to 4 V for the 400 kHz channel. Data for all other differential channels were then scaled relative to that channel. This amplitude scaling typically results in the magnitude of the probe response from four 20% OD holes in the mix channel being ≈ 2.75 V. For phase-angle alignment, the response from the 100% TW hole on the ASME standard was set to 40° at all differential test frequencies prior to generation of the processed channel data. This step results in a phase angle of $\approx 35^{\circ}$ for the 100% TW hole from the mix channel data.

Because the phase angle of the EC probe response affects the measurement of the vertical and horizontal components of data, uniform calibration of data is crucial for reliable measurement of these variables. While the calibration procedure described above serves this purpose for the analyses of the limited database here, for more repeatable measurements when the noise is measured from the mix channel, the amplitude scaling and phase alignment should be performed directly on the mix channel data. Also, as with any other comparative NDE method, a reference standard is used to compensate for differences in probe response due to any manufacturing variability.

3.1.3 Procedure for Measurement of Noise Level

Based on the studies here and elsewhere, several viable methods can be employed for measuring the noise level in EC inspection data. These methods are based on measuring the vertical component (V_{max}) and the magnitude (V_{pp}) of the probe response over the region of interest. Equations for calculation of these indicators are given in Sec. 2.2.3. Several indicators of the noise level in a subset of test sections from the mock-up were calculated using the sliding window approach described earlier in this report and are presented in Sec. 3.2. Measurement parameters and procedures that are common in all calculations are described below.

The measurement variables (i.e., window and segment length) that are provided as input to the computer scripts used to calculate the noise level in the EC inspection data are in units of length. Therefore, data points are initially converted to units of length by using a scaling factor. The axial scaling of bobbin probe data for each test section was first performed by using either the distance between known discontinuities in that test section or a pre-determined scaling factor, calculated from known distances between manufactured flaws in a calibration standard tube. Based on the results of investigations presented earlier in this report, a sliding measurement window length of 20.3 mm (0.8 in) was used in all test cases. The measurement region consisted of a 38.1-mm (1.5-in) data segment on each side of the flawed zone. To avoid interference from nearby discontinuities and potential indications, slightly shorter data segments were used in a few cases. For assessment of the global level of noise, the selected region of interest was away from the flaw signal and included only a free-span region of the tube. Both maximum and average values were calculated over that region. For assessment of the local level of noise, the selected region of interest included the portion of the tube immediately outside the flawed zone (i.e., it included the response from any existing support structures). For cases in which the flaw extended outside the TSP edges, a different procedure was used since the response from the TSP residual signal (potential source of signal distortion at TSP intersections) is not always separable from the flaw signal if the flaw extends beyond the TSP edge. In these cases, the TSP mix residual signal was calculated independently by using the data acquired from a calibration standard tube with a simulated TSP collar. The residual signal obtained in this manner is expected to provide a lower limit on the level of noise that could actually be present at the flawed TSP intersection and, thus, may not provide a conservative estimate of detection capability. In practice, the noise level measured from flaw-free intersections at the same elevation in the SG could be used for such assessments when a flaw extends beyond the edges of the TSP.

3.2 Evaluation of Parameters for Establishing Detection Limit

This section reports the results of measurements of noise level in the EC inspection data from the mock-up. Bobbin coil data from 18 test sections were initially included for analysis. As discussed earlier, the flaws in this database were all identified as being borderline indications because at least one analyst team or a number of individual analysts from different teams did not identify the flaw signal in the test section. Measurements were performed on both the original data and simulated data with a low level of superimposed noise.

3.2.1 Composition of Database for Noise Level Assessments

Figures 3.1 to 3.18 show the processed channel data for all eighteen test sections included in the evaluation. Except for three cases, flaws in these tubes were located at dented and non-dented TSP intersections. Both the original data and simulated data with superimposed noise are shown in each figure. Data are presented in a strip chart and in a lissajous pattern (i.e., impedance plane trajectory) for a small section encompassing the flaw signal. Simulated composite noise in all test cases consisted of a low-amplitude random and a periodic component. Several examples on generating this type of noise were presented earlier in this report. The random noise had an amplification factor of one for both the horizontal and vertical components and was added to every other data point. The periodic noise had an amplification factor of 0.125, which corresponds to a peak-to-peak amplitude of 0.25 V. Other variables for the simulated periodic noise, including periodicity and eccentricity, were adjusted in the same manner as that given in earlier examples.

Figure 3.1(a) shows the original and noise-injected data for the first test section. To demonstrate the statistical nature of noise, Fig. 3.1(b) shows the case where the same level of noise as in Fig. 3.1(a) was added to the original data but with different initial seeding for random noise and 90° phase shift of the periodic component. This test case shows that the same level of noise can lead to a remarkably different degree of distortion of low amplitude signals. As discussed earlier, this difference occurs because noise can interfere both constructively and destructively with the signal. This observation explains why the *S/N* can increase in some cases when the data possess a higher level of noise. However, this phenomenon primarily affects more subtle indications that typically exhibit a low amplitude response. Results of analyses provided below include additional test cases that further demonstrate this effect.

For the analyses presented here, simulated noise was added only once to the mix channel data for each test section. This limitation is considered acceptable since the data were selected so that the signals and noise levels would represent limiting cases for assessing the detection capability. The statistical nature of noise, however, suggests that it would be more realistic to consider the effect of adding the same level of simulated noise with random seeding multiple times to each data segment. The influence of noise would be represented even more accurately by generating noise with variable amplitudes. By means of the analysis tools described in this report, databases could easily be augmented with a statistically significant number of test cases.

Figure 3.2 shows, in addition to display of the EC signal before and after addition of noise to data from the second test section [Fig. 3.2(a)], plots of the spatial distribution of noise level along the tube axis [Fig. 3.2(b)]. The graphics from this intermediate step show V_{max} and V_{rms} values overan $\approx$ 38-mm (1.5-in)-long section on each side of the flawed location.

Measured values of V_{max}, V_{rms}, and V_{pp} over the ROI are used next (Sec. 3.2.2) to determine the viability of these parameters for assessing the influence of noise on detection. As mentioned earlier, the data

from the seventh test section, shown in Fig. 3.7, was excluded from the analyses. The basis for marking this particular test section as an outlier was that the missing of the flaw signal could not be correlated with the level of noise present in the data. Expert judgment concluded that analyst misinterpretation of the probe response was the most likely cause for the missed call. While setting data exclusion criteria is not generally considered as a safe practice for the analysis of EC inspection data from SG tubes, including the outlier data in the analyses here would have resulted in unrealistic assessments for the effect of noise on detection probability.

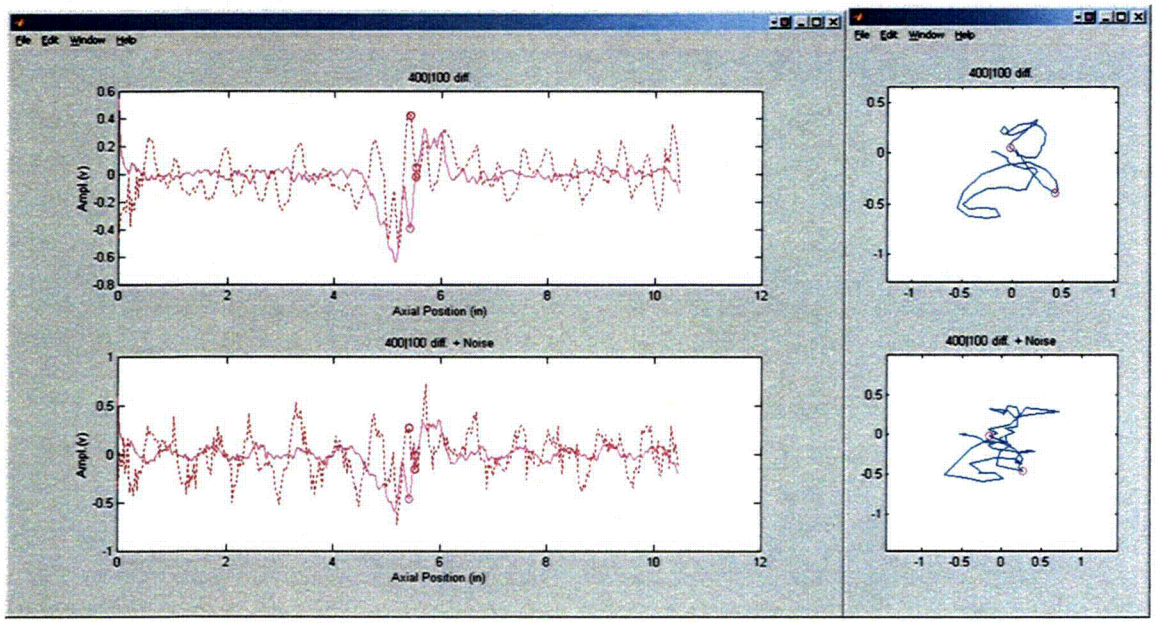

(a)

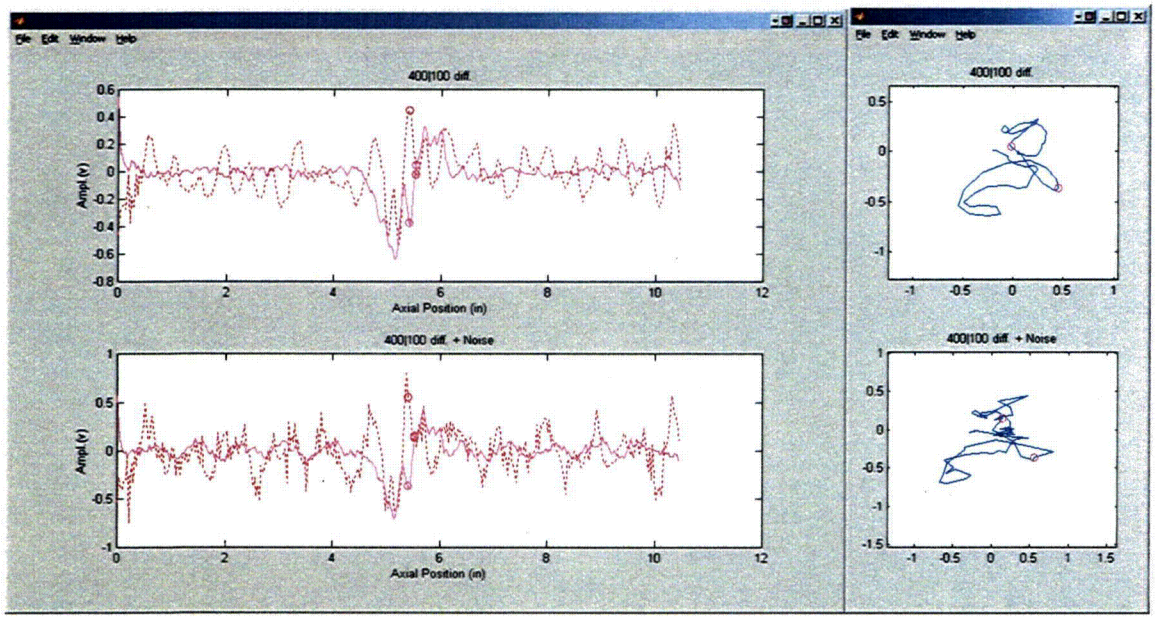

(b)

Figure 3.1 *Eddy current data collected with bobbin coil from test section #1 with flaw at TSP intersection. The figure shows representative displays of data in strip chart (left) and lissajous (right) formats without (top) and with (bottom) simulated composite noise consisting of a small random and a periodic component. The results shown in (a) and (b) demonstrate that the same level of simulated noise added to different points in the original data can distort the signal differently.*

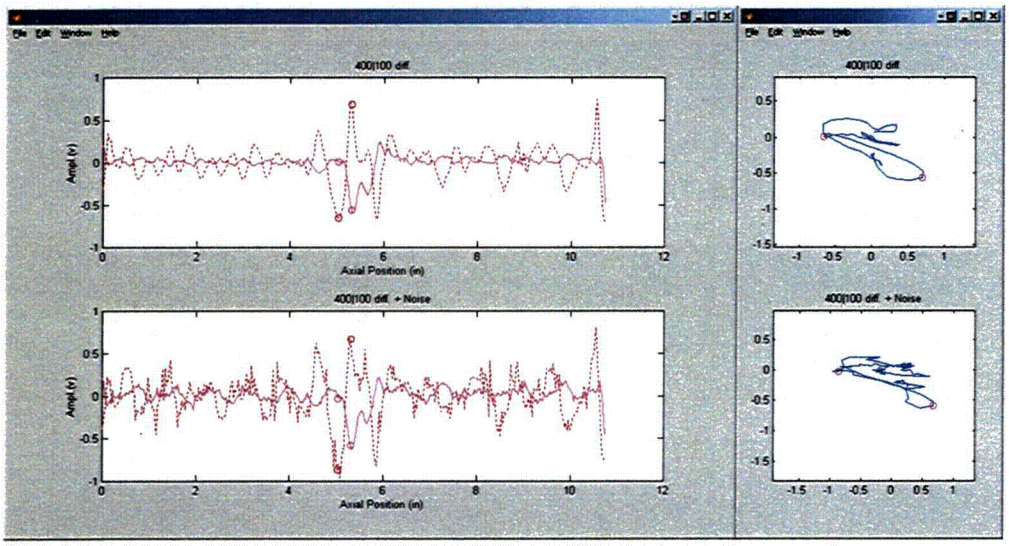

(a)

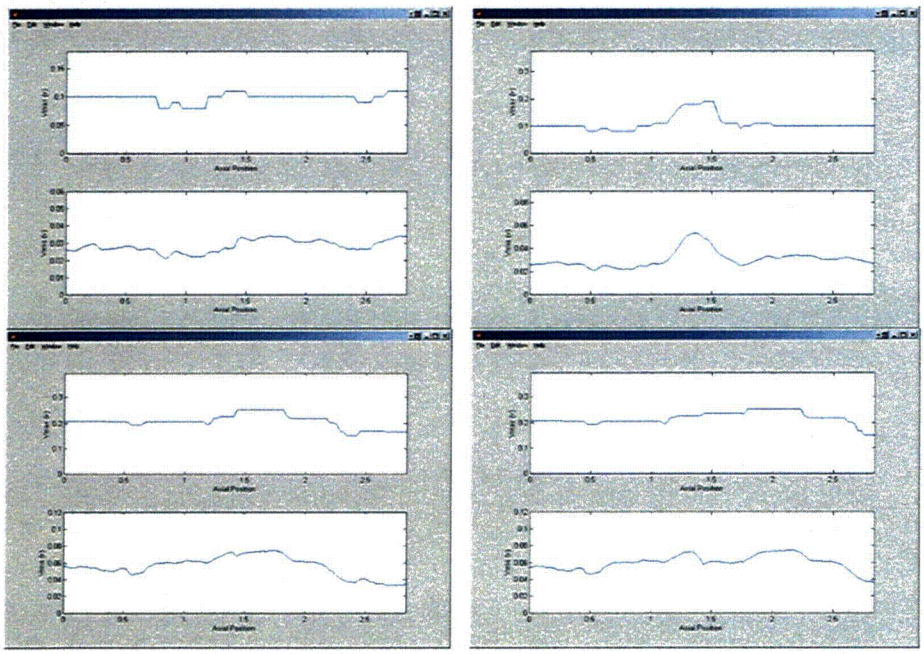

(b)

Figure 3.2 *Eddy current data collected with bobbin coil from test section #2 with flaw at TSP intersection. Graphics show (a) representative display of data in strip chart (left) and lissajous (right) format without (top) and with (bottom) simulated composite noise consisting of a small random and a periodic component. Also shown in (b) are the spatial distribution of V_{max} (upper trace) and vertical RMS (lower trace window) noise level with the ROI encompassing only the free-span region (left) and TSP (right) for the original (top) and simulated data (bottom) with added level of noise.*

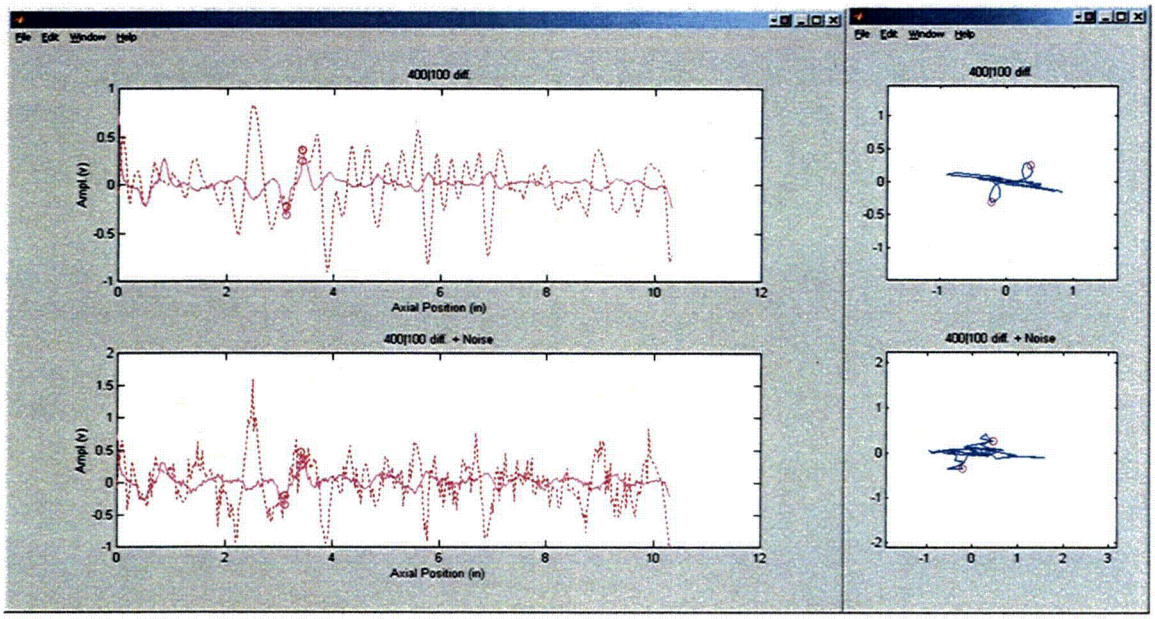

Figure 3.3 *Eddy current data collected with bobbin coil from test section #3 with flaw at free-span region. Graphics show representative display of data in strip chart (left) and lissajous (right) format without (top) and with (bottom) simulated composite noise consisting of a small random and a periodic component.*

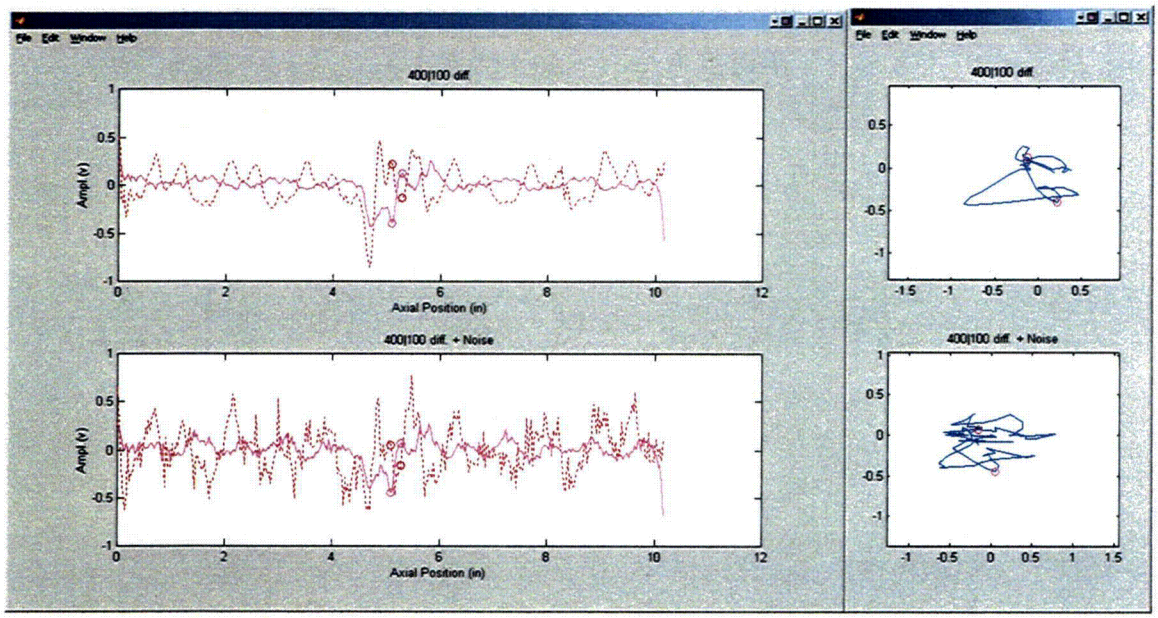

Figure 3.4 *Eddy current data collected with bobbin coil from test section #4 with flaw at TSP intersection. Graphics show representative display of data in strip chart (left) and lissajous (right) format without (top) and with (bottom) simulated composite noise consisting of a small random and a periodic component.*

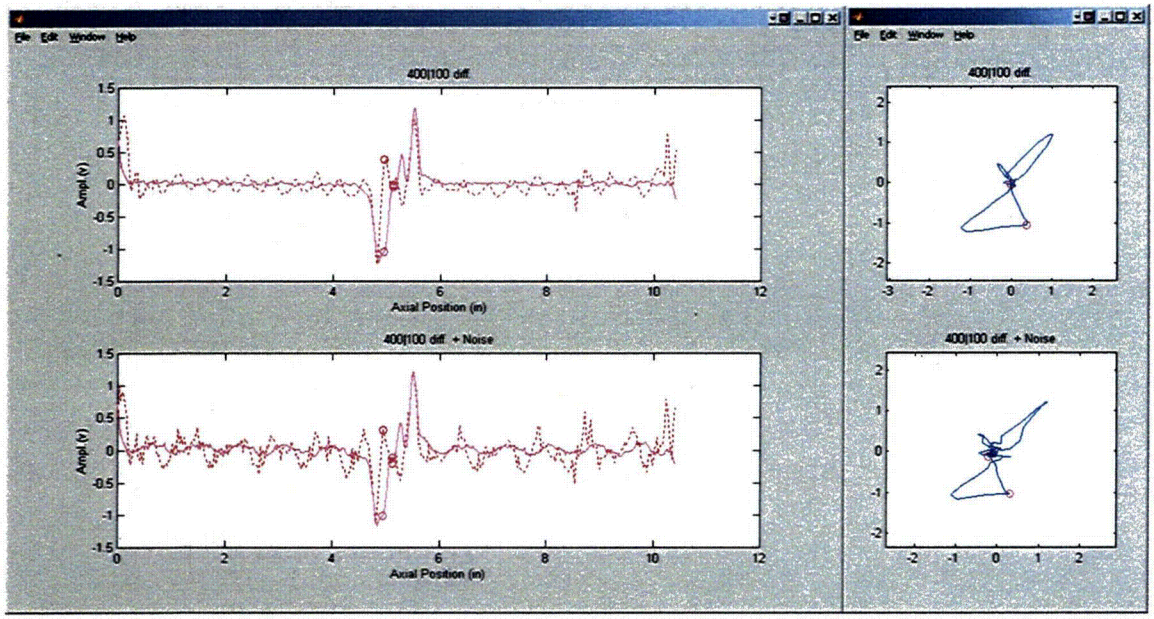

Figure 3.5 *Eddy current data collected with bobbin coil from test section #5 with flaw at TSP intersection. Graphics show representative display of data in strip chart (left) and lissajous (right) format without (top) and with (bottom) simulated composite noise consisting of a small random and a periodic component.*

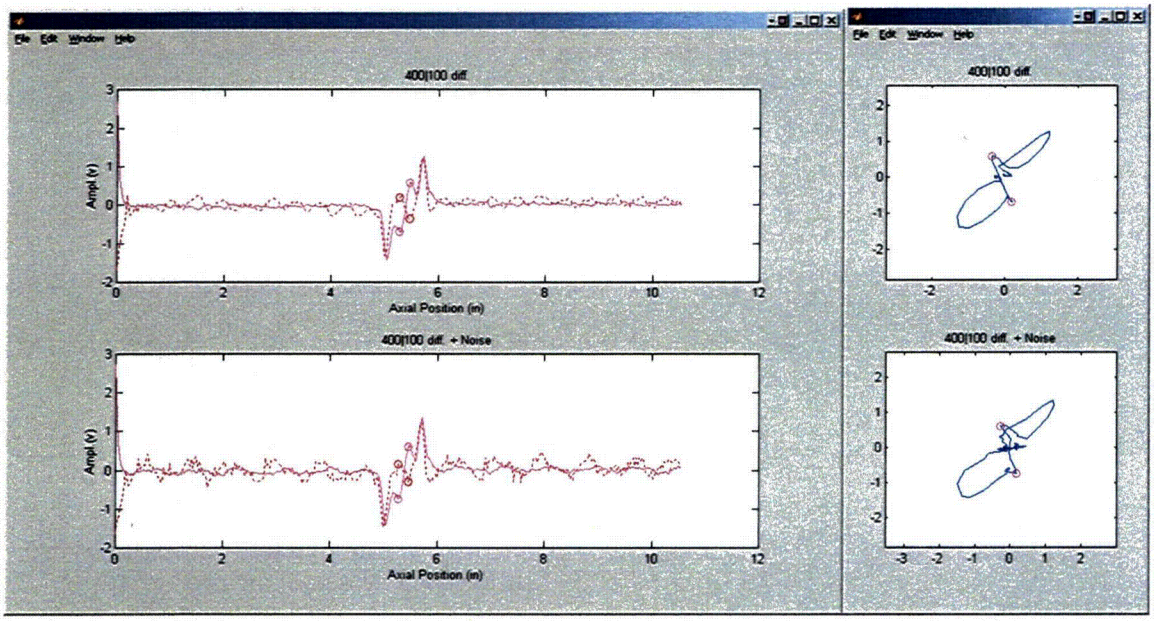

Figure 3.6 *Eddy current data collected with bobbin coil from test section #6 with flaw at TSP intersection. Graphics show representative display of data in strip chart (left) and lissajous (right) format without (top) and with (bottom) simulated composite noise consisting of a small random and a periodic component.*

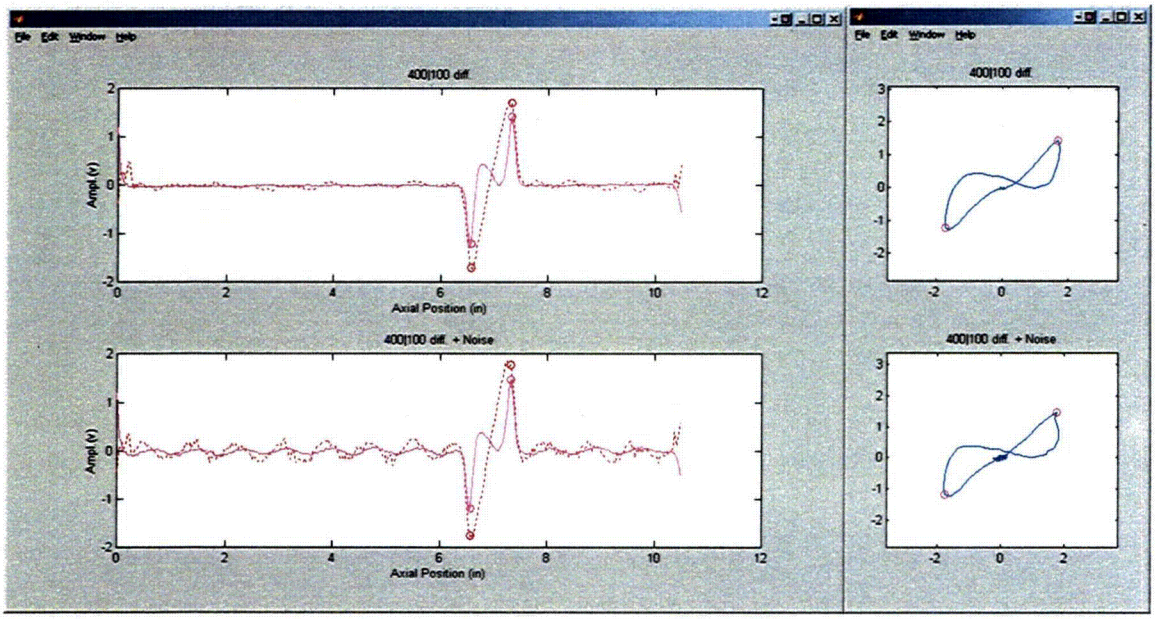

Figure 3.7 *Eddy current data collected with bobbin coil from test section #7 with flaw at free-span region. Graphics show representative display of data in strip chart (left) and lissajous (right) format without (top) and with (bottom) simulated composite noise consisting of a small random and a periodic component.*

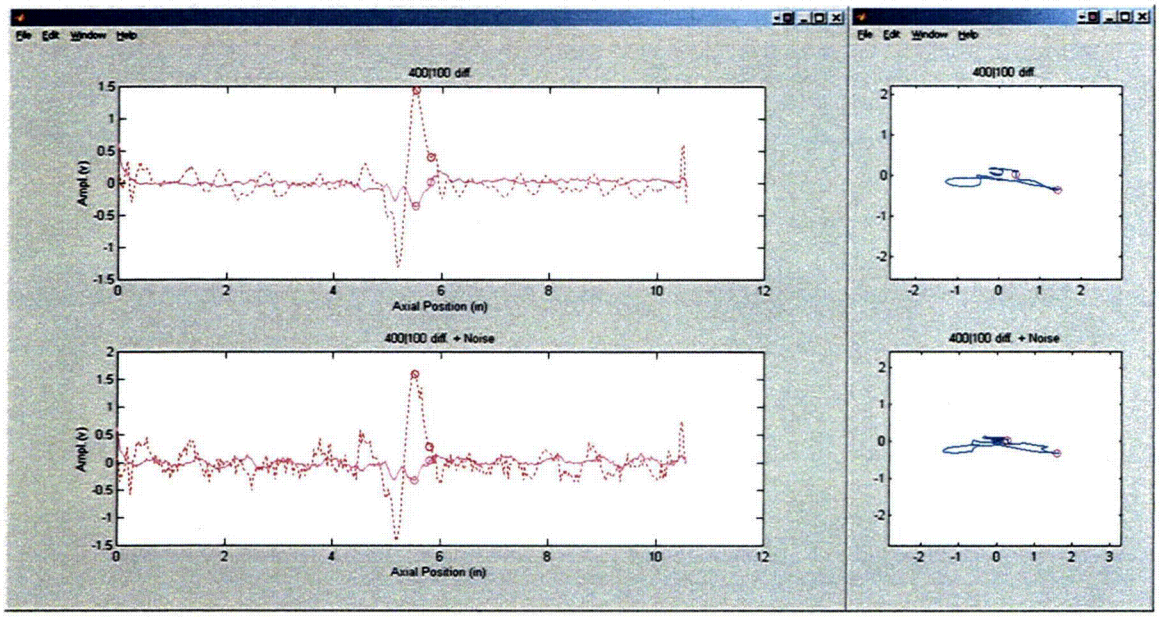

Figure 3.8 *Eddy current data collected with bobbin coil from test section #8 with flaw at TSP intersection. Graphics show representative display of data in strip chart (left) and lissajous (right) format without (top) and with (bottom) simulated composite noise consisting of a small random and a periodic component.*

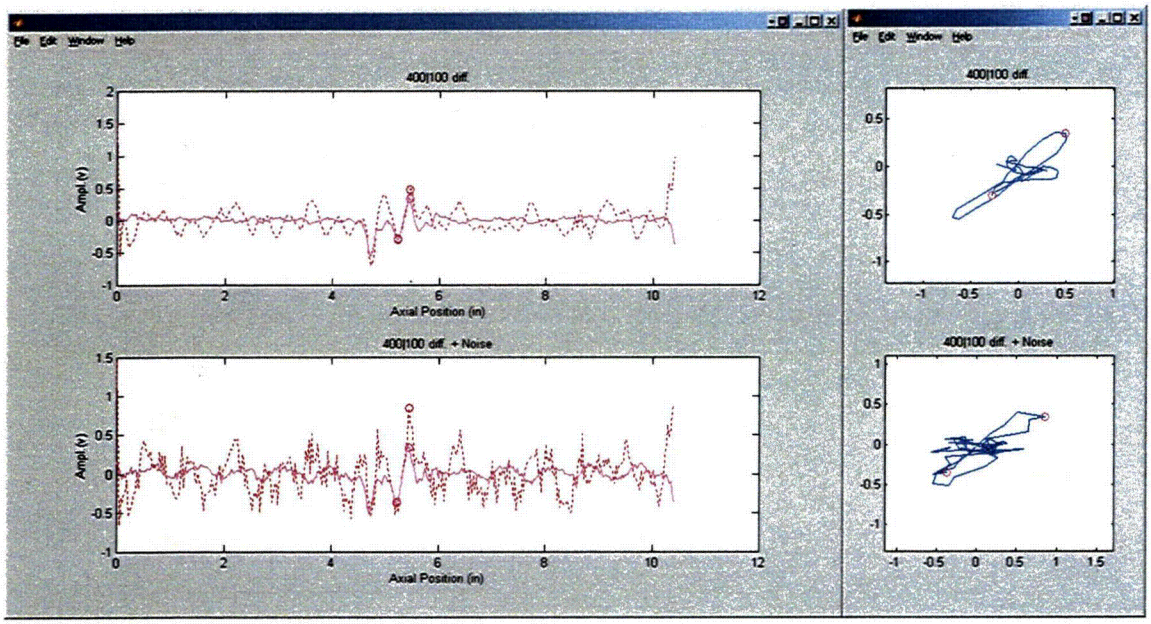

Figure 3.9 *Eddy current data collected with bobbin coil from test section #9 with flaw at TSP intersection. Graphics show representative display of data in strip chart (left) and lissajous (right) format without (top) and with (bottom) simulated composite noise consisting of a small random and a periodic component.*

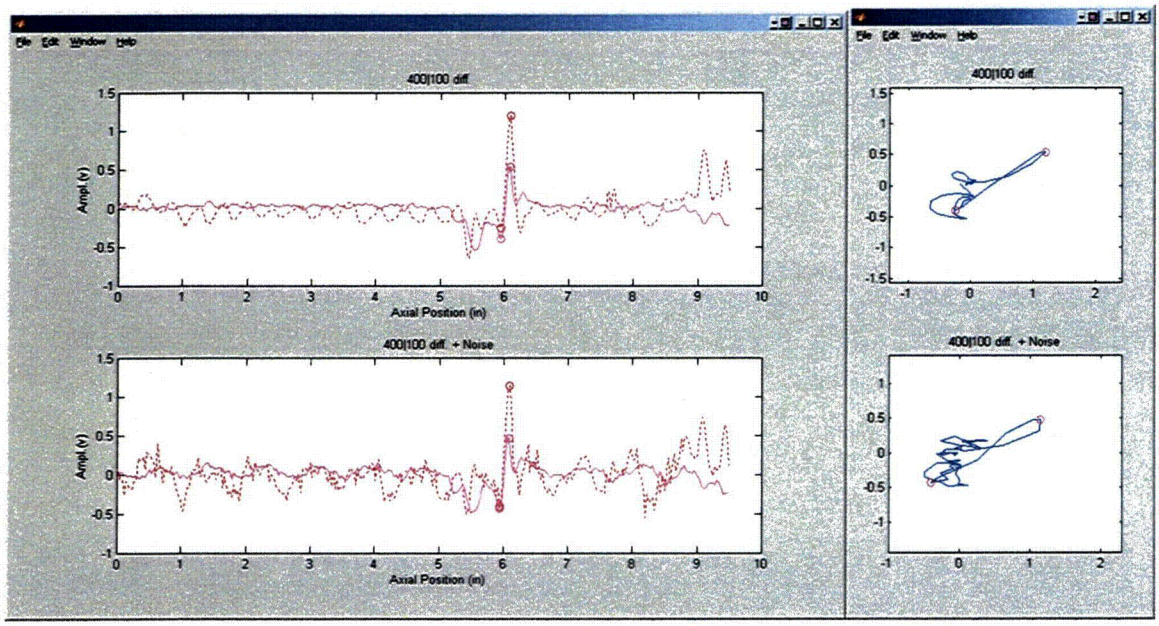

Figure 3.10 *Eddy current data collected with bobbin coil from test section #10 with flaw at TSP intersection. Graphics show representative display of data in strip chart (left) and lissajous (right) format without (top) and with (bottom) simulated composite noise consisting of a small random and a periodic component.*

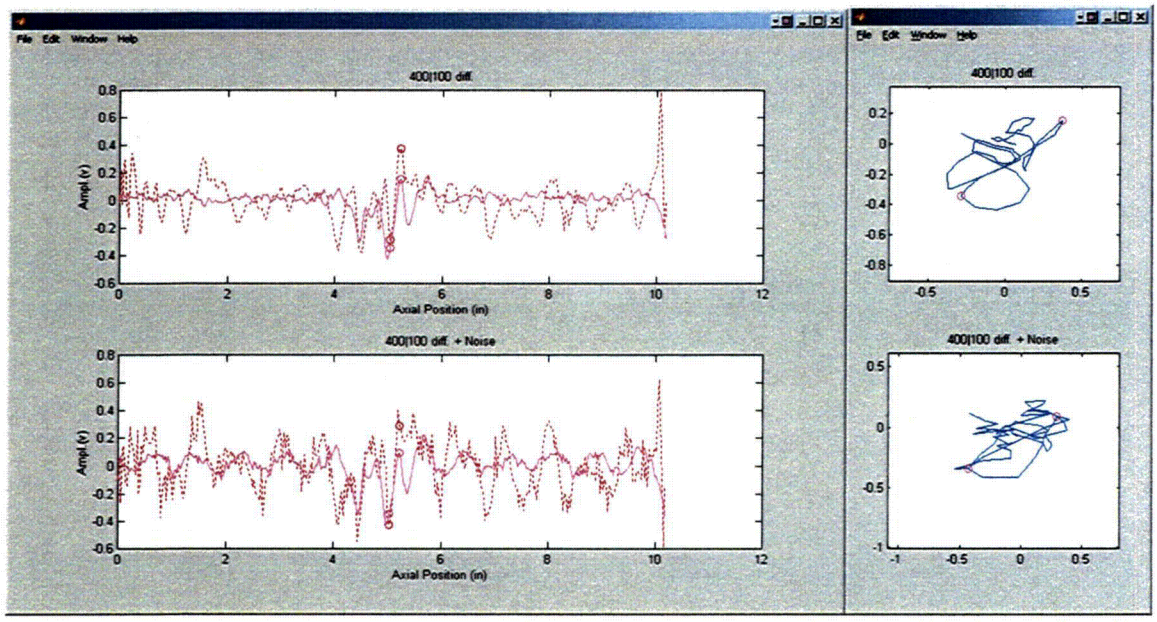

Figure 3.11 *Eddy current data collected with bobbin coil from test section #11 with flaw at TSP intersection. Graphics show representative display of data in strip chart (left) and lissajous (right) format without (top) and with (bottom) simulated composite noise consisting of a small random and a periodic component.*

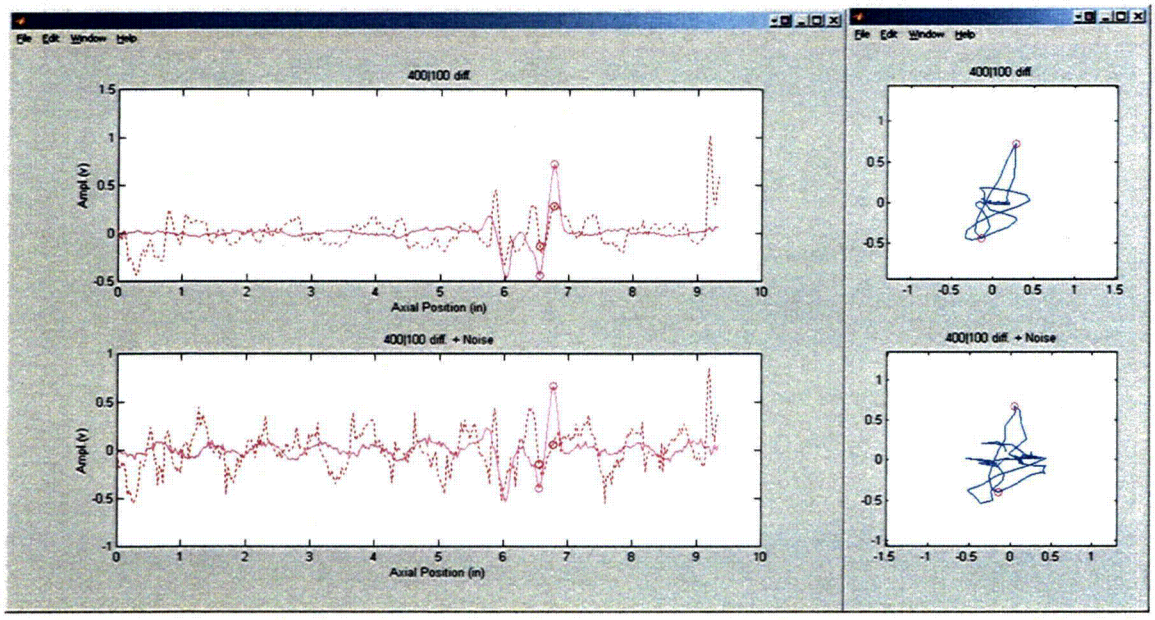

Figure 3.12 *Eddy current data collected with bobbin coil from test section #12 with flaw at TSP intersection. Graphics show representative display of data in strip chart (left) and lissajous (right) format without (top) and with (bottom) simulated composite noise consisting of a small random and a periodic component.*

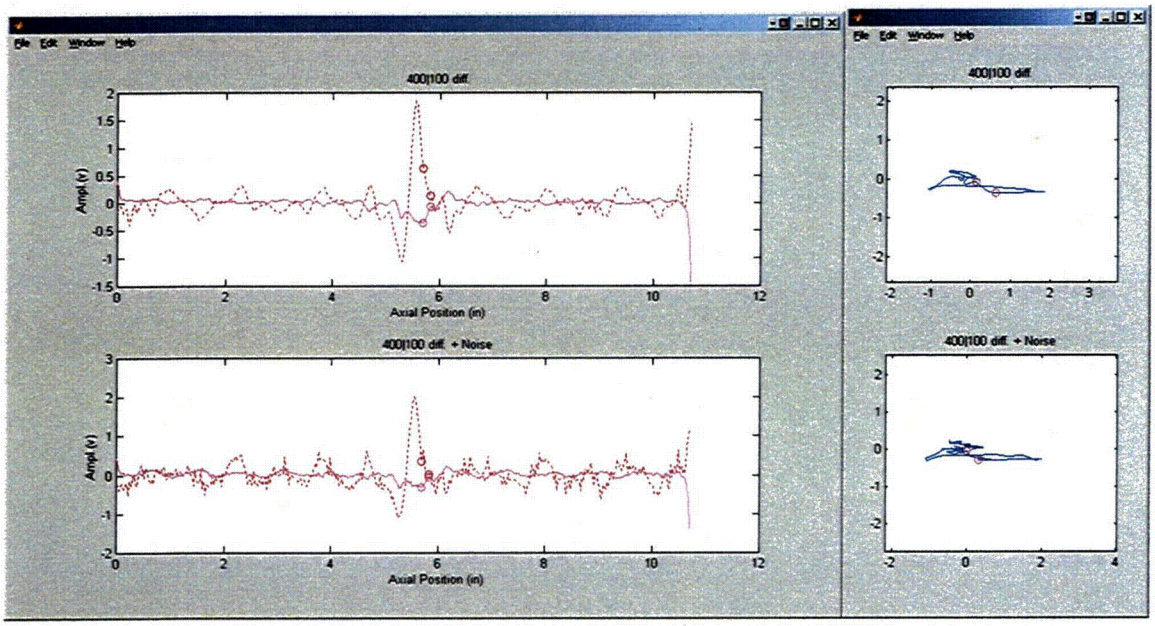

Figure 3.13 *Eddy current data collected with bobbin coil from test section #13 with flaw at TSP intersection. Graphics show representative display of data in strip chart (left) and lissajous (right) format without (top) and with (bottom) simulated composite noise consisting of a small random and a periodic component.*

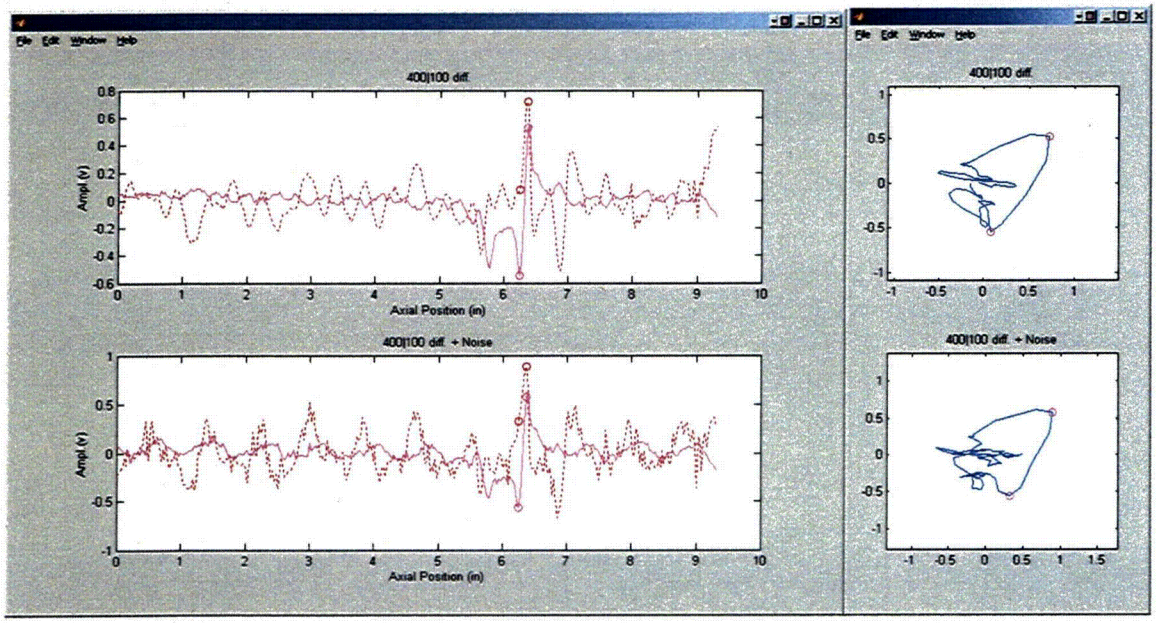

Figure 3.14 *Eddy current data collected with bobbin coil from test section #14 with flaw at TSP intersection. Graphics show representative display of data in strip chart (left) and lissajous (right) format without (top) and with (bottom) simulated composite noise consisting of a small random and a periodic component.*

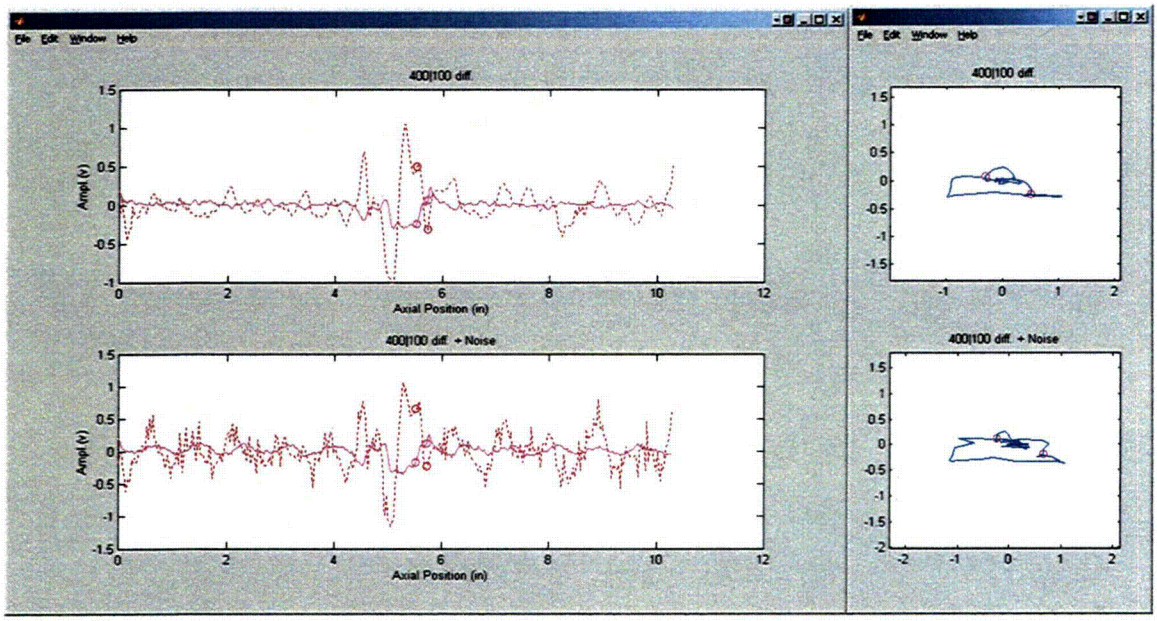

Figure 3.15 *Eddy current data collected with bobbin coil from test section #15 with flaw at TSP intersection. Graphics show representative display of data in strip chart (left) and lissajous (right) format without (top) and with (bottom) simulated composite noise consisting of a small random and a periodic component.*

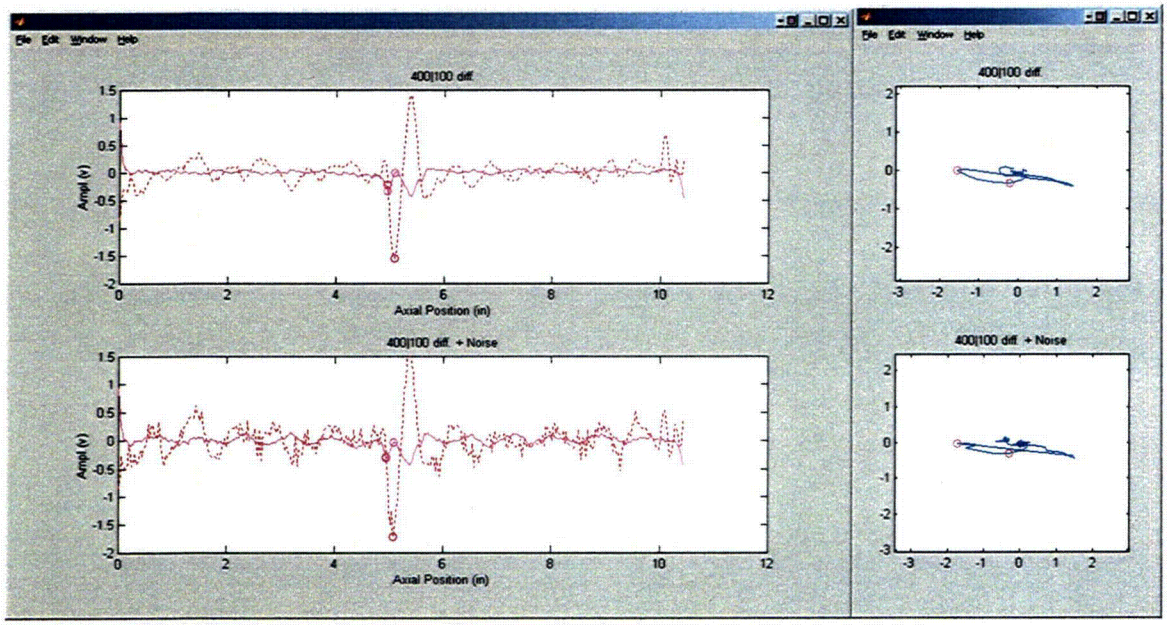

Figure 3.16 *Eddy current data collected with bobbin coil from test section #16 with flaw at TSP intersection. Graphics show representative display of data in strip chart (left) and lissajous (right) format without (top) and with (bottom) simulated composite noise consisting of a small random and a periodic component.*

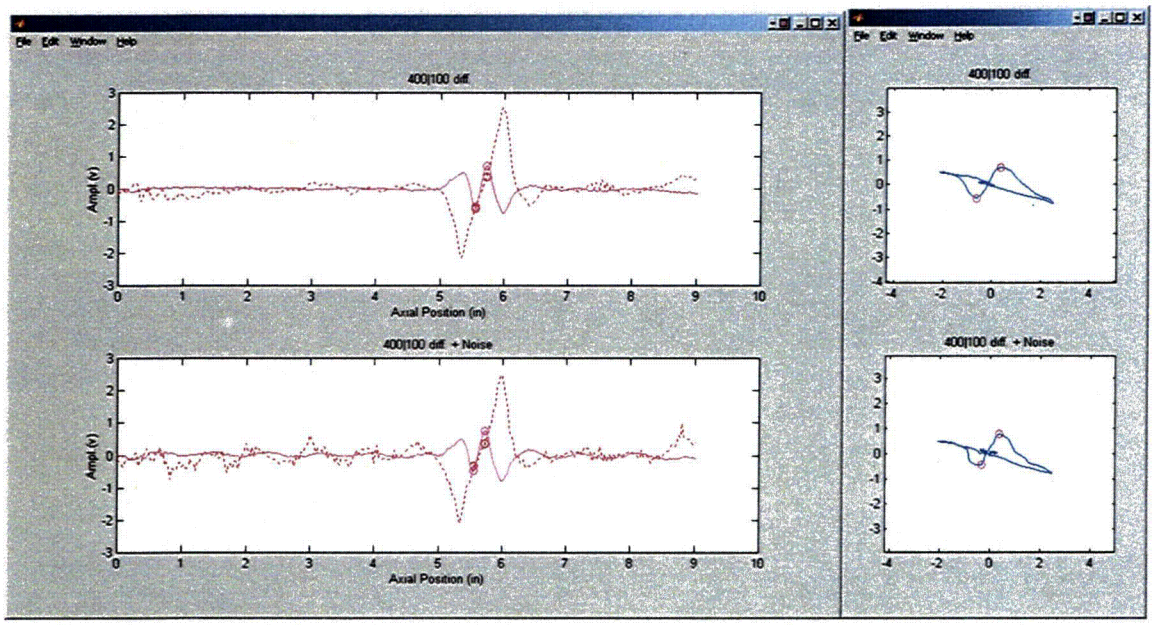

Figure 3.17 *Eddy current data collected with bobbin coil from test section #17 with flaw at TSP intersection. Graphics show representative display of data in strip chart (left) and lissajous (right) format without (top) and with (bottom) simulated composite noise consisting of a small random and a periodic component.*

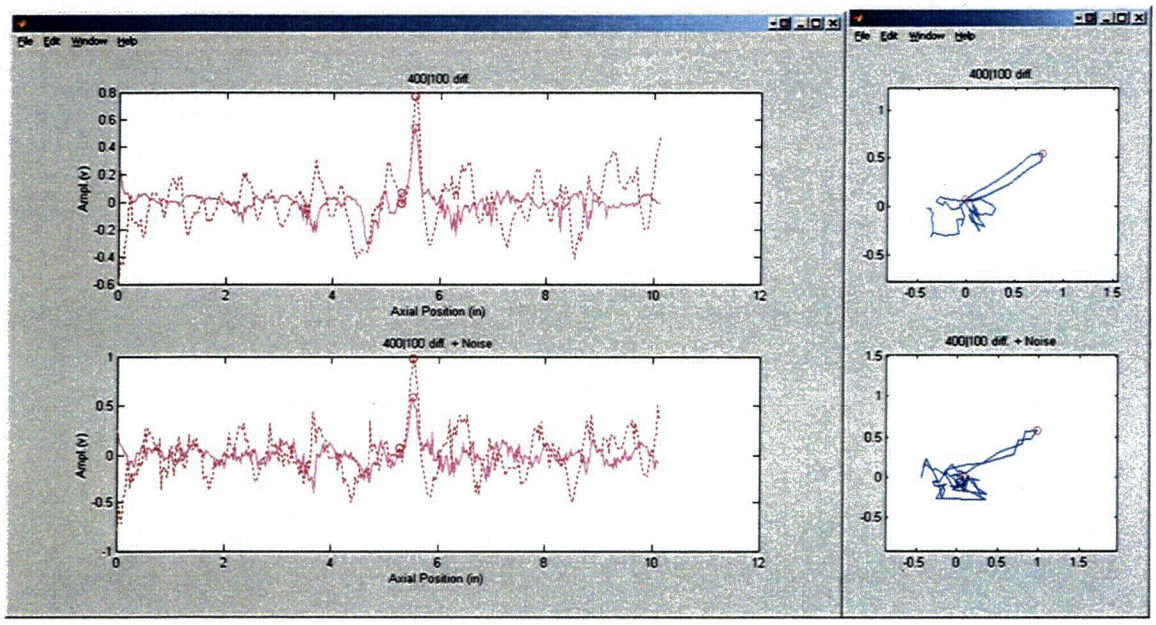

Figure 3.18 *Eddy current data collected with bobbin coil from test section #18 with flaw at free-span region. Graphics show representative display of data in strip chart (left) and lissajous (right) format without (top) and with (bottom) simulated composite noise consisting of a small random and a periodic component.*

3.2.2 Analysis of Measurement Results for Establishing Detection Probability

This section discusses the results associated with measurement of EC noise level in the database of test sections described above (with and without injected noise) and in a calibration standard tube. Investigations so far have shown that one of the sources of bobbin coil signal distortion at TSP intersections is the residual signal in the mix (i.e., processed) channel data. The response from the TSP residual signal, however, is not always separable from the flaw signal if the flaw extends beyond the TSP edge. For such cases, the TSP mix residual signal was calculated independently by using the data acquired from a calibration standard tube with a simulated TSP collar. The residual signal obtained in this manner is expected to provide a lower limit on the level of noise that could actually be present at the flawed TSP intersection and, thus, may not provide a conservative estimate of detection capability. Minimum and average values were also determined for the level of baseline noise, using V_{max} and V_{pp} measurements from non-flawed sections of the reference standard tube. Data obtained from these measurements are listed in Table 3.1.

Tables 3.2 and 3.3 list the measurement results for all the test sections included in the database for the original and noise-injected data, respectively. The measurements in both cases were made over the free-span region of each tube and outside the degraded zone. Parameters shown in those tables are the average and maximum level of noise over the ROI in each test section. Comparisons of the average RMS values for the vertical component and total noise, N^{v}_{RMS} and N^{T}_{RMS}, as well as the average vertical component and peak-to-peak values, V_{max} and V_{pp}, of the measured noise level in Tables 3.2 and 3.3 indicate only a moderate increase due to the added noise. As noted earlier, estimation of the free-span noise level based on the RMS or average value mainly provides a measure of data quality. The noise indices calculated based on the maximum value of all measurements over the ROI on the other hand seem to provide a more conservative estimate of the level of noise and thus its effect on detection.

To assess local noise, which has a greater impact on detection capability, RMS and peak-to-peak values were calculated from the maximum value of these variables computed in one of the windows over the flawed region, which also encompassed the probe response from the TSP. For those cases where the TSP response could not be isolated from the flaw signal, average values (i.e., mean value from multiple measurements of the level of noise associated with the residual signal) from Table 3.1 were used instead. This procedure was used for adjusting the level of noise for two TSP intersections in the entire data set. Tables 3.4 and 3.5 list the calculated results for several measures of noise using the maximum value of all measurements over the ROI in each test section. They include the vertical component and total RMS values; V_{max} and V_{pp} values; and *S/N* values based on the vertical component, $(S/N)^{v}$, and the total or magnitude (corresponding to peak-to-peak value), $(S/N)^{T}$, of signal and noise. Measurements based on V_{max} and V_{pp} are generally considered as indicators of detection capability and sizing accuracy, respectively. Several important trends can be observed from the *S/N* values based on the V_{max} component of signal and noise, $(S/N)^{v}$, that are given in Table 3.4. Most test sections in the database used in this study have $(S/N)^{v}$ values below 2. Flaw signals in five cases were detected by a number of teams at *S/N* levels less than one. This finding reflects the ability of analysts to detect subtle indications in some cases. Based on the available database, the highest *S/N* level at which a flaw signal was not detected is slightly above 2.0. The corresponding values of V_{max} from test sections with the highest *S/N* values may be used to establish a minimum detection limit for the inspection techniques that employ bobbin probes.

The results in Table 3.5 are for the same test sections as in Table 3.4 but with an increased level of simulated noise. In general, the *S/N* values dropped slightly as a result of the added noise. However, *S/N* increased slightly in a few cases because of the constructive interference of noise in them. Since the number of missed calls for the EC indication with the highest *S/N* was small, results of the analyses listed in Table 3.4 suggest that an empirically derived value of $(S/N)^{v}$ slightly above 2 [e.g., $(S/N)^{v} \approx 2.5$] would result in

detection of flaw signals with an acceptable degree of confidence. This information may thus be used to set a lower limit on *S/N* for detection of flaw signals in the mock-up. However, any detection limit established based on the data with the added level of noise may be considered as biased because of the prior knowledge about the location of indications in the original data. A more accurate detection limit can only be established by developing a more extensive database.

The assessments so far have been focused primarily on identifying viable measures of noise and assessing the impact of noise on detection capability. Some general comments can be made, however, regarding the sizing capability based on the results listed in Tables 3.4 and 3.5. While no direct assessments of the effects of noise on sizing capability exits, noise indices based on the magnitude of the probe response are expected to be an indicator of sizing ability. The *S/N* values in those tables based on V_{pp} measurements, $(S/N)^T$, on average, exhibit a considerably lower value than those based on V_{max} measurements, $(S/N)^v$. As explained earlier, this effect is primarily due to the larger influence of common sources of noise on the horizontal component of data. The influence on the horizontal component of the data could result in significant distortion of the phase angle of a signal and, therefore, the estimate of the flaw depth (since the phase angle is commonly used to estimate the flaw depth). The examples shown here suggest that the level of noise, which may minimally affect detection, can have a profound effect on sizing.

Table 3.1 Measured minimum and average values of probe response from calibration standard tube.

Location	Minimum value		Average value	
	V_{max}	V_{pp}	V_{max}	V_{pp}
Free-span section	0.04	0.23	0.09	0.38
TSP	0.31	0.75	0.35	0.9

Table 3.2 Measured average and maximum value of noise level in free-span regions of the test sections shown in Figs. 3.1-3.6 and 3.8-3.18 from mix channel data without simulated noise.

Test section	Average value over ROI				Maximum value over ROI			
	N^v_{RMS}	N^T_{RMS}	V_{max}	V_{pp}	N^v_{RMS}	N^T_{RMS}	V_{max}	V_{pp}
Figure 3.1	0.02	0.11	0.09	0.38	0.03	0.16	0.12	0.50
Figure 3.2	0.03	0.12	0.10	0.42	0.03	0.17	0.11	0.56
Figure 3.3	0.05	0.29	0.17	1.00	0.08	0.47	0.30	1.45
Figure 3.4	0.03	0.13	0.11	0.42	0.04	0.17	0.14	0.52
Figure 3.5	0.02	0.09	0.08	0.31	0.02	0.12	0.11	0.39
Figure 3.6	0.03	0.09	0.11	0.32	0.04	0.13	0.14	0.39
Figure 3.8	0.02	0.10	0.08	0.33	0.03	0.15	0.11	0.46
Figure 3.9	0.03	0.13	0.10	0.46	0.03	0.18	0.13	0.58
Figure 3.10	0.03	0.10	0.10	0.34	0.04	0.14	0.13	0.50
Figure 3.11	0.02	0.09	0.09	0.32	0.03	0.15	0.13	0.49
Figure 3.12	0.02	0.09	0.08	0.32	0.04	0.13	0.12	0.43
Figure 3.13	0.02	0.12	0.10	0.43	0.03	0.20	0.13	0.60
Figure 3.14	0.03	0.11	0.11	0.40	0.03	0.14	0.13	0.48
Figure 3.15	0.02	0.11	0.09	0.38	0.03	0.19	0.13	0.64
Figure 3.16	0.03	0.12	0.10	0.42	0.04	0.20	0.12	0.61
Figure 3.17	0.02	0.09	0.09	0.35	0.03	0.13	0.11	0.47
Figure 3.18	0.07	0.16	0.28	0.60	0.12	0.26	0.39	0.82

Table 3.3 Measured average and maximum value of noise level in free-span regions of the test sections shown in Figs. 3.1-3.6 and 3.8-3.18 from mix channel data with simulated noise.

Test section	Average value over ROI				Maximum value over ROI			
	N^{v}_{RMS}	N^{T}_{RMS}	V_{max}	V_{pp}	N^{v}_{RMS}	N^{T}_{RMS}	V_{max}	V_{pp}
Figure 3.1	0.05	0.20	0.19	0.79	0.06	0.31	0.23	1.07
Figure 3.2	0.05	0.18	0.20	0.70	0.07	0.27	0.25	0.97
Figure 3.3	0.06	0.39	0.24	1.55	0.07	0.66	0.30	2.54
Figure 3.4	0.07	0.19	0.27	0.86	0.09	0.27	0.37	1.11
Figure 3.5	0.05	0.16	0.16	0.62	0.06	0.20	0.20	0.76
Figure 3.6	0.05	0.19	0.19	0.67	0.06	0.21	0.24	0.84
Figure 3.8	0.06	0.16	0.21	0.60	0.08	0.21	0.30	0.81
Figure 3.9	0.06	0.21	0.23	0.84	0.07	0.28	0.27	1.12
Figure 3.10	0.06	0.17	0.21	0.64	0.08	0.30	0.28	1.09
Figure 3.11	0.04	0.17	0.16	0.62	0.07	0.22	0.22	0.72
Figure 3.12	0.05	0.17	0.20	0.75	0.08	0.24	0.27	0.95
Figure 3.13	0.05	0.23	0.18	0.96	0.07	0.30	0.28	1.14
Figure 3.14	0.06	0.18	0.20	0.68	0.07	0.23	0.23	0.81
Figure 3.15	0.05	0.20	0.17	0.82	0.06	0.30	0.19	1.08
Figure 3.16	0.06	0.17	0.22	0.67	0.08	0.24	0.25	0.85
Figure 3.17	0.05	0.15	0.18	0.57	0.07	0.24	0.21	0.97
Figure 3.18	0.11	0.22	0.44	0.88	0.15	0.32	0.57	1.10

Table 3.4 Measured maximum value of noise level and *S/N* over the region of interest, which includes the TSP for the test sections shown in Figs. 3.1-3.6 and 3.8-3.18 from mix channel data without simulated noise.

Test section	Maximum value over ROI including TSP					
	N^{v}_{RMS}	N^{T}_{RMS}	V_{max}	V_{pp}	$(S/N)^{v}$	$(S/N)^{T}$
Figure 3.1	0.22	0.32	0.68	1.05	0.65	0.64
Figure 3.2	0.05	0.17	0.35	0.90	1.80	1.67
Figure 3.3	0.08	0.47	0.30	1.45	2.00	0.61
Figure 3.4	0.18	0.37	0.49	1.42	1.08	0.48
Figure 3.5	0.40	0.54	1.24	1.81	0.83	0.61
Figure 3.6	0.44	0.58	1.44	2.00	0.89	0.70
Figure 3.8	0.10	0.74	0.34	2.81	1.38	0.42
Figure 3.9	0.05	0.19	0.35	0.90	1.86	1.13
Figure 3.10	0.20	0.27	0.56	0.88	1.66	1.96
Figure 3.11	0.10	0.19	0.38	0.61	1.53	1.44
Figure 3.12	0.19	0.30	0.65	1.30	1.78	0.97
Figure 3.13	0.08	0.26	0.35	0.94	0.86	0.83
Figure 3.14	0.15	0.28	0.51	1.01	2.14	1.27
Figure 3.15	0.13	0.66	0.37	2.07	1.38	0.47
Figure 3.16	0.17	0.81	0.51	3.00	0.65	0.34
Figure 3.17	0.27	1.06	0.84	3.18	1.49	0.50
Figure 3.18	0.12	0.26	0.39	0.82	1.23	1.12

Table 3.5 Measured maximum value of noise level and *S/N* over the region of interest, which includes the TSP for the test sections shown in Figs. 3.1-3.6 and 3.8-3.18 from mix channel data with simulated noise.

Test section	Maximum value over ROI including TSP					
	N^{v}_{RMS}	N^{T}_{RMS}	V_{max}	V_{pp}	$(S/N)^{v}$	$(S/N)^{T}$
Figure 3.1	0.19	0.35	0.67	1.32	0.66	0.47
Figure 3.2	0.07	0.28	0.35	1.00	1.96	1.78
Figure 3.3	0.07	0.66	0.35	2.55	2.23	0.58
Figure 3.4	0.15	0.34	0.51	1.37	1.00	0.56
Figure 3.5	0.40	0.52	1.25	1.91	0.73	0.54
Figure 3.6	0.45	0.63	1.43	2.16	0.96	0.67
Figure 3.8	0.11	0.85	0.35	3.09	0.84	0.41
Figure 3.9	0.07	0.28	0.35	1.14	2.21	1.40
Figure 3.10	0.18	0.29	0.57	1.07	1.60	1.69
Figure 3.11	0.14	0.26	0.50	0.93	1.03	1.05
Figure 3.12	0.22	0.35	0.76	1.22	1.40	1.02
Figure 3.13	0.10	0.31	0.37	1.17	0.67	0.81
Figure 3.14	0.14	0.34	0.50	1.26	2.37	1.11
Figure 3.15	0.17	0.72	0.48	2.28	1.04	0.51
Figure 3.16	0.18	0.89	0.59	3.27	0.48	0.32
Figure 3.17	0.32	1.02	0.97	3.03	1.26	0.47
Figure 3.18	0.15	0.32	0.57	1.10	1.00	1.09

3.3 Adjustment of POD Based on Noise Level

As discussed in Sec. 3.2.2, there is a high likelihood that cracks will be detected for $(S/N)^v$ slightly greater than 2, but that is not sufficient to quantify the effect of $(S/N)^v$ on POD. The data developed in Sec. 3.2.2 for signal and noise levels in the mock-up were compared with the actual probabilities of detection as determined in the ANL/NRC steam generator mock-up analysis round robin.[7] The results are shown in Fig. 3.19.

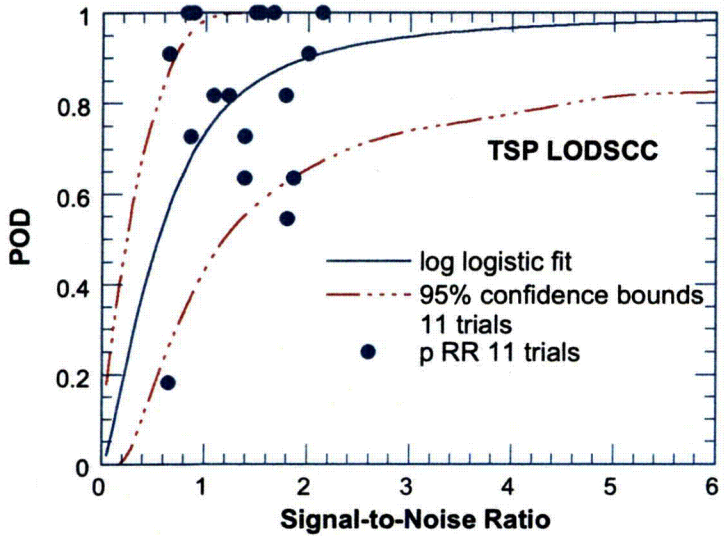

Figure 3.19
Solid dots show probability of detection measured for round–robin (number of hits/11 trials). Solid curve shows log–logistic fit for POD based on round–robin data. Chain-dot curves show estimated bounds (95th percentile) on the expected values of POD obtained in 11 trials if the true binomial POD is given by the log–logistic fit.

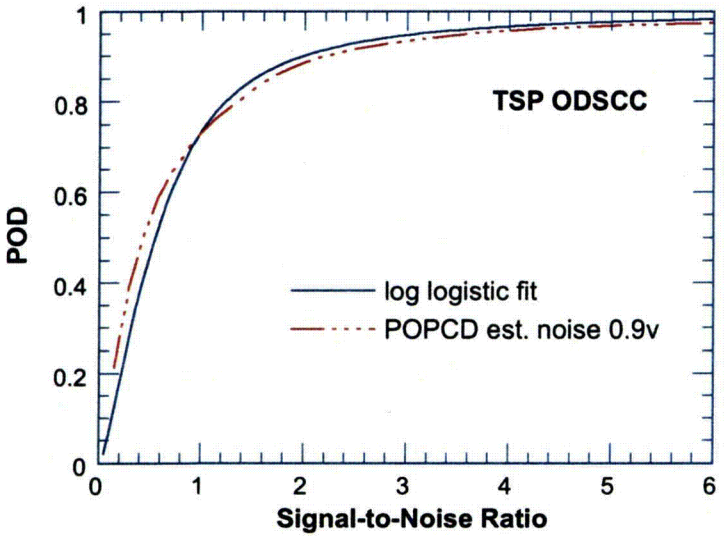

Figure 3.20
Probability of detection as a function of $(S/N)^V$. The log logistic fit to the data from the round–robin is shown as solid curve. For comparison, a POD vs $(S/N)^V$ curve estimated from the POPCD curve for TSPs is also shown. A value of 0.9 V was assumed for all specimens in the POPCD database.

The data from the round–robin shown as solid dots in Fig. 3.19 are simple fractions of the number of teams that identified the flaws to the total number of teams (11). Linear–logistic, log–log, and log–logistic maximum–likelihood fits were examined. The log–logistic curve gave the best fit to the data. Even if the best–fit curve actually does represent the true POD curve, in the 11 trials the observed probabilities would not be expected to lie on the curve. The upper and lower chain–dot curves in Fig. 3.19 are 95th percentile estimates for the observed probabilities for 11 trials. These bounds would become narrower for a larger number of trials. More data lies outside the bounds than would be expected if the log–logistic fit was perfect, but the agreement is reasonably good, although the number of data are limited. For comparison, a curve of POD as a function of *S/N* estimated from the industry probability of prior-cycle detection (POPCD) curve,[8] which gives POD as a function of voltage for ODSCC at TSPs is shown in Fig. 3.20. The signal-to-noise ratios are unknown for this data, but based on the average value of V_{max} for mock-up of 0.6 V and some experience with data from the field, a value of 0.9 V was assumed for V_{max}, and signal–to-noise ratios were then calculated. The resulting POD curve is in good agreement with that based on the data from the round–robin, which provides some increased confidence in the POD curve, despite the limited data on which it is based. The POD curve in Fig. 3.19 is consistent with the previous observation in Section 3.2 that for $(S/N)^{\nu}$ greater than 2, the POD is very high. However, even for a value of $(S/N)^{\nu} = 1$, the POD is 0.7.

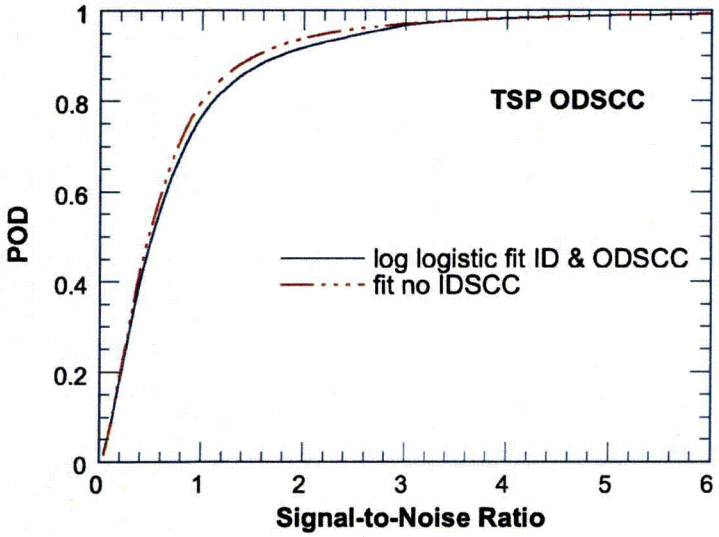

Figure 3.21
Probability of detection as a function of S/N. Although flaws are predominantly ODSCC, the data includes some IDSCC. Excluding the IDSCC data does not significantly change the POD curve.

Although the data in Fig. 3.19 (Table 3.4 upon which Fig. 3.19 is based) are predominantly for ODSCC flaws, four data points for IDSCC flaws are included. In the round–robin, the false call rate for ODSCC was low (1.7%), but because the IDSCC were associated with dents, the false call rates for these flaws is very high (44%). Such high false call rates would usually make detection probabilities associated with these flaws suspect. To verify that these ID data were not unduly distorting the results, the POD curve was recomputed with the ID data excluded. As shown in Fig. 3.21, excluding the IDSCC data does not significantly change the POD curve. Since including the IDSCC results in somewhat lower values of POD, the more conservative curve has been used as the basis for discussion.

It is plausible that POD as a function of $(S/N)^{\nu}$ is more broadly applicable than a POD curve as a function of depth or voltage for a given geometrical condition, but more data from other flaw situations in the mock-up or from field data are needed to determine whether they are consistent with the POD curve derived from the TSP data. A POD curve developed from TSP data may be optimistic for other situations. Since

analysts expect to find cracking at the TSP, there may be a tendency when dealing with the uncertainty associated with a lower $(S/N)^V$ to make the call more conservatively than might be the case in locations where the known likelihood of cracking was somewhat lower.

Conventionally POD is given in terms of voltage or depth rather than $(S/N)^V$ and the POD curve as a function of $(S/N)^V$ can be used to develop a curve in terms of voltage. In Fig. 3.22, a POD curve as a function of signal level (voltage) was derived from the POD as a function of $(S/N)^V$ by multiplying $(S/N)^V$ by the average noise level in the mock-up for TSP locations (0.6 V from Table 3.4). In Figure 3.22 this curve is compared with Figure 3.22 with the POD curve as a function of voltage developed directly from the round robin data and the industry POPCD curve. The use of the average noise level in the mockup instead of the actual noise level associated with each point results in some differences between the POD curve derived from the $(S/N)^V$ and the actual POD for the round robin, but the curves are reasonably close. This suggests that use of an average noise level may give a reasonable overall estimate of the POD. The agreement with the POPCD curve is extremely good. This is probably somewhat fortuitous, since the noise level in the mock-up is presumably somewhat lower than the noise levels expected in typical operating steam generators and as noted by comparison with the round robin curve, use of an average noise level instead of the actual noise level will introduce some error.

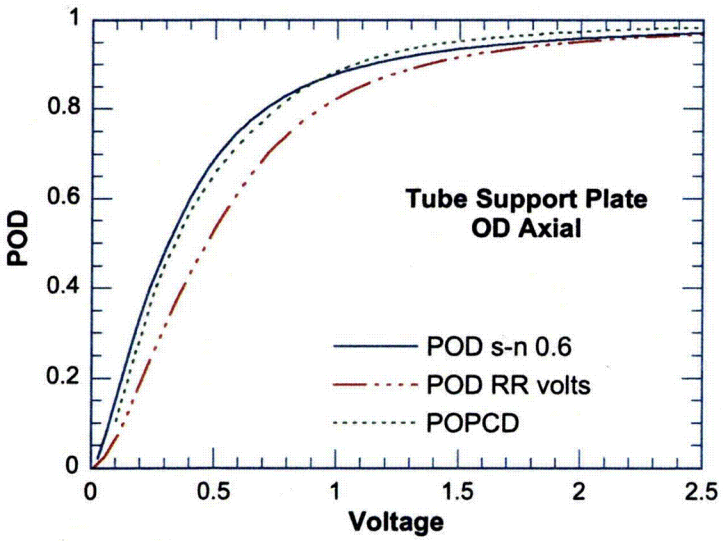

Figure 3.22
Probability of detection as a function of voltage. POD RR denotes the probability of detection

The predicted effect on the POD as a function of signal voltage of an increase in the average noise level from 0.6 V to 0.9 V is shown in Figure 3.23. As expected, for a given signal level, the POD decreases significantly especially at lower signal levels. However, such results don't fully reflect the effect of noise on POD. The results in Table 3.4 suggest that noise is at least approximately log–normally distributed. The log–mean is -0.67 with a log–standard deviation of 0.46. It seems reasonable to assume that noise and signal levels are uncorrelated, i.e., a flaw of a given magnitude (resulting in a given signal level) is as likely to occur at a relatively high noise location as it is at a relatively low noise location. Thus for a given signal level there is a range of POD depending on the noise level. The resulting range for the noise conditions in the mock-up is shown in Fig. 3.24. The mean curve (solid blue) represents the POD at a given signal level for the average noise level. For the same signal level, the POD will decrease in high noise locations and increase in low noise locations. Although the mean value of the POD for a 1 V signal is 0.88, the POD could vary from 0.71 to

0.96 when noise is evaluated at 1.64 standard deviations from the mean (and assuming a normal distribution of noise levels). Similar results are shown in Fig. 3.25 for an average noise level of 0.9 V and a relative range of noise levels similar to that in the mock-up for the TSP region.

In Fig. 3.26, the effect of variability in noise in the POPCD is estimated. It is assumed that the POD as a function of voltage represented by the POPCD curve corresponds to the mean POD curve for a mean noise level of 0.9 V. The relative variability of noise in the field is assumed to be the same as that in the mock-up. The probability of detection of a 1 V flaw signal at the noisiest location (0.72) is considerably smaller that then average POD of such a flaw (0.89) and the POD can approach 1 at the least noisy locations. These results are of course extremely dependent on the actual distribution of noise levels in locations of interest in operating steam generators and results based on the mock-up data can only illustrate the potential impact of the variability in noise on POD.

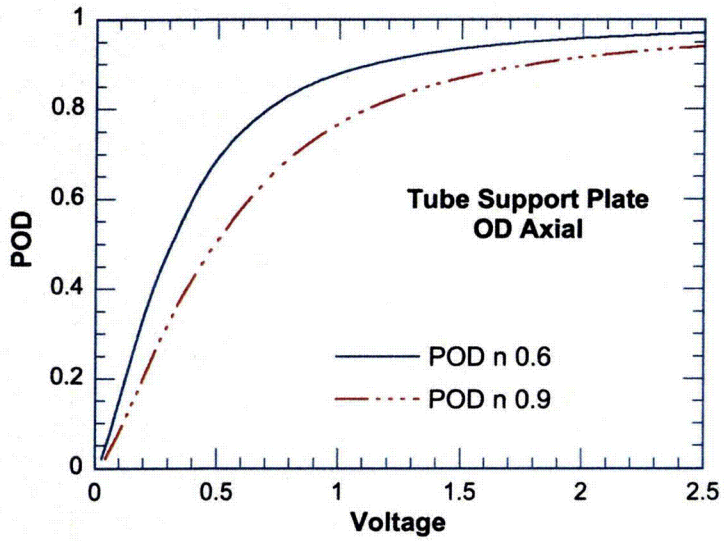

Figure 3.23
Probability of detection as a function of signal voltage for average noise levels of 0.6 V and 0.9 V.

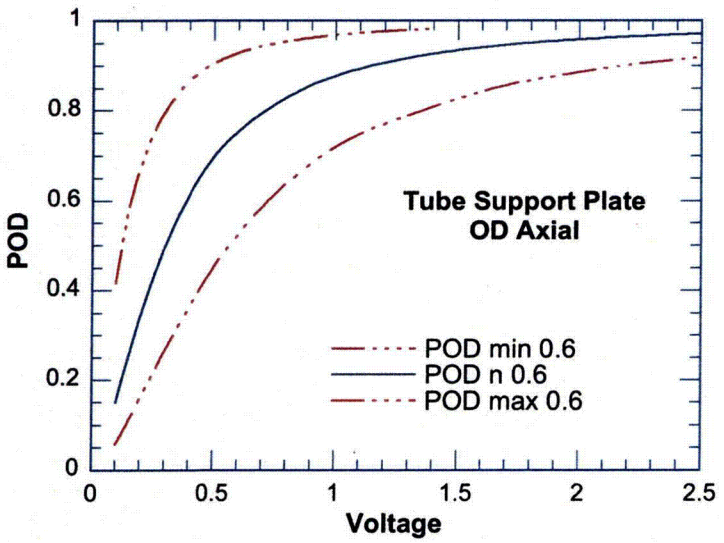

Figure 3.24
Range of probabilities of detection expected for a given voltage for log–normal noise with a mean value of 0.6 V.

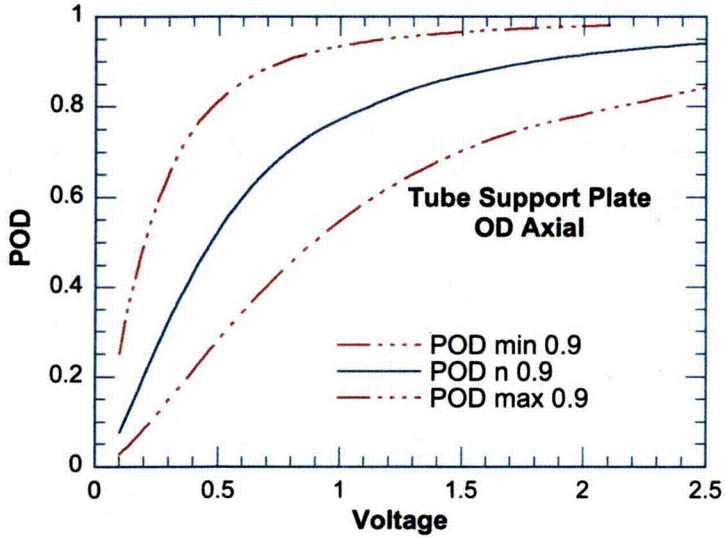

Figure 3.25
Range of probabilities of detection expected for a given voltage for log–normal noise with a mean value of 0.9 V.

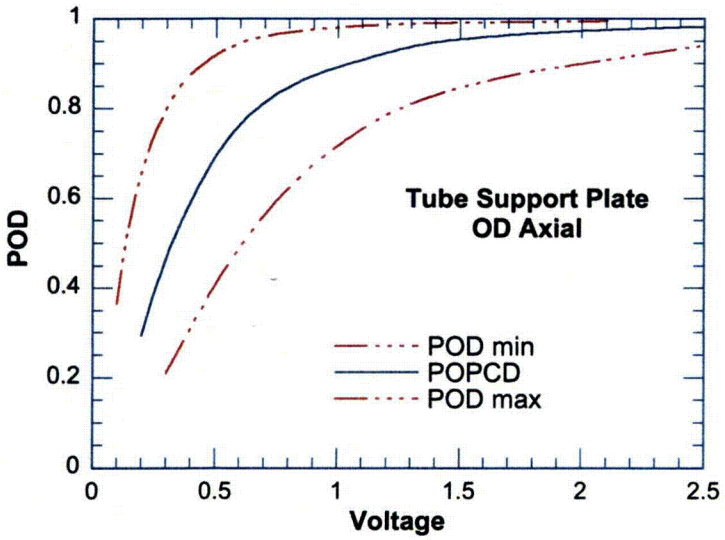

Figure 3.26
Range of probabilities of detection expected for a given voltage for log–normal noise with a mean value of 0.9 V based on the POPCD curve.

4 Concluding Remarks

This report presents results on the assessment of noise level for bobbin coil inspections of SG tubes. It also presents preliminary results regarding the treatment of noise in 2-D EC inspection data pertaining to rotating and array probes, which is an extension of 1-D measurements with bobbin probes. A series of algorithms has been integrated into a software-based tool for the simulation, superposition, and measurement of noise in EC inspection data acquired with standard probes. These tools can be used to perform various computations associated with the influence of noise on detection and sizing in an efficient and systematic manner. Evaluations were carried out to identify the most viable indicators of EC noise influence. Several measurement variables (e.g., window size and the extent and location of the ROI) were examined to determine their effect on estimation of the noise level. Calculations of noise indices were based on the vertical component (V_{max}) and the magnitude (V_{pp}) of the EC data using RMS, mean, and maximum values of all measurements over the region of interest. To reduce measurement variability, a sliding window method was introduced. The results of these investigations were used to implement a procedure for the evaluation of noise level in data collected with bobbin probes from the tube bundle mock-up at ANL.

Test-case results are also reported on the measurement of noise level for establishing a detection limit based on the EC inspection data collected from the mock-up. Bobbin coil data from a subset of intersections were initially included for analysis. Analyses were performed for both the original data and simulated data with a low level of superimposed noise. Based on the analysis of *S/N*, a single indicator was identified as being the most direct measure of noise level. Analyses indicated that the maximum amplitude of the V_{max} component measured over the free-span region of the tubing provides a conservative estimate of noise level for data quality assessments. The same parameter measured over the region of interest that would encompass the probe response from extraneous discontinuities provides a viable measure of detection capability. Typical values of V_{max} and V_{pp} in the available database of mock-up test sections for establishing a detection limit are provided in Tables 3.2 and 3.4. Signal-to-noise ratios may then be used to determine a threshold on the amplitude of the smallest detectable flaw in the presence of a certain noise level. The POD curves may subsequently be adjusted by using the minimum detection limits for a given technique.

Some general remarks regarding the analyses presented in this report should be made if similar procedures are to be used for field applications. Investigations here have revolved around defining and measuring the noise associated with a limited set of test sections from the mock-up. Establishment of reliable limits on detection capability for a particular NDE technique requires a statistically significant database. As noted earlier, the measurement of noise level for the purpose of data quality assessment should be distinguished from measurement of noise for the purpose of evaluating tube structural integrity. Combined information from several semi-independent indicators of noise level could provide complementary information on the influence of EC noise on detection.

The detection capability is more closely correlated with the signal amplitude. Sizing ability could depend on both the amplitude and phase angle of the signal, as well as the NDE technique being employed. Because the same level of noise can affect detection and sizing differently, separate limits might have to be placed on the level of noise when detection and sizing capability are being assessed. Irrespective of the methodology used for measuring the level of noise, results should be treated as probabilistic estimates of noise level rather than an absolute measure of detection. Furthermore, missed indications because of misinterpretation of probe response by an analyst should not be included in the assessments of noise level for establishing a detection limit. This conclusion is particularly important for field applications, where the analysis results can be affected by various sources of signal distortion as well as operator-related factors.

Unless the effect of deterministic sources of signal distortion can be suppressed with reasonable consistency, defining a measure of noise level that could be uniformly applied to all SG locations will inherently lead to placing more conservative limits on the detection capability of a technique. This conclusion is particularly true for specialized techniques that employ EC rotating or array probes with different coil design and sensitivity. Common sources of signal distortion along with hardware- and software-based techniques for reducing their influence, when the EC noise level is found to be excessive, were discussed earlier in this report (see Sec. 2.1). Additional use of digital filters was suggested as one possible approach for improving the detection capability. Applying frequency and spatial domain filters to EC data for suppression of various random and deterministic sources of signal distortion is not a common ISI practice. This is attributed primarily to the variability in the analysis results that could be introduced by arbitrary adjustment of filter parameters by the operator. Improper application of filtering schemes could lead to distortion and potential elimination of low amplitude signals. The limited number of digital filtering techniques that are currently used for ISI applications are thus employed for screening purposes only.

Finally, adjustment of POD based the level of noise is discussed in Sec. 3.3. Data from the ANL mock–up round robin is used to develop a POD curve as a function of signal–to–noise. It is plausible that POD as a function of $(S/N)^v$ is more broadly applicable than a POD curve as a function of depth or voltage for a given geometrical condition, but more data from other flaw situations in the mock-up or from field data are needed to determine whether they are consistent with the POD curve derived from the TSP data. This curve can be used to estimate the impact on the more conventional POD curve as a function of voltage as the average noise level is increased from 0.6 V in the mock–up to 0.9 V, which may be more representative of some field conditions. The results also suggest that there can be significant variability in the detectability of a given flaw signal from location–to–location within a given steam generator due to variability expected in noise.

5 References

1. S. Bakhtiari and D. S. Kupperman, *Advanced NDE for Steam Generator Tubing*, NUREG/CR-6638, ANL-99/9 (Jan. 2000).

2. S. Bakhtiari, J. Y. Park, D. S. Kupperman, S. Majumdar, and W. J. Shack, *Final Report on Advanced Nondestructive Evaluation for Steam Generator Tubing for the Second Steam Generator Tube Integrity Program*, NUREG/CR-6814, ANL-03/4 (July 2003).

3. *MATLAB, the Language of Technical Computing, Using MATLAB Version 5*, MathWorks, Inc., Natick, MA (1998).

4. W. H. Press, B. P. Flannery, S. A. Teukolsky, and W. T. Vetterling, *Numerical Recipes*, Cambridge University Press, Cambridge, UK (1986).

5. *Pressurized Water Reactor Steam Generator Examination Guidelines: Revision 6, Requirements*, Electric Power Research Institute, Palo Alto, CA (2002).

6. S. L. Meyer, *Data Analysis for Scientists and Engineers*, John Wiley & Sons, Inc., New York (1975).

7. D. S. Kupperman, S. Bakhtiari, W. J. Shack, J. Y. Park, and S. Majumdar, Eddy Current Reliability Results from the Steam Generator Mock-up Analysis Round-Robin: Revision 1, NUREG/CR–6791 Rev.1, ANL–08/30, (2009).

8. Special Report 06-02 - Results of Steam Generator (SG) Tube Inspections for Diablo Canyon Power Plant Unit 2 Thirteenth Refueling Outage. ML062400518 (2006)

NRC FORM 335
(9-2004)
NRCMD 3.7

U.S. NUCLEAR REGULATORY COMMISSION

BIBLIOGRAPHIC DATA SHEET

(See instructions on the reverse)

1. REPORT NUMBER
(Assigned by NRC, Add Vol., Supp., Rev., and Addendum Numbers, if any.)

NUREG/CR-6982

2. TITLE AND SUBTITLE

Assessment of Noise Level for Eddy Current Inspection of Steam Generator Tubes

3. DATE REPORT PUBLISHED

MONTH	YEAR
March	2009

4. FIN OR GRANT NUMBER

Y6588

5. AUTHOR(S)

S. Bakhtiari, D.S. Kupperman, and W.J. Shack

6. TYPE OF REPORT

Topical

7. PERIOD COVERED *(Inclusive Dates)*

8. PERFORMING ORGANIZATION - NAME AND ADDRESS *(If NRC, provide Division, Office or Region, U.S. Nuclear Regulatory Commission, and mailing address; if contractor, provide name and mailing address.)*

Argonne National Laboratory
9700 South Cass Avenue
Argonne, IL 60439

9. SPONSORING ORGANIZATION - NAME AND ADDRESS *(If NRC, type "Same as above"; if contractor, provide NRC Division, Office or Region, U.S. Nuclear Regulatory Commission, and mailing address.)*

Division of Engineering
Office of Nuclear Regulatory Research
U.S. Nuclear Regulatory Commission
Washington, DC 20555-0001

10. SUPPLEMENTARY NOTES

M. Stambaugh, NRC Project Manager

11. ABSTRACT *(200 words or less)*

This report provides an overview of research activities associated with eddy current (EC) inspection of steam generator tubes carried out at Argonne National Laboratory (ANL) as part of the Steam Generator Tube Integrity Program sponsored by the U.S. Nuclear Regulatory Commission. The primary focus is on spatially one-dimensional calculations for bobbin probe noise, with limited investigations on noise measurement in rotating probe data. First, the report reviews the basic concepts and common sources of signal distortion in ED data from in-service inspections. Next, various algorithms for the simulation, superposition, and measurement of noise that were developed at ANL are described. The effect of measurement variables (e.g., sample size and region of interest) on various measures of noise level is also presented. Viable indicators of the noise level are identified and the associated measurement procedures are outlined. The second part of the report deals with measurement of the level of noise present in the ANL tube bundle mock-up. Selected tubes were identified as having flaw signals that were borderline for detectability. Inferences were made regarding the limit of detection. Finally, implications of the results concerning detection probability and applications of the proposed methodologies for the measurement of noise are discussed.

12. KEY WORDS/DESCRIPTORS *(List words or phrases that will assist researchers in locating the report.)*

Eddy current
Steam generators
Inservice inspection
Data analysis
Noise assessment

13. AVAILABILITY STATEMENT

unlimited

14. SECURITY CLASSIFICATION

(This Page)
unclassified

(This Report)
unclassified

15. NUMBER OF PAGES

16. PRICE

PRINTED ON RECYCLED PAPER

Federal Recycling Program